Quantitative Chemical Tagging: Empirical Constraints on the Identification of Dispersed Coeval Stellar Groups

by Arik W. Mitschang

A thesis submitted in fulfilment of the degree of
Doctor of Philosophy at Macquarie University

ASTRONOMY, ASTROPHYSICS AND
ASTROPHOTONICS RESEARCH CENTRE

December 13, 2014

Except where acknowledged in the customary manner, the material presented in this thesis is, to the best of my knowledge, original and has not been submitted in whole or part for a degree in any university.

Arik W. Mitschang

Contents

Abstract

The long term evolution and the origin of the Galactic stellar disc are the subjects of intense study. Much is surmised about the evolution of galaxies in general by studying those at cosmic scales, yet there are still significant issues in explaining phenomena in our own Galaxy. It is only a single case, but of universal importance due to our ability to resolve individual stars and stellar populations. Amongst the important open questions are the origin (or indeed the reality) of the thin and thick stellar discs, the role of intra-disc stellar migrations, the merger history, in-situ star formation history and the chemical evolution of the disc. Kinematic information, though crucial to understanding the Galactic environment, is short lived in the disc and thus astronomers are turning to stellar chemical abundances, which remain unchanged for most of a star's lifetime, to reveal history. In particular, the technique of chemical tagging may be able to use this "fossil" information to link groups of stars in the disc which have formed concurrently from the same molecular cloud, but have since dispersed. Though it has been established that open clusters have tight abundance scatter, the empirical evidence for the viability of chemical tagging has for the most part gone unstudied. With a large survey dedicated to tagging – GALAH – just on the horizon, we perform several empirical investigations of this technique. An empirical coeval probability function, which quantifies the likelihood that a pair of stars originated from the same star formation event, is developed and characterised. We then perform a real world test by conducting the first ever blind chemical tagging experiment, with several important implications.

Preface

This thesis is presented in the style of thesis by publication. The original research and distinct contribution to scientific understanding of the universe has been previously published in major refereed journals in the field of astrophysics, and is placed in context within this thesis. The papers appearing are the following:

1.) **In Chapter 3**: "Elemental abundances of intermediate-age open cluster NGC 3680" appearing in Monthly Notices of the Royal Astronomical Society, 2012, volume 422, pages 3527-3534. All writing, data analysis work, and figure creation was carried out by the candidate. The second and third authors are the candidate's supervisors.

2.) **In Chapter 4**: "Quantifying chemical tagging: towards robust group finding in the Galaxy" appearing in Monthly Notices of the Royal Astronomical Society, 2013, volume 428, pages 2321-2332. All writing, data analysis work, and figure creation was carried out by the candidate. The second and fourth authors are the candidate's supervisors. The third author is credited for significant support and advice in the development of ideas presented.

3.) **In Chapter 5**: "Quantitative chemical tagging, stellar ages and the chemodynamical evolution of the Galactic disc" in Monthly Notices of the Royal Astronomical Society, 2014, volume 438, pages 2753-2764. All writing, data analysis work, and figure creation was carried out by the candidate. The second and third authors are the candidate's supervisors. The fourth author is credited for significant support of and advice in the development of ideas presented. The fourth and fifth authors are credited for providing the unpublished dataset used in the analysis, and for assistance in editing the article.

The author wishes to acknowledge the support of the following individuals, groups or organizations: his thesis advisers Daniel B. Zucker and Gayandhi M. De Silva, without whom this certainly would not have come together. They both practiced the art of guidance at the same time as leeway, being advocates at the same time as critics, and above all placed their trust this candidate, for which he is ever grateful. The Australian Astronomical Observatory (AAO) for a top-up scholarship that has supported this work over the past three years. The Macquarie University and AAO HERMES group – Borja Anguiano, Daniela Carollo, Valentina D'Orazi, Gayandhi De Silva, Sarah Martell, Colin Navin, and Daniel Zucker – for their interest in this topic that fostered many discussions and thoughtful direction. Michael Fitzgerald for the countless office beers and pub crawls, and whose own passion and motivation for astronomy was a

constant inspiration. All the strange and wonderful people who have made up the astronomy post-grad office at Macquarie University over the years for keeping things interesting and never taking things too seriously. His wife, Kayo Nishida, for not questioning his sanity in deciding to undertake this task, despite all signs of impending doom. His son, Kai Matthew Mitschang, for so many smiles and making this the most interesting year yet. And finally his daughter to be, in hopes that she is welcomed with good health.

Chapter 1

Introduction

As the night sky fades over time to the dull glow of smog and city lights, by virtue of the advancement of human civilisation and ingenuity, it seems easy to forget altogether what motivates us in understanding our place in the universe. Yet, for tens of thousands of years, as far back as physical archaeological evidence is available, through war, famine, and earth shattering natural disaster, humans have been looking to the heavens for context to our lives on this tiny blue planet. It's no mystery why. Imagine, for a moment, you are on a mountain top, high above the tree line. You are standing on a slab of cold granite on this biting clear moonless night. The dull groan of the light breeze echoing in the valley below, and the trickle of a small, rocky creek, are the only sounds to be heard. Its pitch dark, but a soft shadow looms beneath your feet. You look up to see the Milky Way painted across the full breadth of the sky, its veins as bright as day. Thousands of twinkling points dot the dark canvas, each one much like our own Sun, possibly harboring a planet with a being looking right back at you. You even see another galaxy, maybe two. Each one is made of yet more stars, and you begin to wonder how far it extends. Just how big is it? How insignificant is this beautiful planet we call home, and how did it even all come to this? The freedom in these thoughts, the freedom in imagining the vast expanses of space captivates your mind, your subconscious, and never escapes.

The past four hundred years, since the invention of the modern astronomical telescope by Galileo Galilei, have seen immense progress in answering some of those questions. We now have a good idea of the origin, extent, and structure of the universe. We have an incredibly precise picture of the Solar System, the motion of objects within it so well mapped that we can successfully land a spacecraft on a comet. We now know that the Sun, Earth and Solar System are located within a much larger structure, an immense spiral galaxy, and that such large structures

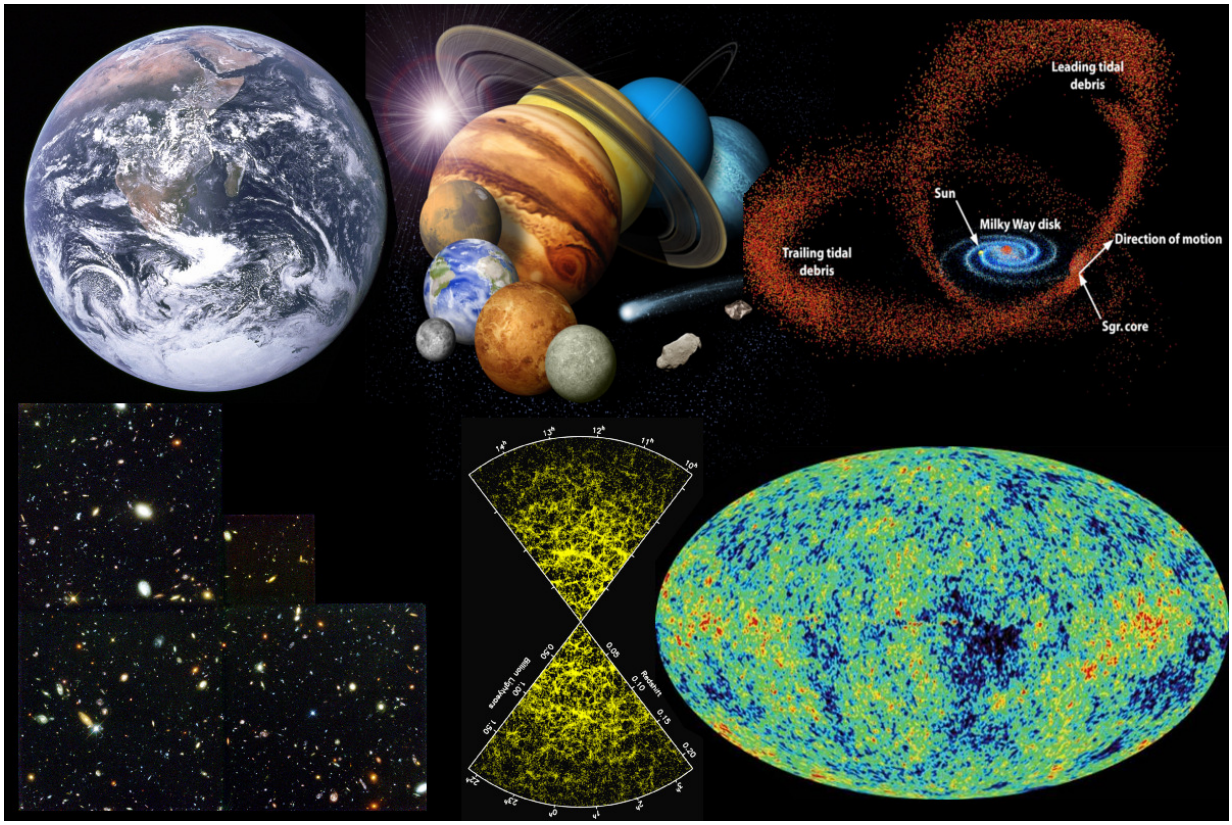

FIGURE 1.1: Our place and time in the universe. Clockwise from top left, (a) Earth, as seen from Apollo-11 (NASA) (b) Planets of the Solar system (NASA) (c) A simulated view of the Galaxy and its streams (David R. Law, UCLA) (d) The Hubble deep field image, showing galaxies everywhere (NASA) (e) A 2dF Galaxy Redshift Survey (2dFGRS) view of the large scale structure of the local universe (http://www.roe.ac.uk/ jap/2df/) (f) The cosmic microwave background (CMB) as measured by WMAP, the temperature fluctuations seen in color space are micro-kelvin scale (NASA).

are ubiquitous. We even have an age for the universe, 13.7 billion years old, and have looked back, several times now, to the primordial light emitted when it was only a tiny fraction of that age. Figure 1.1 illustrates the current understanding of the scope of, and our place in, the universe at large.

It is often said that we know more about the far reaches of the Solar System than we do about the deepest depths of the oceans on our own planet. One might say, similarly, that we have a greater understanding of the large scale structure and evolution of galaxies out to the edge of the visible universe and time, than we do about the events which led to the Milky Way we see today.

1.1 Galactic Archaeology Primer

Just as archaeologists dig for fossils, the preserved remains of ancient cultures or living organisms, here on earth, Galactic archaeologists search for *fossils*, or any unchanging evidence of the evolutionary history of the Milky Way (commonly referred to simply as "the Galaxy", noting the capitalization). The Galaxy, though most of it is obscured by thick lanes of dust and our position in it renders study of the opposite side impossible, is nonetheless an ideal laboratory for studying the evolution of its class of galaxies, and, by proxy, the evolution of structure in the universe itself. Even in the upcoming era of extremely large telescopes (those with diameters exceeding thirty meters), very few other galaxies are close enough to enable resolving single stellar populations. Given that stars are the primary light source in the universe, and that light is the fundamental information transport mechanism, it follows that in order to gain insight to the processes that formed the Galaxy, one must understand the origins and evolution of its stars. The rest of this chapter serves to briefly introduce our current understanding of the basic structure of the Galaxy, and the importance of certain stellar populations for Galactic Archaeology.

1.2 The Galaxy

1.2.1 Structure and Dynamics

Thin and Thick Discs

Figure 1.2 shows an edge-on view of the Galactic disc as seen by 2MASS (The 2 Micron All Sky Survey;Skrutskie et al. 2006) in the left panel, and a face-on view of the Whirlpool galaxy, which is likely quite similar in morphology to the Galaxy, in the right panel. The disc is clearly visible in the 2MASS image, where a very high density, thin disc shape is accentuated by intervening dust lanes. A squint of the eye helps to recognise that stars extend more diffusely above and below the inner dense region. Of course, in reality, a lot of this is due to the projection effects of the image being taken from inside the disc itself; however, it is well known that spiral galaxies exhibit real vertical extension of their most obvious side-on stellar components (e.g. Yoachim & Dalcanton 2006). As an example, Figure 1.3 shows both a shallow and deep image of the same edge on galaxy, the thickness escaping detection in the shallow image, but clearly visible in the deep one.

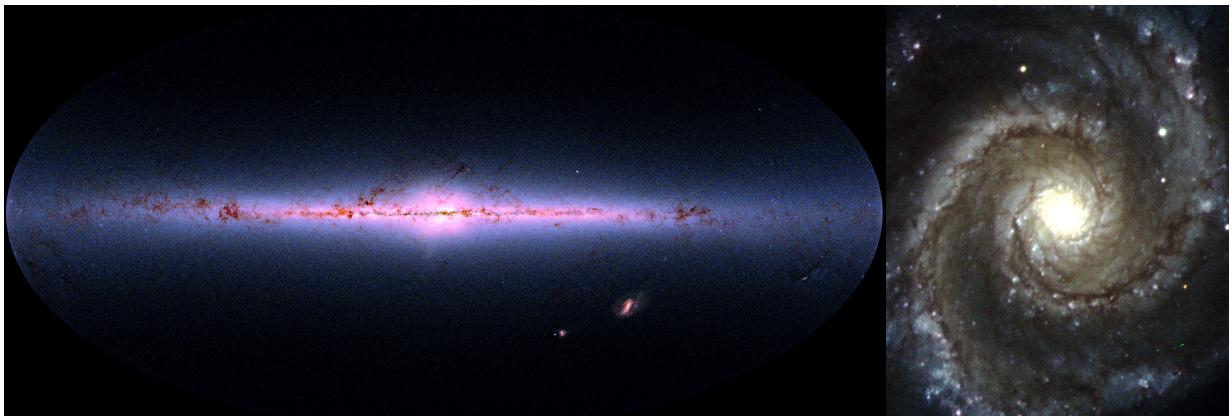

FIGURE 1.2: The Galaxy. Left image from 2MASS compiled by T. Jarrett (IPAC), the right image taken by the Mary Erskine School as a part of the Faulkes telescope project.

Gilmore & Reid (1983) were the first to propose that such a dichotomy exists in the Milky Way. Using the technique of photometric parallax on a sample of stars near the Solar neighbourhood, they derived a vertical density function that required two exponential components at distinct scale heights to fit. These they named the "old disc" for the thin component with a scale height of $\sim$ 300 pc (which, paradoxically, is now known to comprise of the younger component of the Galaxy), and the "thick disc" for the component with a scale height closer to 1 kpc. The "old disc" is now commonly referred to as the thin disc. Much work has been done in the intervening years to characterise the Galactic disc components (Bensby et al. 2003, Nordström et al. 2004, Bensby et al. 2005, Reddy et al. 2006, Haywood et al. 2013, Anguiano et al. in prep.). Several large-scale surveys have contributed, notably including the Geneva-Copenhagen Survey (GCS; Nordström et al. 2004), which contains over 14 000 stars with parallax, radial velocity and photometric measurements, the Radial Velocity Experiment (RAVE; Steinmetz et al. 2006), over half a million spectra which allow velocity determination to $\sim$ 2 km/s, and the Sloan Extension for Galactic Understanding and Exploration (SEGUE; Yanny et al. 2009), which now contains over 300 000 spectral measurements of stars.

One reason that all of the above mentioned surveys have a spectroscopic component is that the kinematic structure of the disc is essential to understanding its nature. For example, the thick disc is found to have a systematically higher vertical velocity dispersion in its population than the thin disc. The events or processes which led to the kinematic heating of the thick disc are still up for debate, however two major categories exist: internal, secular processes such as radial migration (Sellwood & Binney 2002), and external events such as galaxy mergers (Quinn et al. 1993, Abadi et al. 2003). Quillen & Garnett (2001), using the 189 star sample of Edvardsson

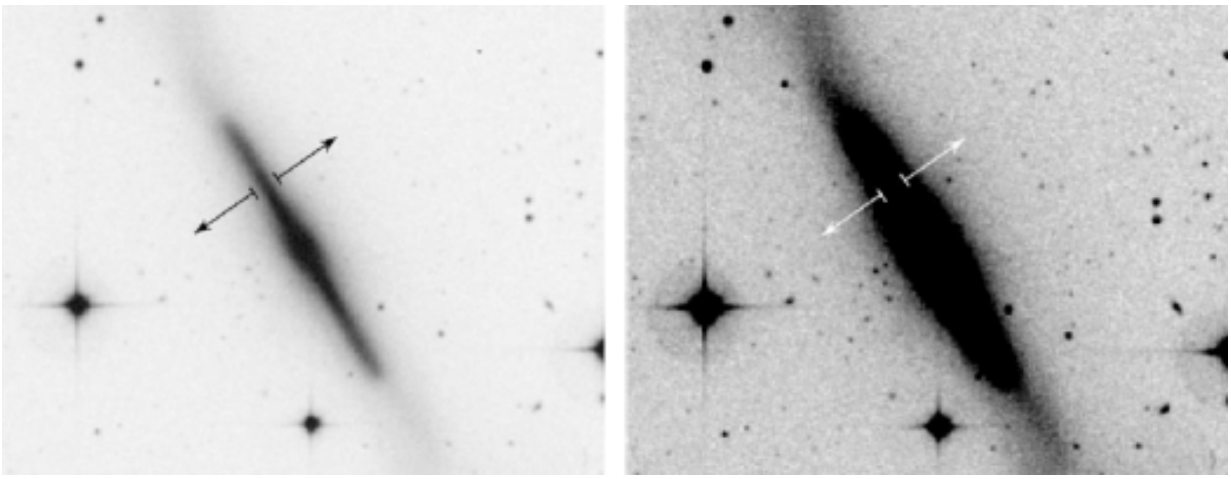

FIGURE 1.3: Shallow and deep images of an edge on galaxy illustrating the thin and thick discs and their scale lengths (Tsikoudi 1980).

et al. (1993) with updated parallaxes from Hipparcos (Perryman et al. 1997) and ages from Ng & Bertelli (1998), found a sharp break of roughly 20 km/s in the velocity dispersion of stars older than 9 Gyr, and little trend from then to the present epoch. This result argues heavily for a single ancient heating event such as in the merger scenario (e.g. Bekki & Freeman 2003), the infall of such a satellite giving a vertical kick to the stars of the present disc, after which new stars form in a new, the thin, disc. More recently, and with a much larger dataset, Nordström et al. (2004) found no such saturation exists in the disc heating, but rather a smooth monotonic signature with the exception of a slight increase in dispersion at $\sim$ 10 Gyr, which they note could be attributed to the thick disc. It is not clear if this result argues strictly against a merger event, but does require a mechanism supplying a constant source of heating, likely one amongst the secular variety. The Nordström et al. (2004) result probably represents the true relationship better than that of Quillen & Garnett (2001) due both to the higher quality of data and much larger, more statistically significant, sample size.

Merger History

This is not to suggest that mergers haven't been important in the history of the galaxy. Clever analyses of sky survey photometric catalogues, primarily from the Sloan Digital Sky Survey (SDSS; York et al. 2000), have revealed a rich population of faint dwarf galaxies and stellar streams in various states of dynamical interaction around the Milky Way (e.g. Irwin et al. 1990, Martin et al. 2004, Willman et al. 2005, Belokurov et al. 2006b,a, Zucker et al. 2006). Most

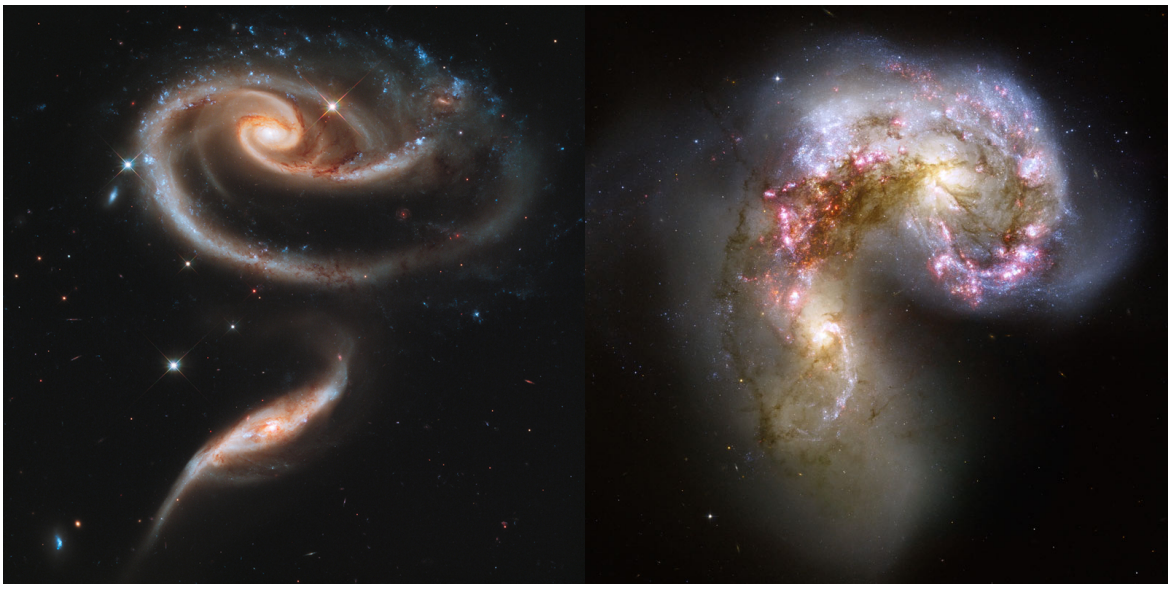

FIGURE 1.4: HST images of galaxies in different phases of interacting. The left hand image shows UGC 1810 and UGC 1813, both appearing tidally stretched from their gravitational interaction. The right hand image is the Antennae galaxies, a merger probably a few hundred million years in progress. Images from http://hubblesite.org.

notably, the Sagittarius dwarf spheroidal galaxy (Sag dSph), discovered by Ibata et al. (1994), appears to have made two passes over and through the Galactic plane, leaving a tidal tail of stars which will presumably eventually merge with the disc and halo populations (see also Hyde 2014). Sag dSph is a particularly remarkable example in our own Galaxy, but the plethora of other dwarfs, and the rich dwarf galaxy environment of our nearest large galaxy neighbour M31 (Martin et al. 2009, Richardson et al. 2011, Conn et al. 2013), imply merging is ongoing. Further, observations beyond the local environment reveal even larger scale mergers between spiral galaxies is a factor which cannot be ignored (for example, Figure 1.4 shows two examples of interacting galaxies as viewed by the Hubble Space Telescope).

Cosmological models, particularly in the current dark matter and dark energy paradigm (Λ CDM) have been considered highly successful at recovering the observed large scale structure of the universe, and generate galaxy halos that generally resemble those observed (see, e.g., the Aquarius Project simulations of Springel et al. 2008). Thus it has become widely accepted that the Milky Way was built up of at least several major mergers in its history, although the ERIS simulation (Guedes et al. 2011) does a remarkable job of mimicking the Galaxy and does so with only a comparatively moderate merger history. Observables of this are incredibly difficult to

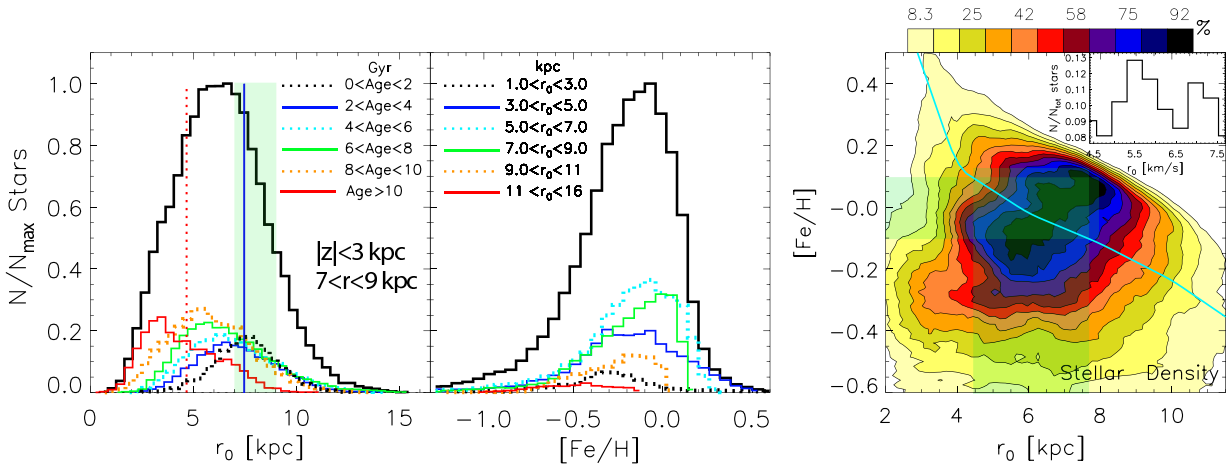

FIGURE 1.5: Results of simulations accounting for radial migration (Figure 3 of Minchev et al. 2013). The left and middle plots show birth radii probability distributions for stars in the Solar neighbourhood as a function of age and metallicity, respectively. The right hand plot is a reprojection of the middle plot also showing the possible birth radii of the sun (shaded cyan region).

decipher, but it is crucial to test this hypothesis with observations. The implications reverberate wider than simply testing the Milky Way's merger history; the modified Newtonian dynamics (MOND) paradigm offers an alternative explanation to the "missing mass" problem than dark matter, explaining flat rotation curves in galaxies, and, though it does not include cosmology per se, it certainly challenges the CDM description (see, e.g., the recent review by McGaugh 2014 and references therein). Such tests will also aid in sorting out these questions.

Stellar Migrations

Among the secular processes that may be occurring in the disc, stellar radial migration has been receiving a lot of attention in the literature from both theoretical and observational perspectives. Sellwood & Binney (2002) are widely regarded as the pioneers of the idea of stellar radial migration, which they referred to equally as churning. As its name suggests, radial migration involves stars moving inward and outward within the disc generally perpendicular to its rotational axis. It was proposed as a solution to the problem that, though the inter-stellar medium (ISM) of the Galaxy shows decreasing metallicity with radius (e.g. Luck et al. 2006, Boeche et al. 2013), stars in the local vicinity do not show a tight correlation between age and metallicity (see also Section 1.2.2).

It has been suggested that the outward movement of stars from the central portion of the disc heat in the vertical direction, in order to conserve angular momentum, and this may be sufficient

to explain the origin of the thick disc (Loebman et al. 2011). There is contention in the literature as to how efficient radial migration is, however; for example, the simulations of Minchev et al. (2012) show that flaring is not a significant effect and thus cannot explain the thick disc. However it is clear from the simulation context that stellar migration is an important consideration and may be able to explain observed metallicity gradients across the Galactic disc. Figure 1.5, taken from Minchev et al. (2013), is a nice illustration of radial migrations based on the latest simulations. The left hand panel shows the radius of origin of stars in the Solar region as a function of age, while the middle plot shows the metallicity of Solar neighbourhood stars as a function of birth radius. Significant overlap exists in distributions for both age and metallicity, lending to the difficulty in disentangling this process through observation. It is also evident from the left and middle panels that migrations occur in both directions (inward from the outer disc and outward from the inner disc). The right hand plot shows the metallicity density distribution for stars in the Solar neighbourhood as a function of radial origin. An interesting feature of the right hand plot is the cyan shaded region, which shows a region of possible birth radii for the Sun based on the models and an error of ± 1 dex in Fe.

A large portion of the recent work has been in the theoretical realm (e.g. Roškar et al. 2008b,a, Minchev et al. 2011, 2013). Haywood (2008) notably utilised stellar orbital information in the GCS in bins of metallicity to argue that radial migration could be observed in the orbital patterns of stars. The higher metallicity stars tend to have inward orbits while the lower metallicity stars had more outward orbits, which, assuming a relatively static ISM, would imply the metal rich component came from closer to the bulge while the metal poor component from the outskirts of the disc. Significant overlap between the two orbital populations in this study in particular, along with the uncertainty in assumptions of the ISM, mixing efficiencies and ages of stars, in general, make interpretation of the current observational evidence rather subjective. Until significant advances in observation, e.g. Gaia and its spectroscopic counterparts Gaia-ESO and GALAH, are upon us, it is clear the primary domain of stellar migration studies lies in theory.

1.2.2 Chemical Composition

The chemical composition and evolution of the Galaxy is a separate, but equally important, mechanism to the kinematic evolution. Remembering that, aside from Li in the Big Bang and an inconsequential amount in human-made accelerators, all metals in the universe (metals in astrophysics, of course, being any element heavier than He) have been created through the cyclic processes of stellar evolution and subsequent radioactive decay. Each such cycle will further

enrich the interstellar medium upon the death of a star, the resulting dust and gas contributing to the creation of a new cluster of Solar systems, many of which are likely harbouring planets (see, e.g., Kepler mission resources at http://www.nasa.gov/kepler). Hence, tracking the chemical enrichment over time and space can lead to an understanding of when and where star formation events have occurred, what types of stars were involved, and can shed light on the merger history of the Galaxy.

The relationship between metallicity and age, the age-metallicity relation (AMR), in the Galaxy is extremely important in testing theories not only of star formation, but also of galactic and cosmic evolution. Its measurement and understanding is a pinnacle of astrophysics, yet it remains elusive in a large part due to the difficulties in determining ages of stars. This has not stopped concerted efforts to model it, and significant progress in observing it. Galactic chemical evolution models generally predict a monotonic increase of the Fe abundance ([Fe/H]; see Section 3.2 for details on notation) of stars with age, where the oldest stars are metal poor, and youngest are metal rich as compared to the Sun (Rocha-Pinto et al. 2000, Feltzing et al. 2001, Nordström et al. 2004, Kobayashi et al. 2006, Haywood 2006, Soubiran et al. 2008, Roškar et al. 2008b, Casagrande et al. 2011, Minchev et al. 2013) . Figure 1.6 in the left hand panel shows an example of one such model, from Kobayashi et al. (2006). The right hand panel shows the observed AMR from the GCS for a large sample of stars. The large scatter places only weak constraints on models and bears little resemblance to the prediction in the left panel.

This example is a bit unfair. The model on the left does not account for uncertainties in observations and processes like radial migration or churning that would tend to induce scatter about the mean relation. Meanwhile, new techniques and calibrations have slightly improved the determinations of both age and metallicity for the same stars in the GCS sample (Casagrande et al. 2011). Recent modeling efforts combine analytic chemical evolution with N-body and/or smoothed particle hydrodynamics codes to arrive at a prediction of the true observable AMR taking into account mixing processes (e.g. Roškar et al. 2008b, Minchev et al. 2011). These combined have brought theory and observations substantially more in-line, yet it is still important to appreciate the inadequacy of stellar age calculations for individual field stars and how this may affect the observed AMR, which would in turn require the careful reconsideration of theory.

An important tracer of the thin and thick disc populations that has recently come to light is the position in the α-element versus Fe abundance plane. Fuhrmann (1998) was likely the first to identify the distinct sequences of thin and thick disc stars in such a diagram using Mg and Fe abundances, and kinematically identified disc membership. In this diagram, the thick disc stars inhabit the metal-poor (i.e., Fe poor) but α-rich portion of the diagram, while the thin

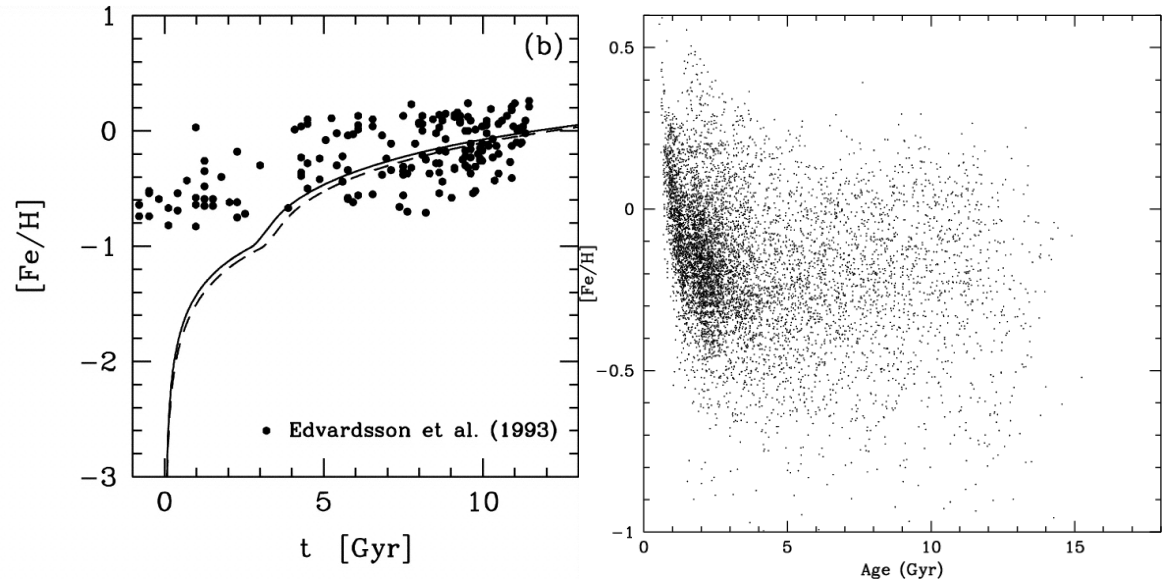

FIGURE 1.6: The age-metallicity relationship in theory and observation. The left hand panel shows a chemical evolution model realisation in the Solar neighbourhood of Kobayashi et al. (2006), where the solid line is the model and dots are observed values. The right hand panel shows the observed AMR from Nordström et al. (2004) for about 7500 stars with "well-defined" ages. Note the opposite sense of the horizontal axis: in the left panel t is the time from beginning of model, i.e. the youngest stars are to the right, while in the right panel the youngest stars are to the left.

disc stars inhabit the metal-rich but α-poor portion. There is overlap in both dimensions, but a notable gap between them along a diagonal ordinate. This empirical relationship has been further investigated and generally supported in the intervening years with larger samples of stars and high quality abundance measurements (e.g. Feltzing et al. 2003, Bensby et al. 2003, 2005, Reddy et al. 2003, 2006, Navarro et al. 2011). Figure 1.7, modified from Haywood et al. (2013), shows a sample of stars (taken from Adibekyan et al. 2012) in both the α abundance versus age and α versus metallicity planes. The stars were categorised by their position in the former plane, where thick disc stars are the oldest segment, but appear to separate well across the dividing line in the latter plane. Though its significance is not well studied, there appears to be a knee at the separating age, with a steeper slope for thick disk stars suggestive of a distinct evolutionary path for each component.

Most modern studies of the Galactic disc are in the context of the thin/thick dichotomy, but this need not be so. Many lines of evidence argue in favour of distinct components, but some contradict this picture; for example Bovy et al. (2012) used SEGUE survey data to argue that a single-component fit of "mono-abundance populations" (MAPs; groups of stars with similar

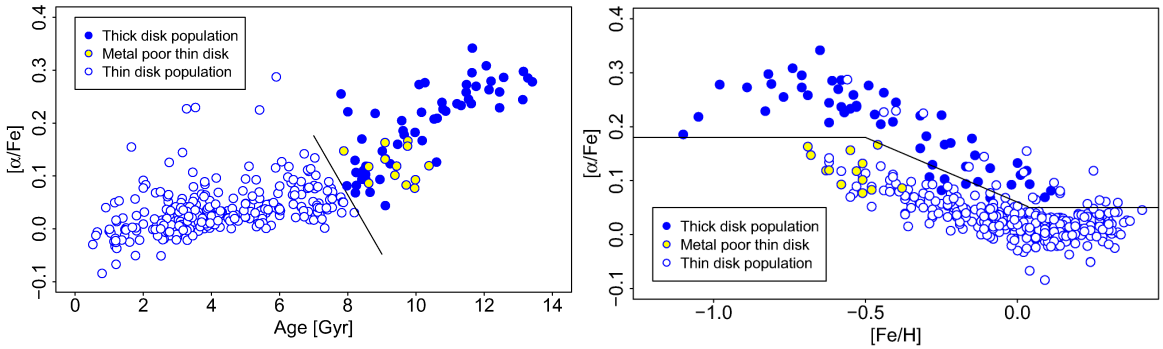

FIGURE 1.7: The α versus Fe abundance plane for stars of Haywood et al. (2013). The left panel shows the thin/thick dichotomy from an age perspective, while the right panel shows the abundance plane with an illustrative line marking the boundary between populations. Modified from Figure 8 of Haywood et al. (2013) to be landscape (from portrait).

abundances) describes the data well. They caution that improper accounting of survey selection functions can lead to inappropriate classifications such as the dual component disc. Rix & Bovy (2013) further warn of selection functions and again point to MAPs as a natural way to model the Galactic disc. Whether the disc is truly bi-modal, in that there is a clearly distinct evolutionary history for each part, or this bimodality is a product of observational bias, or merely comes from a human psychological predisposition to categorise everything, is a question for future history books. One thing for certain is that to pin this question down requires theory and observations to come in line with one another, necessitating advances in both fields.

1.3 Obstacles to Understanding the Galaxy

Though our picture of the current state of the Galaxy, and the distribution of its stars over space is fairly comprehensive, there exist many challenges in understanding how it evolved over cosmic time. The motion of stars at this epoch helps to understand the Galactic potential and identify populations of stars in bound associations. Field stars in the disc, which account for a majority of Galactic stars have, however, been subject to dynamical processes which make their kinematic properties short-lived and thus are of little use in trying to unravel their origin.

The chemical patterns in the disc – the radial metallicity gradients and age-metallicity relationship, for example – require an understanding of the dynamical evolution to explain them, which is still an ongoing mission in astrophysical theory. It may be possible to overcome this

seemingly degenerate problem by means of a simple fact: the photospheric abundances of element species in most stars are not modified while they are on the main sequence and lower giant branches. Unlike the kinematic properties of stars, this chemical information is a *fossil* record of the epoch of formation.

In the next chapter and remainder of this thesis, we introduce and discuss the concept of "Chemical Tagging", which aims to leverage the fossil nature of chemical abundance patterns in stars to trace back their origin. The technique has a great deal of promise for making the next leap in understanding the Galaxy, much like the advent of the CCD detector enabled sky surveys such as SDSS, which allowed great headway to be made in mapping the distribution of stars and unveiling dwarf galaxies and streams. Moreover, it has the possibility of improving age determinations for stars, which is critical for studies of evolution but remains a difficult problem for field stars. Finally, identifying the birth cluster of the Sun is a compelling problem which also may be tackled through chemical tagging.

Chapter 2

Chemical Tagging

To circumvent some of the complications in studying the Galaxy noted in the previous chapter, astronomers are beginning to turn to a technique called "chemical tagging", which postulates that field stars can be linked to one-another as having been created from the same molecular cloud (conatal), based solely on their unique abundance patterns. The concept of chemical tagging, in the present sense, was introduced by Freeman & Bland-Hawthorn (2002). They noted that much progress had been made in the decades prior on understanding the Galaxy, but that significant issues like stellar mixing, preventing construction of reliable time-lines, require a fossil record that can only come from studying the chemical patterns of stars. A fantastic suggestion that was based loosely on theory, is now the goal of a very large observational undertaking, motivating the commissioning of an entirely new instrument. In this chapter we detail the arguments that form the basis for chemical tagging, the tests that have been done prior to this thesis, and provide some details of the instrument and survey that motivate this work.

2.1 The Formation and Enrichment of Star Clusters

A star is a complicated physical object with a strikingly simple origin: a cloud of gas and dust collapses under its own gravity, becoming dense enough to ignite nuclear reactions in its core, from whence begins a delicately balanced dance of inward and outward forces in dynamical equilibrium. It is an often accepted tenet of modern astrophysics that stars do not form alone, but in dense clusters of gas and dust, termed molecular clouds. These structures then typically dissolve on timescales much shorter than the lifetime of the low mass stellar population ($\sim$ 100 Myr), contributing to the stellar field population (Janes et al. 1988, Lada & Lada 2003). Open

clusters are an interesting exception to the rule, though young and intermediate aged clusters such as the Hyades may represent the tail end of the disruption lifetime, as there are significant numbers that date back to early epochs of the galaxy (Phelps et al. 1994, Liu & Chaboyer 2000, Bragaglia et al. 2008a, Sestito et al. 2008a, Randich et al. 2009). The process occurs deeply embedded in dust, which obscures observation, and at scales that make resolving individual proto-stars difficult; however infrared and millimeter wavelength studies have been able to probe the environment of nearby molecular clouds such as the Orion Trapezium complex to show that this scenario is acceptable (see, e.g., Muench et al. 2008 and references therein). We must note, though, that the current epoch of star formation may not be representative of those past, and for many purposes open clusters are considered to represent typical star formation clusters yet are, by the numbers, almost certainly not typical.

The low mass stars (close to, or below, Solar mass) of a star forming cluster will not contribute further to the enrichment of stars at the current epoch, since their lifetimes are long compared to the cluster disruption time (and the age of the Universe itself) and their mass loss on the main sequence is negligible. High mass stars on the other hand have short main sequence lifetimes, stellar winds of O-stars will enrich the inter-stellar environment even on their main sequence through significant mass loss, and their post-main sequence processes and deaths generate the most metals available to a new generation of stars. Individual high mass stars will result in a supernova, which itself is a powerful nuclear processing engine but importantly also provides a mechanism to eject large amounts of enriched material to form a new molecular cloud. We discuss some of the specifics of nuclear processing in stars in the next section.

It is this cyclic process that results in the chemical enrichment of the Galaxy, and given that the precise conditions for formation of the high mass stars in any given molecular cloud must be stochastic (McKee & Tan 2002), this also means that each subsequent cloud should have a unique pattern of metal abundances. Assuming that within a molecular cloud, ejecta from all contributing sources are well mixed, all stars formed within will share the unique chemical pattern. This is the hypothesis behind chemical tagging, and tests on several open clusters confirms that measured abundances of member stars are indeed the same to within the measurement uncertainties (see 2.3 below).

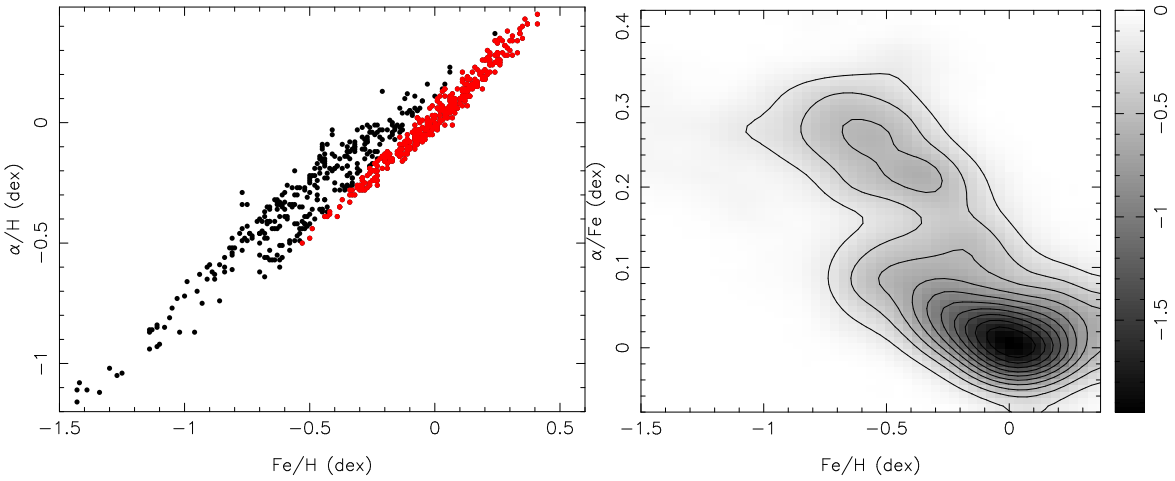

FIGURE 2.1: The α-Fe abundance plane for Hipparcos stars within 150 pc of the Sun. The left hand panel shows the individual abundances where the thin disc population is highlighted in red. The break is visible in this figure but not exceedingly obvious. A clever re-projection using α/Fe on the vertical axis (right hand panel) shows a much clearer separation between the populations, here accentuated by the histogram representation. The red points were selected from this right hand plot as those in the lower right lobe.

2.2 The Multi-Dimensional Chemical Space

Freeman & Bland-Hawthorn (2002) termed the parameter space making up the patterns of abundances "$\mathcal{C}$-space". The number of true independent dimensions that make up this space is important to the success of practical experiments. As an example, consider the α-Fe abundance plane as a tracer of thin and thick disc stars pictured in Figure 2.1. The diagonal shape of the lobes representing each population means that a projection in either axis results in a reduction of information. Considering only Fe, for example, there is a regime where few thick disc stars exist, but that region comprises only a fraction of all thin disc stars. The additional dimension introduced here unveils important information, even though the distribution of stars in this space clearly shows both dimensions are not independent.

The example extends to chemical tagging where the scale to which we attempt to identify structure is significantly smaller, meaning that a higher dimensionality of $\mathcal{C}$-space is also necessary. It must be noted, however, that increasing the measured dimensions of $\mathcal{C}$-space does not simply correspond to measuring more elements. Many groups of elements are generated in the same processes in stars (Wallerstein et al. 1997), for example the iron-peak elements Fe, Ni, Cr, Mn, Zn are generated in type Ia supernovae (SNe Ia), or the α-elements Ti, Ca, Mg, Si, and O, which are built up by successive capture of α particles in core collapse supernovae (SN II), and

are also likely responsible for synthesis of the rapid neutron capture (r-process) elements, Eu being the most commonly measured (Kratz et al. 2007). The slow neutron capture (s-process) elements such as Ba, Y, La, and Nd are generated during the asymptotic giant branch (AGB) phase (Busso et al. 1999, Karakas & Lattanzio 2007)[1]. Though their abundances will not be identical to one another because of differing nucleosynthetic requirements, they will evolve more or less in lock-step, implying that there may not be much information gained by measuring multiple elements in a single group. Ting et al. (2012) did a comprehensive principle component analysis (PCA) on abundance patterns of several stellar groups in order to identify the true underlying dimensionality of $\mathcal{C}$-space, and what elements (or linear combinations of elements) make up those dimensions. PCA involves re-projecting natural dimensions onto sets of orthogonal eigenvectors, each of which is some linear combination of the natural dimensions. The contribution of total variance of each eigenvector (principle component) can be computed. The components making up most ($> 90\%$) of the variance then gives the true underlying dimensionality. In the Ting et al. (2012) analysis, the open cluster sample with 13 distinct element abundances measured could be described (90%) by between 6 and 9 separate dimensions, depending on the assumed measurement uncertainties. This of course implies that the evolution of several species of the 13 elements is interdependent.

A factor further complicating the $\mathcal{C}$-space is that its dimensionality is not static. Bland-Hawthorn et al. (2010a) describe a chemical evolution model accounting specifically for star clusters based on an assumed initial cluster mass function (ICMF). Figure 2.2 shows the results of their model for r-process elements as a function of [Fe/H] abundance (a generational indicator) for two values of the ICMF slope parameter γ, and two assumptions of intrinsic abundance scatter. Also shown is a simulation using a less sophisticated closed-box evolution model but over a wide range in [Fe/H] for [Eu/Fe] abundance scatter evolution from Bland-Hawthorn & Freeman (2004a). In all simulations clustering is clear particularly at low metallicities, but becomes significantly more homogeneous even by [Fe/H] of -2 dex, which is rare in the Galactic disc, even the lower metallicity thick disc (see, e.g., Schlesinger et al. 2012). One interpretation of this figure is that the clustering signature is easily detected with only a single dimension (e.g. the r-process element in the left panel of figure 2.2) at very low metallicities, but, if detectable, requires more dimensions as the scatter narrows in the one dimension.

[1] Some neutron capture elements, including Ba, may be generated through both the s-, and r-processes depending on the environment (M/H, for example).

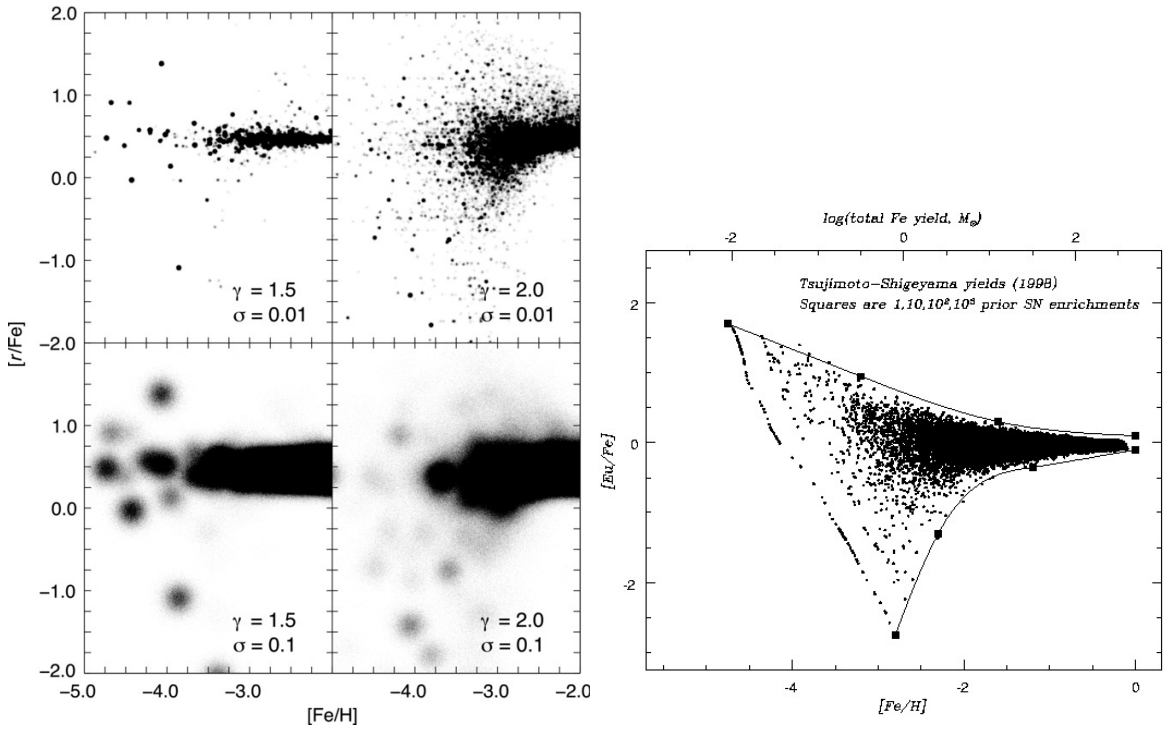

FIGURE 2.2: Clustering chemical evolution models. The left panel shows r-process scatter as a function of [Fe/H] where top and bottom sub-panels are intrinsic cluster internal abundance scatters of 0.01 and 0.1 dex, respectively, and left and right sub-panels assume different ICMFs (Figure 9 of Bland-Hawthorn et al. 2010a). The right panel shows Eu abundance scatter as a function of [Fe/H] up to Solar metallicity (Figure 1 of Bland-Hawthorn & Freeman 2004a).

2.3 Tests of Chemical Tagging

In the intervening years since chemical tagging was proposed in Freeman & Bland-Hawthorn (2002), several studies have sought observational support of the presupposition that abundance patterns of conatal stars are homogeneous. The most obvious candidates to test against are open clusters, since these objects probably represent precursors to most stars in the Galaxy not presently in associations – in other words, field stars are likely to be from evaporated open cluster-like star formation events. Moving groups have also been tested in the literature, where chemical tagging has been utilised to distinguish between either a purely dynamical origin or a disrupted star cluster. Finally, the technique has been used on small scales as an association membership test. In this section, we describe some of these tests.

An important early test in this vein was performed on the well studied intermediate-age Hyades open cluster in De Silva et al. (2006). The Hyades is a particularly good lab for this

type of study because its proximity enables high quality observations and abundance determinations, and the membership criteria are well established. De Silva et al. (2006) specifically targeted heavy elements in the s-, and r-process elements (Zr, Ba, La, Ce, and Nd) for the same reasons outlined above, and estimated the intrinsic scatter (taking into account the uncertainties in observations and analysis) in all cases to be below 0.05 dex and most cases below 0.02 dex for a sample of $\sim$ 50 stars. This wasn't the first study to establish chemical homogeneity in cluster environments; earlier work by Friel et al. (2003), Schuler et al. (2003), Tautvaišiene et al. (2000a) and Gonzalez & Wallerstein (2000a) established homogeneity in elemental abundances in Collinder 261, M61, M34 and M11, respectively, however the number of stars in those studies was more limited, being between 4 and 9 stars per cluster.

Moving groups (e.g., Eggen 1963 and other publications by the same author in the same decade) are another important lab for testing chemical tagging. These are associations of stars that have some common motion but may be rather loosely associated in spatial coordinates; they may be actively dispersing open cluster-like structures, the chemical homogeneity of which would tend to confirm the premise of chemical tagging field stars. De Silva et al. (2007b) studied a sample of stars in the HR1614 moving group in a wide variety of elements including Na, Mg, Al, Si, Ca, Mn, Fe, Ni, Zr, Ba, Ce, Nd, and Eu. They concluded that, apart from four stars that were probable non-members or background contamination, the remaining 14 stars had an 80% probability of having intrinsic abundance variations on average 0.03 dex and no more than 0.08 dex.

Though not strictly tests of chemical tagging, several studies have used the concepts of chemical tagging to determine association of stars to nearby clusters. For example, in De Silva et al. (2011) and Tabernero et al. (2012), abundances were used to probe membership of stars thought to be associated with the Hyades supercluster association, finding four stars that are chemically and kinematically consistent with having originated from an early Hyades star formation event in the first case, and expanding on that in the second case, 28 stars were found to be consistent with the core Hyades open cluster. A stream in the same vicinity as the Hyades cluster has also been thought to be associated with the star formation events of the Hyades cluster, however Pompéia et al. (2011) did a chemical analysis on a sample of stream stars, finding that only a small fraction ($\sim$ 10%) could have formed in the Hyades, and the more likely origin of the stream is an orbital resonance. The Argus association, an unbound group of spatially concentrated stars, was chemically tagged to a probable origin in the open cluster IC 2391 by De Silva et al. (2013). Utilising chemical tagging in the opposite sense, Carretta et al. (2012) claimed that chemical information for stars of open cluster NGC 6752 points to several distinct populations – a result

that has been well studied in globular clusters in recent years, but not before in open clusters. The positive results from these studies give support to the idea of chemical tagging the Galaxy at larger scales.

2.4 HERMES and GALAH

An exciting new development since the Freeman & Bland-Hawthorn (2002) review, and a substantial motivation for the present work, is the new High Efficiency and Resolution Multi-Element Spectrograph (HERMES) for the Anglo-Australian Telescope (AAT). The four camera fibre fed spectrograph was installed and tested on site during October-December 2013, with commissioning observations delivering results within, and sometimes exceeding, the design specifications. In this section we give a brief description of the instrument itself (detailed descriptions can be found in Barden et al. 2010, Heijmans et al. 2012), why it is an important tool for galactic archaeology, and describe the chemical tagging survey planned for the coming years which will utilise it, the Galactic Archaeology with HERMES (GALAH) survey.

2.4.1 The HERMES Instrument

The HERMES camera setup and light path schematic are shown in Figure 2.3. The four cameras target four separate narrow spectral regions: Blue, from 4718 to 4903 Å; Green, from 5649 to 5873 Å; Red, from 6481 to 6739 Å; and Infra-Red, from 7590 to 7890 Å. The fibre slit provides a nominal resolution of R=28,000, with a slit mask providing an additional R=50,000 mode. Each of the cameras is equipped with a 4096x4096 pixel Charge-Coupled Device (CCD) detector which can image up to 392 spectra from the incoming fibres of the 2-degree field (2dF) robotic positioner.

The four narrow spectral regions were chosen specifically with the goals of chemical tagging in mind, though the range of elements is well suited for any chemo-dynamic stellar study. The bottom panel of Figure 2.3 illustrates the spectral bands and the elements that each was designed to target. Figure 2.4 is a Solar spectrum taken with HERMES during commissioning observations in all four channels, showing excellent performance over the entire range.

In spite of the positive results thus far obtained with HERMES, as with any technology developed on the cutting edge, there are some mysterious issues with the instrument. Glass in the gratings of the Blue, Green, and Red arms appears to be radioactive, causing unusual cosmic

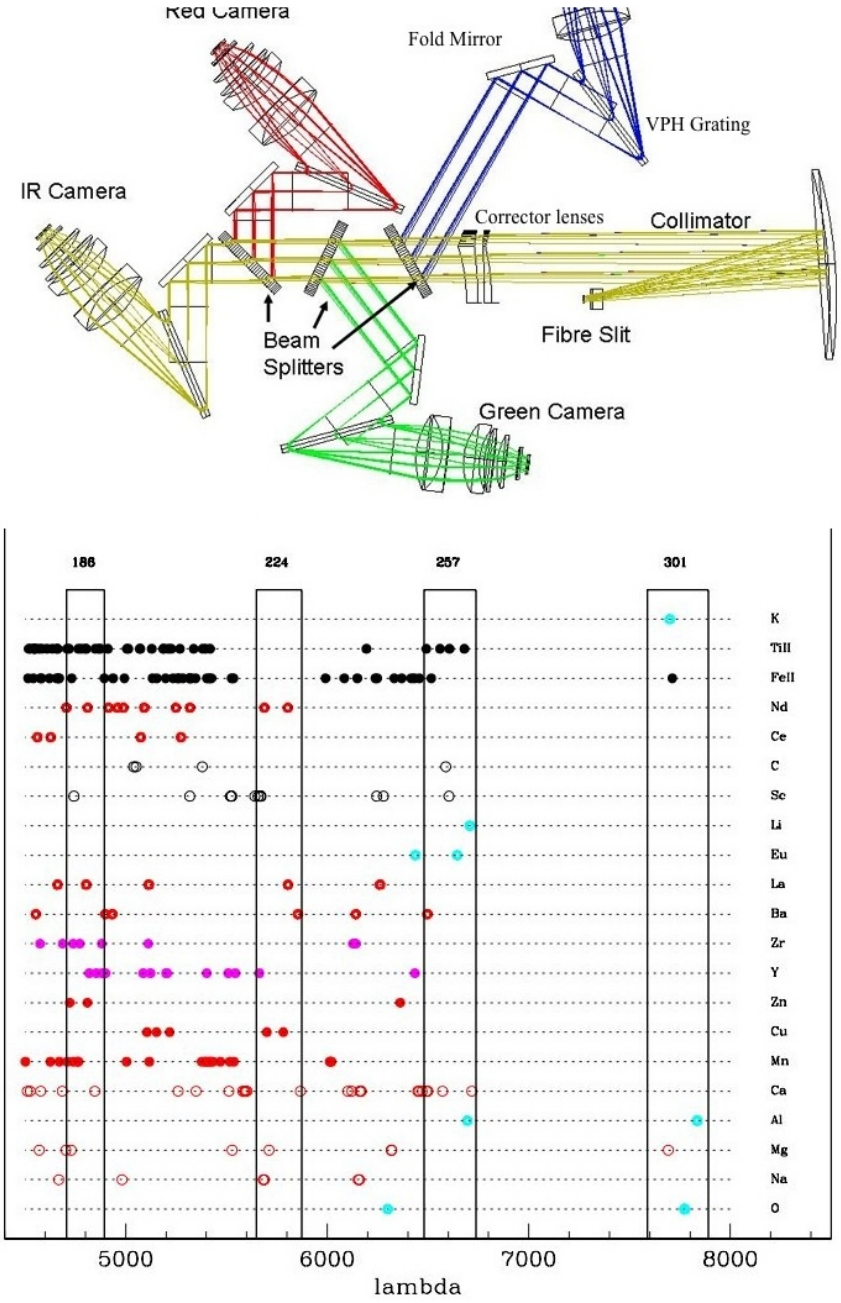

FIGURE 2.3: The top panel shows the HERMES light path from the fibre slit to each of the four cameras. The size of the instrument is about 4m from the collimator mirror at right to the IR camera at left. The bottom panel shows the four spectral bands as boxed regions along with particular lines of species they were designed to target.

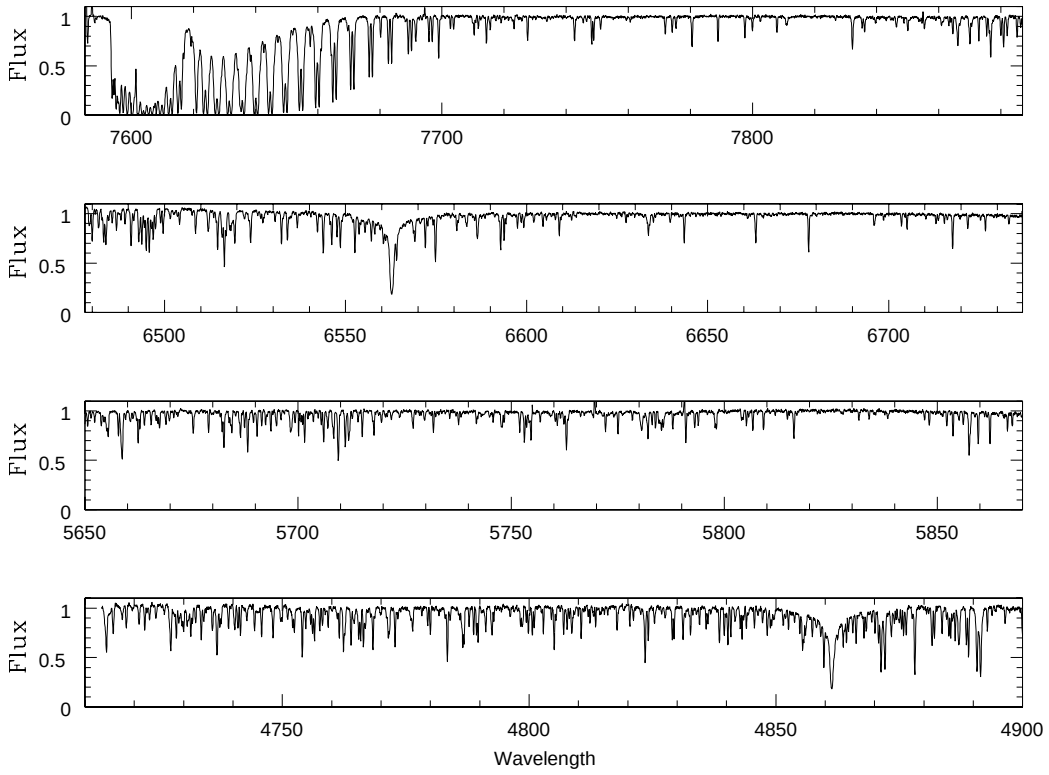

FIGURE 2.4: Solar spectrum in all four HERMES bands. From top to bottom these are the Infra-red, Red, Green and Blue channels.

ray-like events which saturate pixels and leave a "streak" on CCD readout, which may be incident on spectral features in one or more fibres. In subsequent frames, for some time, the hot pixels appear to bleed toward the readout amplifier. It is yet unclear if this phenomenon has a significant ill effect on the measurement of absorption features in affected spectra. Another issue is a light-leak in the Green camera, coming from a warning LED situated inside the instrument which fails to switch off. A procedure is known to fix this issue, but at the expense of a lost frame, until a more permanent solution is implemented. Nevertheless, the instrument is now in facility mode and producing usable results, we look forward to a flood of interesting investigations using HERMES in the near future. More details on the instrument and facility can be found on the Internet site: http://www.aao.gov.au/science/instruments/current/HERMES.

2.4.2 The GALAH Survey

Given the specific design goals of the HERMES instrument, it should be no surprise that a survey of the size and scope of GALAH would be planned for its use. GALAH (described in detail in Freeman et al. 2014) will obtain spectra of 1 million stars mostly in the Galactic discs between magnitudes of about 12-14 in the V-band, in the R=28,000 mode. This is orders of magnitude larger in size than current inventories of high-resolution stellar spectra; homogeneous high level products (e.g., stellar parameters, abundances, radial velocities, etc.) will be made publicly available, yielding a truly rich and revolutionary catalog that will likely enable major advances in the field of Galactic archaeology, even without the planned chemical tagging component.

An important goal and planning factor of the survey is to achieve a S/N of 100 per resolution element, which simulations have shown should be sufficient to obtain random errors on abundance determinations nominally to 0.05 dex (for [Fe/H]). This translates to 1 hour exposures for a 14^{th} magnitude star, allowing sufficient time to fully configure the fibre positions for the next field while observing, at the same time enabling the million star target to be achieved in a reasonable time-frame ($\sim$ 5 years). One hallmark of the GALAH design is to minimise any selection bias by creating as simple a selection function as possible. This is done by restricting the selection criteria to obtaining full fields that are not overly crowded, and keeping field configurations within a set magnitude range to limit the ill-effects of cross-talk. In the end, there are 6546 potential fields of which 3300 must randomly be observed – in order to achieve a million star minimally biased survey – as illustrated in grey circles in Figure 2.5.

At the time of writing this thesis, the GALAH pilot survey program has been completed, and several of the main survey fields have been observed, after a successful large program application to the Australian Time Assignment Committee (ATAC). Figure 2.5 shows the fields observed thus far for pilot and main survey programs. The progress indicates several survey components are on track including the observation planning component "ObsManager" and the target input catalog. There are still areas needing attention including improving the reliability and automation of the abundance analysis pipeline "Theremin", and fine tuning the data reduction system for the HERMES instrument, in addition to some of the instrument challenges mentioned above.

The abundance analysis pipeline is at the core of GALAH's mission of chemical tagging, but has a difficult task; one which at present humans still tend to do better at than modern microcomputers. The next chapter introduces stellar spectroscopy and high resolution abundance analysis.

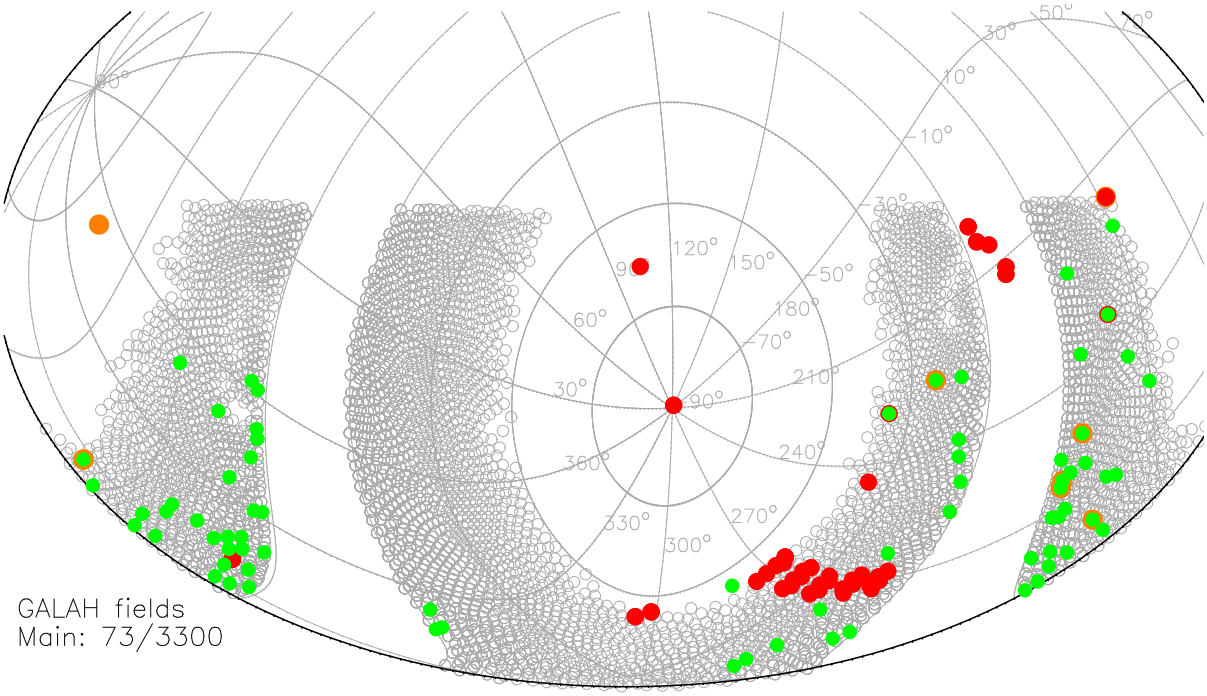

FIGURE 2.5: Planned and observed GALAH fields (as at 29 April, 2014). Each field is at least dense enough to approximately fill all $\sim$ 400 fibres. Green symbols are completed survey fields, red are pilot survey fields and orange are commissioning test data fields. Plot is shown in celestial coordinates with Galactic latitude and longitude grid overlayed.

Chapter 3

Stellar Spectroscopy and Abundance Analysis

At the heart of our quest to understand the chemical enrichment history of the Galaxy, and a fundamental requirement for chemical tagging, is elemental abundance analysis from stellar spectra. What may appear at first glance to be a relatively innocuous task, is in fact incredibly tricky business – where even seasoned experts in the field will disagree, to a significant degree, with one another over the results derived from the same spectrum. The challenge is compounded when facing the necessity to automatically compute abundances for large samples of stars, as is the case for the Gaia-ESO and GALAH surveys, the details of which are, at the time of writing this thesis, still very much in their infancy. This chapter presents a brief introduction to the field of spectroscopic abundance analysis, finishing with the first journal publication in this thesis.

3.1 Spectra of Stars

Stellar spectroscopy begins with splitting incoming starlight, typically using diffraction gratings such as slit-type, surface relief, echelle, or volume phase holographic (VPH), as is the case in HERMES. Noting that the angle of reflectance or diffraction of incident light is wavelength dependent, with a carefully designed detector placed in the path of the diffracted light we can obtain a map of intensity versus wavelength, which is, of course, a spectrum. Figure 3.1 top panel shows a particularly high quality spectrum of a Hyades target, HIP 20082, observed with the recently commissioned HERMES instrument.

The spectra in Figure 3.1 are normalised with respect to the continuum, or the bulk white light

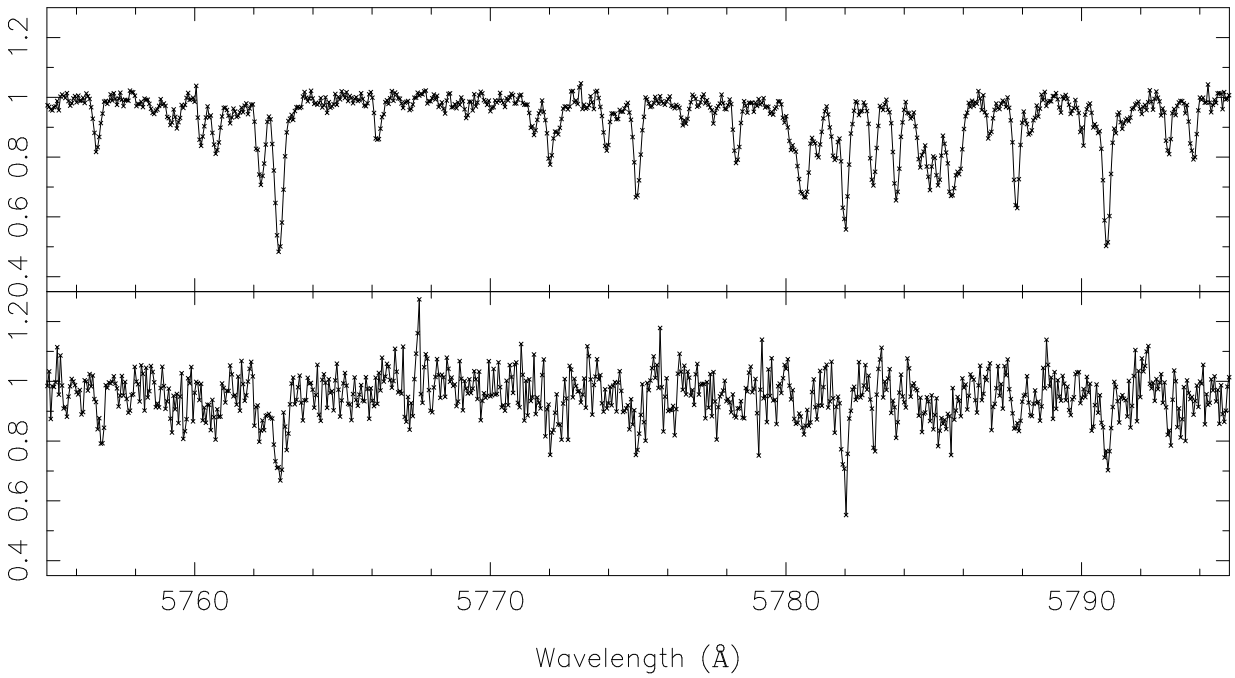

FIGURE 3.1: Slices of example spectra observed with the green arm of the HERMES spectrograph. The top panel shows HIP 20082 with a S/N of approximately 80, while the bottom panel shows 47 Tuc star S-962, having a S/N ratio of close to 20 per resolution element. Both spectra are normalised to have continuum at 1, making the Y-axis unit-less.

emitted from the base of the star's photosphere. The lower intensity dips are absorption features caused by the absorption of white light continuum photons by electron transitions from lower to excited states in a particular atom. Similar absorption features can be seen in a different view in Figure 3.2, right hand panel, which beautifully shows a wide band visible wavelength spectrum of the Sun in the imaging plane, with dark features being absorption lines. Due to the quantum mechanical nature of electron transitions in bound states, each unique transition in a given atom (in a given ionization state) absorbs a photon at a very specific energy (equivalently a specific wavelength) equal to the difference in potential energy between the lower and excited states. Figure 3.2, left panel, shows an energy level diagram depicting specific electron transitions for Ca II (that is, singly ionised Ca). The wavelength and energy at which these transitions occur is precisely calculated from quantum mechanics and can be measured with high accuracy in the lab. The probability of excitation and spontaneous re-emission is an important factor that can also be measured in the lab. Armed with an appropriate stellar model, astrophysicists convert measurements of the strength of individual absorption features into an abundance of that element.

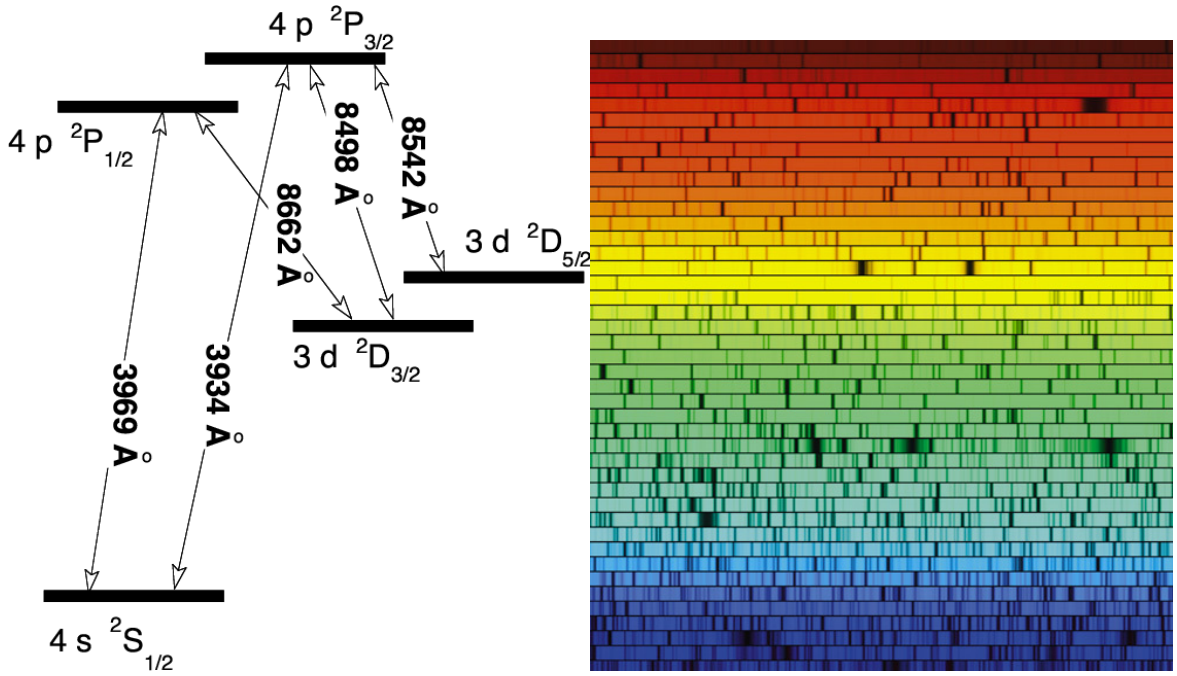

FIGURE 3.2: Grotrian diagram of the electron transitions for Ca II, showing the wavelength in angstroms where the H and K and IR triplet line transitions occur (Figure 5 of Derouich et al. 2007). The right hand panel shows a large number of absorption features in the Solar spectrum in the visible wavelengths.

This incredibly simple task (that was a joke!) is discussed in slightly more detail in the next section.

The spectra in Figure 3.1 were obtained with HERMES using the R=28,000 resolution mode, where resolution, R, is defined as

$$R = \frac{\lambda}{\delta\lambda}$$

and is one of the fundamental properties of spectrometer configurations. Higher resolution allows for the detection of separate close features and is a requirement for detailed abundance analysis, with a large portion of such literature data being taken at R=20,000 or above. Low resolution modes serve an important purpose, though, due to the fact that higher resolution necessarily comes at some cost; in the case of HERMES, which has an additional R=50,000 mode, this cost is roughly $\sim 50\%$ reduction in throughput, precluding the ability to reliably measure fainter stars.

Figure 3.1 shows another stellar spectrum, one of a 47 Tuc member star, at the same resolution

as the top panel, but clearly of lower quality. Matching features can be seen in the two examples, but in the bottom panel the centroids of absorption features in many cases are ambiguous and it is difficult to distinguish weak features from the noise. The difference in quality of these two examples is related to another fundamental quantity of observed spectra: Signal to Noise ratio (S/N), which, as its name suggests, is a measure of the amount of intrinsic signal that is present relative to the underlying noise. Looking at these examples it is easy to recognize that measuring any quantity from the low S/N spectrum is not as reliable as measuring the same in the high S/N spectrum. Though low S/N spectra can produce high quality radial velocity and rough metallicity estimates, S/N is a key factor in abundance analysis and likewise a driver for the design goals and specifications of instruments and surveys aimed at abundance analysis.

3.2 Elemental Abundance Analysis

The dependence of the shape of spectral lines on temperature, optical depth, pressure, etc. generally precludes making direct comparisons between spectral features in different stars. This of course means that we cannot compare some star's spectrum to that of the Sun, whose abundances we assume are known, and derive its abundances. We instead must use some model of the star, based on theoretical calculations, that describes the physical conditions in its atmosphere, and follow the spectral line dependencies to arrive at the observed line shape.

Before moving on, it is important to briefly introduce the notation that is ubiquitous in stellar abundance studies. Absolute abundances, ϵ(X), are expressed as number densities on a logarithmic scale and made relative to Hydrogen, which arbitrarily has an abundance of 12:

$$\epsilon(X) = log_{10}(\frac{N_X}{N_H}) + 12$$

Most commonly in the literature, abundances are given relative to Solar values, which either are assumed to be known from meteoritic sources (e.g. Anders & Grevesse 1989, Asplund et al. 2009), or analysed from a Solar spectrum captured with the same instrument as program stars. The notation is as follows, where the X is the element species, H is Hydrogen abundance and the square brackets specifically refer to the comparison to Solar values:

$$[X/H] = log_{10}(\frac{N_X}{N_H})_\star - log_{10}(\frac{N_X}{N_H})_\odot$$

Commonly [X/Fe] is also used:

$$[X/Fe] = [X/H] - [Fe/H]$$

Though many different models exist describing stellar photospheres, the most commonly used today are 1-D plane-parallel models under the condition of local thermodynamic equilibrium (LTE). The plane-parallel treatment and LTE are simplifications that make the radiative transfer calculations treatable analytically, but are generally considered appropriate for stars of F, G and K type on the main sequence, turn-off and lower giant branches. The models tabulate at least the source flux and pressure at layers of differing opacity in the stellar photosphere, which can be used to calculate the radiation transfer and thus the absorption profile for a given line to be compared to an observed spectrum.

Two methods exist to estimate the abundance of an element from an observed spectrum: equivalent width (EW) measurement and spectrum synthesis. The former can be done simply and quickly for many lines in a spectrum where the level of blending with neighbouring features is minimal. Equivalent width is a measure of the strength of an absorption feature and is defined as length (in wavelength scale, typically Angstroms) of one side of a box with height one that has the same area as that of the line in a normalised spectrum. See Figure 3.3 for a graphical representation of the definition of equivalent width. When a line is deeply embedded in a forest of other lines, a synthetic spectrum is calculated from the model, considering the contribution from as many lines as possible in the region surrounding the line of interest. Spectrum synthesis is complicated partly due to the necessity of knowing the abundances for all species in the vicinity other than the one being estimated, in addition to the added computational costs. Both methods require a model of the stellar continuum emission in order to consider only absorption from the line itself. Deep wings of strong lines, complicated detector response, and spurious emission spikes (e.g., due to cosmic rays) all make estimating the continuum difficult. Typically polynomials or base-splines are used, which do not account for the physics of the continuum and thus can be problematic.

Automated analyses, especially in cases where quality checking by human eye is impractical, can be particularly error prone for these reasons. Non-physical continuum fitting is an exercise in pattern recognition. The human brain is a sophisticated machine for such tasks, while microcomputers still lag behind. For example, local continuum during automated line fitting is sometimes over- or under-fit because the computer cannot decide if continuum regions used in the fit were appropriate, resulting in non-systematic errors in line strength measurements. The problem is often exacerbated in low S/N situations. As a result, automated codes often have to be specifically tailored to instrument configuration and must be equipped with detailed knowledge of the

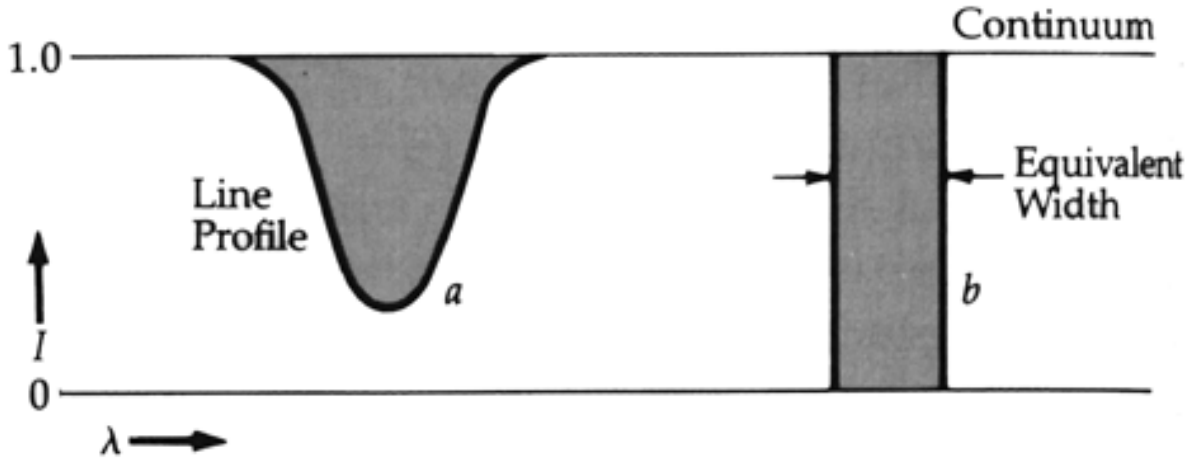

FIGURE 3.3: Graphical representation of the definition of equivalent width. The shaded grey regions *a* and *b* have the same area. The spectrum is normalised so that continuum emission is at unity. Taken from http://ircamera.as.arizona.edu/astr_250/Lectures/Lecture_15.htm.

environment of lines being studied, and may not perform well for all stellar types.

Individual stellar models are computed for stars of specific effective temperature, surface gravity and metallicity. When these quantities are not previously known or estimated (which is most often the case), they are most commonly determined via a trial and error test of a range of stellar models. In this technique, commonly referred to as ionization equalization, each trial is attempting to find the model which yields the same abundance for all measured lines of Fe I and Fe II (though in some cases also Ti I and Ti II are used). Due to the scatter of measurement induced uncertainties in the abundance estimate for each line, the balance of abundances is achieved not through requiring equality, but through minimisation of trends with line Excitation Potential (E.P.), reduced equivalent width (EW/λ), and wavelength. Each of these is important for their sensitivity to different model input parameters.

Once these parameters are estimated, by minimisation of the line slope in the trends listed above, either by eye or by machine, a likely suitable stellar model has been selected. For equivalent width abundance analysis, it is now a matter of computing curves of growth for individual lines and matching the measured EW to the abundance at that EW in the curve. For spectrum synthesis analysis, the model is used to compute several possible line profiles based on varying abundances and minimising the difference between that and the observed spectrum. An important step prior to either of these types of analysis is to compensate for the motion of the subject star relative to Earth (termed radial velocity), which will either shift line positions toward longer

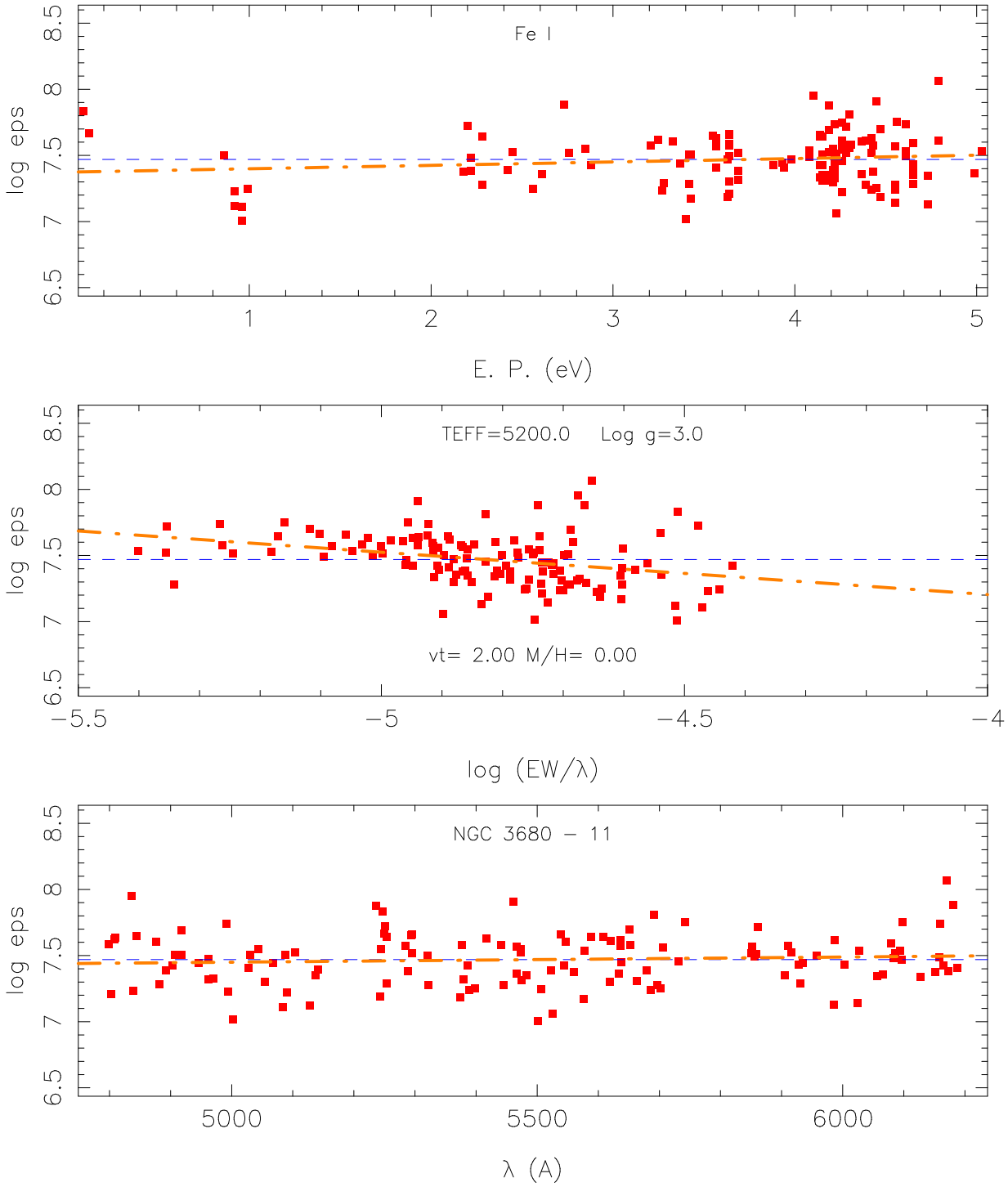

FIGURE 3.4: MOOG view of ionization equalization panel for determining stellar parameters log g, $T_{\rm eff}$, microturbulence and Fe/H, for a program star from Mitschang et al. (2012).

(receding motion) or shorter (advancing motion) wavelengths by means of the Doppler effect. Compensation can be achieved simply by identifying an ensemble of "clean" lines with known laboratory wavelengths and shifting the spectral wavelength scale to best match all lines. Another common method is to obtain a differential velocity by cross-correlating the observed spectrum with a suitable template spectrum (synthetic or observed).

One of the most popular software packages for performing abundance analysis calculations is MOOG, named after the early analog music synthesizers (for its spectrum synthesis component) (Sneden 1973). Figure 3.4 shows part of a MOOG session for determining basic stellar parameters. In each panel the red points are EW measurements of Fe I lines from a normalised spectrum; the text in the middle panel indicates the loaded model is one with an effective temperature ($T_{\rm eff}$) of 5200 K, surface gravity (log g) of 3.0 and microturbulent velocity of 2.00. A trend is clearly present in the reduced equivalent width plot, this being the starting point for analysis. New model parameters would be set (in this particular case microturbulent velocity would be adjusted first), and resulting trends re-examined until minimised in all quantities.

Different quantities with respect to abundance are particularly sensitive to different parameters. The top panel is line excitation potential versus abundance, which probes $T_{\rm eff}$. The middle panel is reduced equivalent width versus abundance and is a particularly good probe of microturbulent velocity. The bottom panel serves to ensure that the equivalent width measurements are reasonable, as there should be no trend in abundance with spectral line position. What is not shown is the same set of plots for Fe II, but log g is well constrained by ensuring the Fe II abundance matches with that of Fe I (and similarly no trends should exist). This iterative process is well suited to a human touch, and is made quicker when some suitable starting conditions are derived from e.g. photometry. Automatic computer algorithms exist to do this balance and are essentially a requirement when it is necessary to process large libraries of spectra. In these cases, however, it is crucial to take care to avoid local minima in optimization either by deriving very reliable starting conditions or fully exploring the parameter space.

3.3 Comparative Analysis and Systematics

The methodology of spectral analysis and the choice of atmospheric models and atomic line data can have a marked effect on the outcome of abundance analysis. The effect, however, is largely overcome in studies by doing a differential analysis, where the overall trends – strictly within the one dataset – are in focus, as opposed to the absolute physical scale. Nevertheless, it is the goal of most scientists to provide the most accurate values possible, and occasionally it is useful or

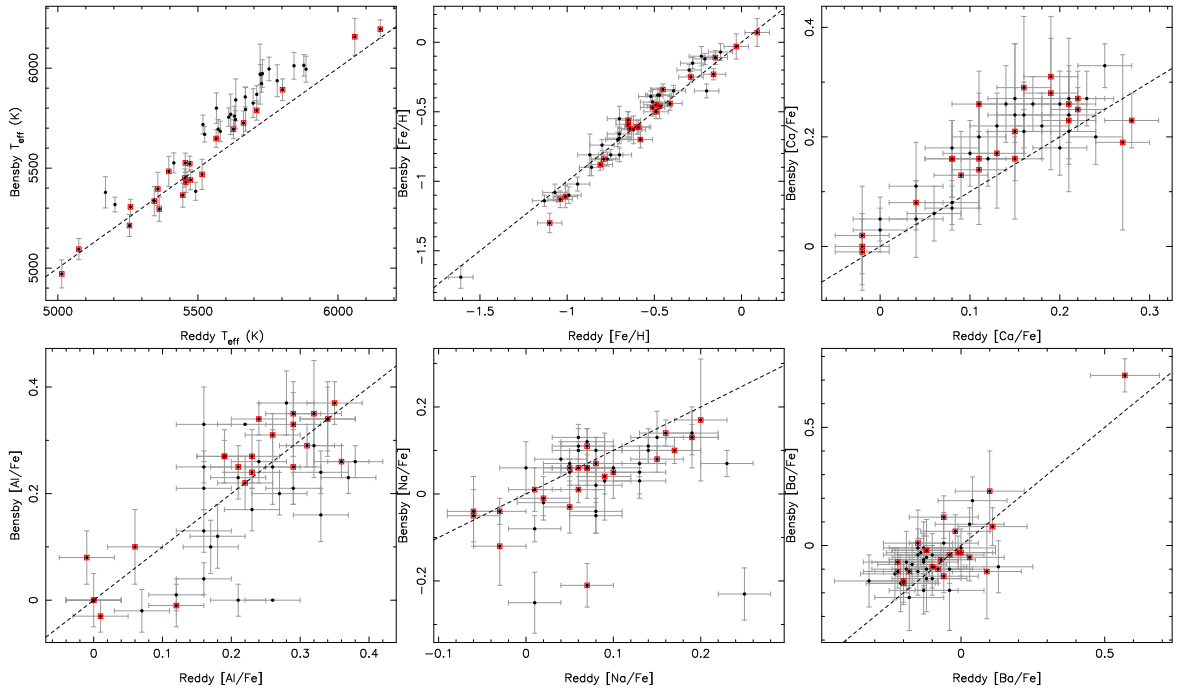

FIGURE 3.5: Comparison of temperatures and abundances calculated in two separate high-resolution spectral analyses. Each comparison plot shows all matching stars in the two studies whose absolute difference in T_{eff} is less than 250 K. The red squares are stars whose absolute difference in T_{eff} is less than 100 K. In each plot the equality relationship is represented with a dashed line.

necessary to include more than a single abundance dataset in a study as, indeed, will be the case later in this thesis. It is thus worthwhile to briefly discuss issues with comparative abundance analysis, and to do so by specific example.

We focus this exercise on a comparison of two high-resolution abundance datasets of Galactic field stars by Reddy et al. (2006) and Bensby et al. (2014). At high resolution the effect of discrepancies in the measurement of the line equivalent width will be minimized, and thus any difference will presumably be primarily related to analysis choices such as atmospheric models, atomic parameters and fitting techniques. Figure 3.5 shows a comparison of T_{eff}, [Fe/H], [Ca/Fe], [Al/Fe], [Na/Fe] and [Ba/Fe] values for 49 stars that are in common between the two studies with absolute temperature differences smaller than 250 K. Highlighted in red are those stars where the temperature differences are smaller than 100 K, where it should be less likely that any discrepancy is due to measurement of spectroscopic features.

A first notable feature of Figure 3.5 is that the red points, those with temperature differences between the studies of less than 100 K, do not appear to be distinct from the rest of the group.

This is likely simply a testament to the true underlying precision of temperature determination. Some disagreement in $T_{\rm eff}$ is likely due also to differing analysis methods – where Reddy et al. (2006) used predominantly Strömgren photometry, Bensby et al. (2014) used the spectroscopic ionization equalization method. Clear signatures of systematic uncertainties are displayed for most quantities, as exemplified in the behavior of both $T_{\rm eff}$ and Na abundances. Fe abundances are in reasonably good agreement, with small reported internal uncertainties. The ubiquity of iron absorption features in stellar spectra spectra at visible wavelengths affords a greater precision in abundance computation (there are roughly 200 in the case of the Bensby et al. 2014 set) and speaks greatly to the necessity for a large number of lines to be measured when aiming for an absolute of comparative study. Many other species will have only a handful of lines measured and some (e.g. Ba or Eu) in many cases only one.

Finally, a source of disagreement between studies may come from the atomic parameters used, e.g. line excitation potential and transition probability. The log *gf* values, in particular, are commonly drawn from either a reverse solar analysis – where abundances are assumed to be known such that log *gf* may be derived – or from tabulated lab values from a variety of sources. Obviously, when the adopted atomic parameters disagree, derived abundances cannot be compared on a level playing ground.

This may sound like a hopeless situation in an era where new instruments and technology are affording unprecedented precision spectroscopy. However, it is still the case that many studies only draw conclusions from a homogeneously analysed dataset, largely avoiding these issues. Further, up-coming stellar abundance surveys will deliver large homogeneous samples, potentially vanquishing issues with comparative abundance analysis (until such a time when combining several survey samples seems sensible).

3.4 An Open Cluster Spectroscopic Abundance Analysis

In this section we present a journal article detailing the spectroscopic abundance analysis of the intermediate age open cluster NGC 3680. The investigation was motivated in a large part to get hands on experience with high resolution abundance analysis via both EW and spectral synthesis methods, including preparation of the spectrum and measurement error analysis.

The cluster of study was selected both because data were readily available and due to the limited number of high resolution abundance studies of this cluster – particularly for the high atomic number elements. Using the automated code ARES (Sousa et al. 2007) for EW measurements, we aimed insofar as was possible to determine abundances for the elements Fe, Na, Mg,

Al, Si, Ca, Ti, Cr, Ni, Zn, Y, Ba, La, and Nd. We could not resolve Eu in any of the stars, but surprisingly were able to make inferences on the abundance of Gd in the giant stars, a rare earth element with little mention in the literature.

The work on this paper ultimately led to the idea of quantitative chemical tagging, which is the main topic of this thesis, and the derived abundances formed part of the open cluster literature abundance database used later in this thesis.

Pages 36-43 of this thesis have been removed as they contain published material. Please refer to the following citation for details of the article contained in these pages:

A. W. Mitschang, G. M. De Silva, D. B. Zucker, Elemental abundances of intermediate-age open cluster NGC 3680, Monthly Notices of the Royal Astronomical Society, Volume 422, Issue 4, June 2012, Pages 3527–3534, https://doi.org/10.1111/j.1365-2966.2012.20866.x

Chapter 4

Empirical Chemical Tagging

Having established the practicability of abundance analysis of stellar spectra, we turn once again to its application to chemical tagging. The discussion of chemical tagging tests in Section 2.3 conspicuously did not include tests of the abundance differences between separate conatal star formation sites. This is because detailed study into this matter has not – to date – been done. The usefulness of chemical tagging relies both on conatal stars being homogeneous in their composition (which has been established for several clusters), and equally on stars formed in distinct sites having measurably distinct compositions. Given that many uncertainties yet exist in our understanding of star formation on local, and galactic, scales – as an example consider the new boom in research into sub-populations of Galactic globular clusters which were once assumed to be examples of "simple" stellar populations (e.g. Kraft et al. 1997, Gratton et al. 2001, Carretta et al. 2010) – it seems necessary to turn to the observed universe in deriving a quantitative approach to practically apply chemical tagging to any real data. A major deliverable of this thesis is the development of such a quantitative approach, detailed in this chapter, which presents the second published peer-reviewed journal article in this series.

A particular challenge in approaching this task has been obtaining a suitable sample of abundances from open clusters. Until data products from Gaia-ESO and GALAH come out, there is no large homogeneous source of stellar elemental abundances. The prospect of collecting a heterogeneous sample of spectra from telescope archives and analysing them in a uniform way was an attractive option, but time constraints prevented this from being done in a reasonable time frame for either this thesis or for preparing for science from these surveys. Instead, a sample from the literature was pieced together based on criteria including spectral resolution of analysed data, number of stars in individual cluster samples, and uncertainties on abundances. Tables of all

types of formats appeared in the chosen sample; these had to be converted to a uniform format, and in some cases hand transcription was necessary from the published table to the final database format, but in the end, a sample of 2775 individual abundance values from 291 stars from 22 literature sources, all at R $>\sim$24,000, was compiled (see Appendix B for more details). Compared to the goals of the upcoming high resolution surveys this may seem a rather small sample, but serves to exemplify the state of this field at present and the timeliness of those surveys.

An important issue in using a sample like this is that the comparisons between abundances of stars in the different studies are affected by differences in their absolute scales. Within each study we consider it safe to compute an abundance difference and believe these accurately represent the true differences. This cannot be done with confidence when computing differences in abundance between different studies, even if their abundances were scaled to the same representation of the Sun. Accounting for this proved to be very difficult; in the end the take-home message is that the probability function is best computed on a sample of open clusters observed with the same survey instrument (e.g., HERMES for GALAH) at the target resolution to really understand the controlling effect of chemical abundance similarities between stars of different clusters.

The remainder of this chapter presents a journal article published in early 2013 in Monthly Notices of the Royal Astronomical Society. The major deliverable of the work in the following paper is an empirical conatal probability function, which describes the probability that two stars observed with a number of similar abundances are compatible with being born out of the same star formation event.

Pages 47-58 of this thesis have been removed as they contain published material. Please refer to the following citation for details of the article contained in these pages:

A. W. Mitschang, G. De Silva, S. Sharma, D. B. Zucker, Quantifying chemical tagging: towards robust group finding in the Galaxy, Monthly Notices of the Royal Astronomical Society, Volume 428, Issue 3, 21 January 2013, Pages 2321–2332, https://doi.org/10.1093/mnras/sts194

4.1 Additional Notes

4.1.1 On the Delta C Weighting Parameter

A weighting factor, $\omega_{\rm C}$, has been included in the definition of the $\delta_{\rm C}$ metric. $\omega_{\rm C}$ is actually a vector of element specific weights, the length of which, naturally, is the number of elements in common in a given pair. For this analysis $\omega_{\rm C}$ has been left as unity, primarily because the literature abundance sample was deemed insufficient to fully explore its application. The ideal sample would be large both in numbers of clusters and numbers of stars per cluster, would have a relatively complete range of measured abundances (i.e. most stars could be compared against the same number of element abundances), and the number of species would be large ($>\sim$ 12 say). A sample of these characteristics will be available soon, either in a data release of Gaia-ESO or after abundance analysis of HERMES commissioning and pilot survey data is stable and complete.

Estimating the optimal values of $\omega_{\rm C}$ is non-trivial; an exhaustive approach would be to evaluate the conatal probability function on a grid of all possible permutations within some limits and to some resolution, maximizing the $\delta_{\rm C}$ at which the conatal probability is 68%. Given the large number of dimensions that is evidently required to identify conatal pairs, this must be an intractable problem. A more promising approach, at least for an initial guess, would use the coefficients of the first several principle components (say, those comprising 90% of the variance) for open clusters from a PCA analysis like that presented in Ting et al. (2012).

4.1.2 On the Coeval Probability Function

The normalisation on each of the intra-, and inter-cluster probability distributions was largely ignored in the previous discussion. The relative normalisations are related to the *a-priori* probability that two stars are associated with one-another regardless of chemical (or any other) information. This prior then is related to the number of distinct star formation sites and the number of stars in each of them, and can be expressed as:

$$A = \sum_{i}^{N} \frac{n_i \times (n_i - 1)}{2}$$

$$B = \sum_{i}^{N} \sum_{j=i+i}^{N} n_i * n_j$$

$$P_{prior} = \frac{A}{A+B}$$

where N is the number of clustered star formation events which have occurred in the Galaxy, n is the number of stars in a given event which contribute to the field, and P_{prior} is the *a-priori* probability that any two stars considered are members of the same coeval group. A and B are then the volumes of the intra-, and inter-cluster probability distributions, respectively.

As an example, consider the unlikely case that field stars in the Galaxy were created in one of two star formation events of 100,000 stars each. In this case A and B each equal almost identically 1×10^{10} (A is just marginally less than B), meaning that $P_{prior} = 0.5$, and the volume of each distribution would be equal. A more likely scenario for the Galaxy as a whole is that there were hundreds of thousands of clusters with varying numbers of stars (in the tens to hundreds of thousands per cluster). To get an idea of the effect, consider a scaled down version of a galaxy where we have eleven clusters with numbers of stars between 5 and 20:

$$\mathbf{n} = \{10, 11, 12, 9, 6, 20, 15, 12, 10, 5, 8\}$$

$$A = 661, B = 6242$$

$$P_{prior} = \frac{A}{A+B} = \frac{661}{661+6242} = 0.096$$

B is ten times as large as A, thus the blue distribution introduced in this chapter would be ten times as large as the red, making the coeval probability function fall off very steeply at small values of δ_{C}. It must be noted, though, that the inter-cluster distribution is particularly uncertain due to systematic uncertainties in the sample and its small size – it may be that the prior does not dramatically reduce the efficacy of chemical tagging.

Unfortunately we do not know N or n, though they may be guessed for the Galaxy as a whole. The more insidious problem is that P_{prior} is very likely to be dependent on the survey volume, or some other spatially constrained scale, given that Galactic mixing is may not be efficient at a global scale. Note that the prior introduced here was not discussed explicitly in the paper in the next chapter, however it would be prudent to keep in mind these caveats when considering the scenarios proposed therein.

Chapter 5

The First Blind Chemical Tagging Experiment

Having developed the coeval probability function for chemical tagging, a natural progression is to test out chemical tagging on a field star sample to test predictions of efficiency and begin to understand challenges facing larger surveys. An important requirement for this experiment is a sample with as homogeneous properties as possible, particularly in the method used to derive abundances. Selecting a sample was fairly straightforward, as there are not a huge number of high-resolution abundance datasets with enough stars. The sample of Bensby et al. (2014) was deemed most appropriate given the large sample size ($\sim$ 700), the number and range of elements analyzed (12 including Ba but excluding O due to very large measurement uncertainties), the resolution enabling precision in abundances (from 40,000 to over 100,000), and importantly the fact that they are all Hipparcos stars and thus have distance and kinematic information as well. Of course, these data were not publicly available at the time this experiment was conceived, but we had been made aware of them through meetings, and the abundances had been used in the literature. There was every indication that data were fully prepared and simply awaiting a writeup of the analysis to release them publicly.

It could not have been surmised at the time that this was not the case, though retrospective thought urges caution when considering utilising data that are not released and described publicly, and that have not gone through the rigour of peer review. Nevertheless, these likely were (and still are) the highest quality measurements of their type and most appropriate for testing our chemical tagging experiment. Bensby was contacted personally and agreed to supply the data for this project.

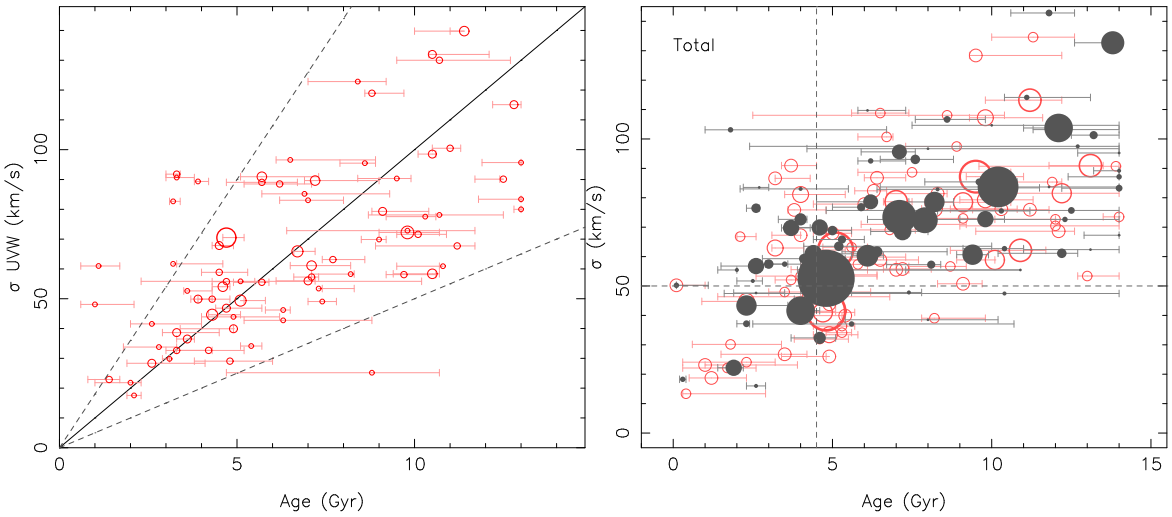

FIGURE 5.1: The left-hand plot shows the age-internal velocity dispersion relation for the first set of data from Bensby using a δ_C cutoff value corresponding to 90% pair probabilities. The solid line traces the mean relation while the dotted lines trace the widening of the distribution with age. Symbol sizes correspond to relative group sizes. The right-hand plot is the figure appearing in the published version, with grey symbols indicating groups identified with 68% pair probabilities.

Building the machinery to link groups from δ_C values was simple, and the first run at analysis came quickly after initially receiving the data. Detailed descriptions of this and other analyses are presented in a published refereed article later in this chapter. The results looked quite encouraging for the prospect of chemical tagging. In particular, with groups of stars ages can be more accurately determined using isochrone methods, and the groups provide a natural binning to inspect the age versus velocity dispersion relationship. One might expect that, if stars form in groups with small velocity dispersions and eventually dissolve, older stars would have proportionally greater spans of time to dynamically interact with components of the galaxy and thus their internal dispersions would increase with age. Due to the stochastic nature of Galactic dynamical interactions, we would also expect a larger spread in the group velocity dispersions overall as time goes on (in other words, the dispersion of the dispersion increases). Figure 5.1 (left panel) shows the very first analysis of the data, and appears to support this reasoning quite clearly.

However encouraging and unexpected that first result might have been, it was not the final word in this experiment. We ended up receiving three updates of the abundance tables, i.e., four different iterations in total, each one yielding different results and with none as seemingly clear as the first (though admittedly part of this was likely a psychological effect). The final iteration,

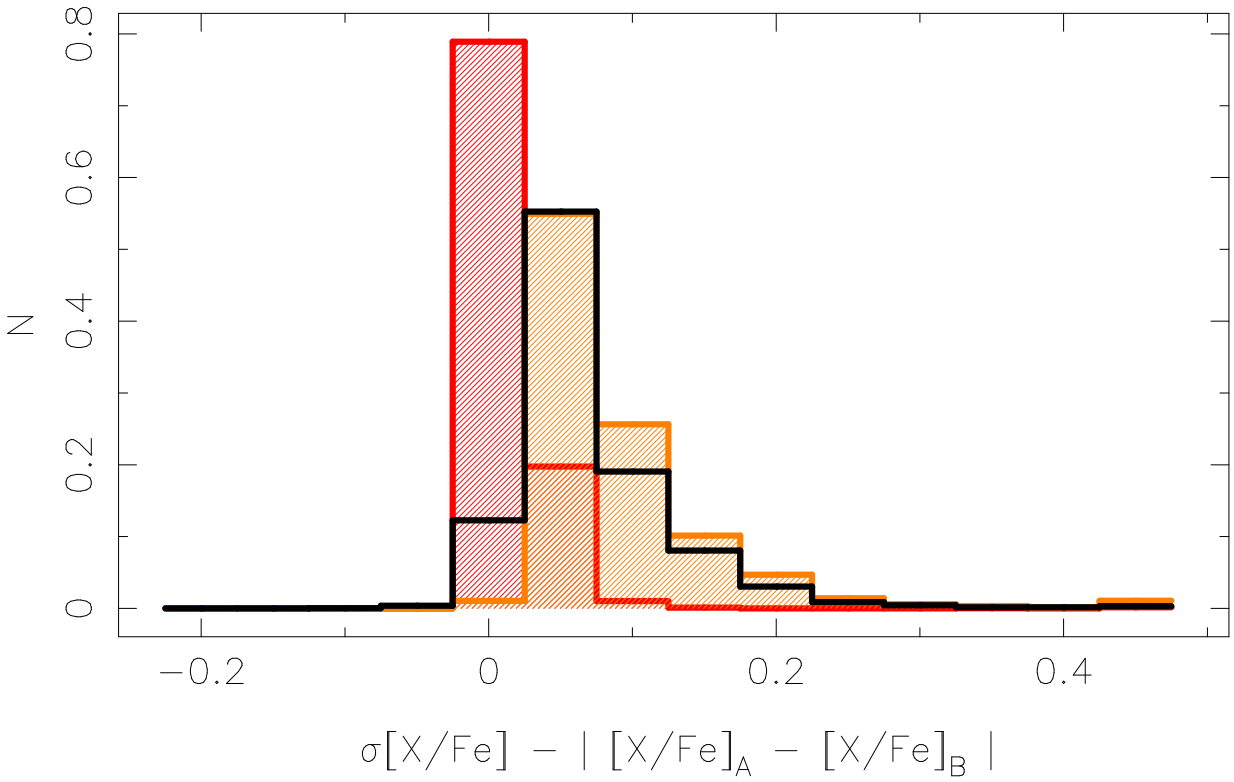

FIGURE 5.2: Estimated uncertainties as compared to calculated abundance differences for different iterations of the Bensby data (black). Also shown are the uncertainties (σ[X/Fe] term; orange) and differences ([X/Fe]$_{\rm A}$ - [X/Fe]$_{\rm B}$ term; red). The positive value of the mode of the black distribution indicates that the uncertainties were likely appropriately estimated.

shown in the right hand panel of Figure 5.1 and which appears in the published paper in this chapter, exhibits a qualitatively similar trend, but note that the layout of groups themselves is quite different from the previous figure. Part of this effect is due to the over-sensitivity that the 90% threshold imposes, which turns out to be too close to the measurement uncertainties. For that reason the 68% pair probability threshold was the primary focus of analysis, and appears as the dark circles in the right-hand plot.

Figure 5.2 shows the difference in calculated abundances for different iterations of analysis as compared to the estimated uncertainties on the abundance values (black histogram). This shows that the uncertainties were appropriately estimated, since the differences in analysis were in general less than the error estimate. Given that the 68% threshold corresponds well with the mean in uncertainties, the difference in groups indicates that group linking has sensitivity to uncertainties beyond those of a single coeval pair (to which the probability is relating). It is

thus important to appreciate that groups and their properties are likely only meaningful when considered globally. In a physically motivated approach to group linking, where a single star can only inhabit a single group, as was taken here, uncertainties prevail, while in a probabilistic approach in which a star can inhabit multiple groups, we clearly cannot discuss the properties of any single group per se.

Even though these repeated re-analyses delayed the submission of the paper, the effect they had on the chemical tagging results led us, in the end, to a much more careful consideration of what the groups and their properties tell us, and what the limits are in the scope of measurement uncertainties. For example, had we proceeded with the first analysis, we quite likely would have ignored the fact that the chemical tagging efficiency appears considerably higher than expected, which becomes an important discussion point later in this work.

5.1 On Computing Stellar Ages

The conclusions of this chapter are dependent substantially on the computation of the ages of stars, either considered individually, or as members of a coeval group. It is thus useful to elaborate on the discussion presented in the next section before proceeding. Other than the special case of the Sun, where meteoritic data can, presumably, give at least a minimum age, astronomers must rely on the theory of stellar evolution to give an indication of a stars age. In the most typical fashion, we compare the observed properties of stars to an isochrone, a tabulated list of theoretical properties of stars spanning a range of masses calculated at a given age (a popular set is the Yale-Yonsei version 2, abbreviated Y^2;Demarque et al. 2004). The list of properties typically includes observables (or, more precisely, derivables) such as colour in a number of bands, absolute magnitude, luminosity, effective temperature, and surface gravity, along with stellar mass.

When determining and age via this method for a group of stars such as an open or globular cluster, we must make the fundamental assumption that the stars are all of approximately the same age, and thus a single isochrone can describe the entire population well. When we have equal confidence on all of our measurements, finding the appropriate isochrone is as simple as minimizing the cumulative scale-independent distance of all parameters between observed values and those predicted by a set of models. With a large sample of stars – and where the same-age assumption holds – statistical confidence can be had in the resulting age.

When fitting a single point, on the other hand, we implicitly assume that theory is perfect and the only source of uncertainty is that associated with our measurements; this is an assumption that is at odds with studies of clusters with precise photometry, which show observations scatter

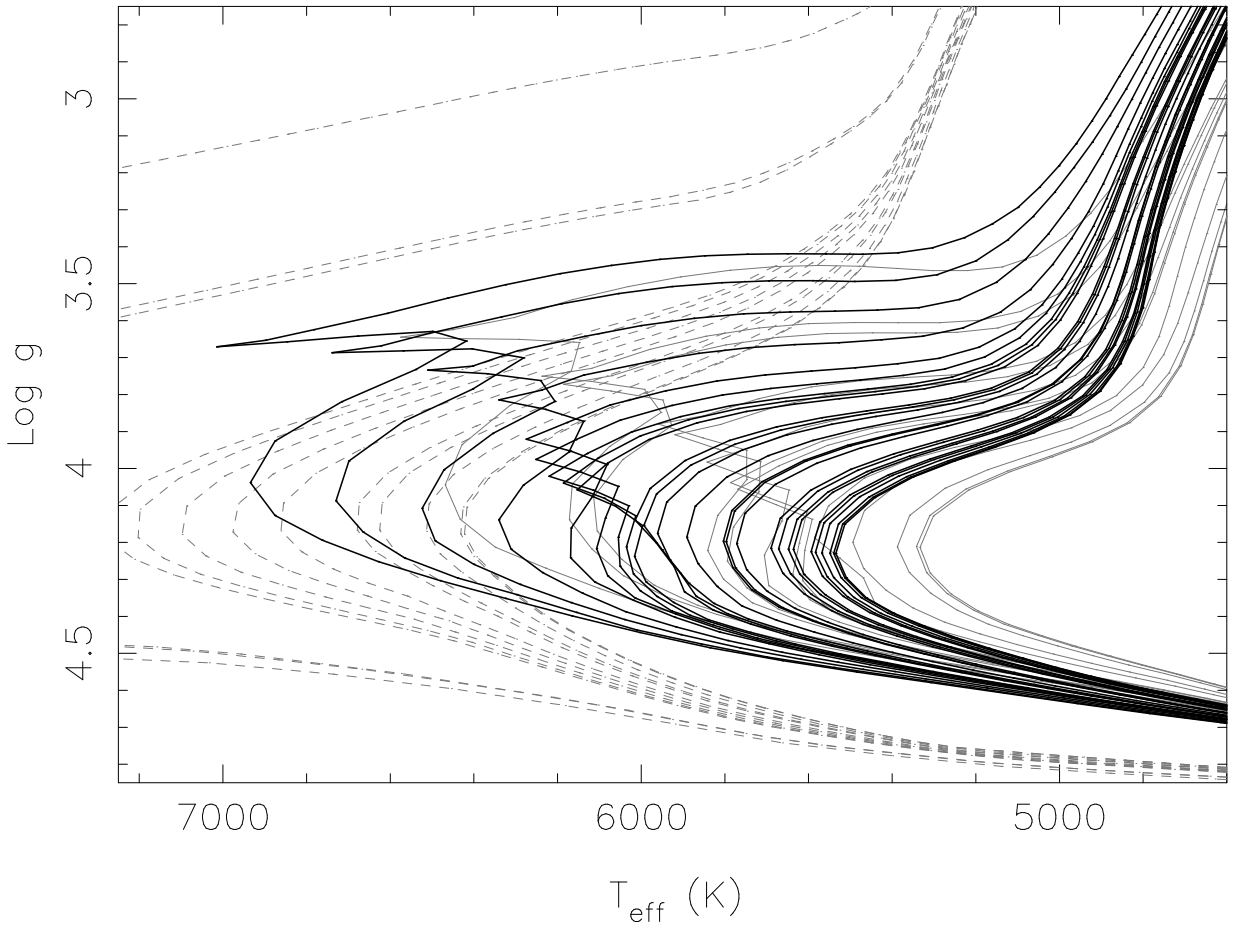

FIGURE 5.3: A grid of Y^2 isochrones for solar iron and α abundances highlighting the dwarf to giant turn-off region (dark solid lines). The grid separation is 500 Myr, increasing from 0.1 Myr (at far left) to 13 Gyr (at far right). Also shown are low metallicity (Fe/H = –1.5; dashed lines) and high metallicity (Fe/H = 0.4; light solid lines) grids for comparison.

significantly about an individual isochrone. It could be that members of such clusters have large age-spreads, or, more likely, it is a result of both imperfect theory and inappropriate assumptions about the conditions of cluster formation. The second major flaw with computing ages for single stars from isochrones is illustrated in Figure 5.3, which shows a range of isochrones at solar metallicity from 0.1 to 13 Gyr. It should be immediately clear the difficulties for dwarf and giant stars, where isochrones are tightly arranged. Though they appear to monotonically evolve with similar morphology from young to old, moving left to right in this diagram, it is clear that towards older ages the separation of isochrones is not linear with age – there are several areas with large age differences between two tightly spaced isochrone tracks. Finally, note the complicated

structure for the solar metallicity isochrones seen in the center of Figure 5.3, between roughly 5800 and 6600 K and log g of 3.5 to 4.5, where overlaps occur between a number of different tracks. Without further constraints, e.g. stars of different mass known to be the same age, there is clearly no way to reasonably select the appropriate best fit isochrone.

If chemical tagging can indeed deliver on its promise to find groups of coeval stars that would otherwise be considered in isolation, it is poised to be a major advancement in the determination of stellar ages in the Galaxy, circumventing some of the issues raised above. Exploring this possibiliy is a focus of the remainder of this chapter, which presents an article published in MNRAS in early 2014 describing a blind chemical tagging experiment and discussing the implications of the results. A further description of the group finding algorithm and the full Table 2 are given in Appendix C. Before moving on, there are two clarifications that should be made with respect to the published work. First, in section 3.2 of the text it states that there are 38 members in the largest group at the 68% probability level, yet, as indicated in Figure 1 and Table 1, there are in fact 42. This was an error propagated from a previous version of the analysis (as described above). Second, we have referred to the $T_{\rm eff}$ vs. log g plots as CMDs (colour magnitude diagrams), which, technically speaking, they are not, even though in appearance and interpretation they are quite similar and are often interchangable in discussion.

Pages 67-78 of this thesis have been removed as they contain published material. Please refer to the following citation for details of the article contained in these pages:

A. W. Mitschang, G. De Silva, D. B. Zucker, B. Anguiano, T. Bensby, S. Feltzing, Quantitative chemical tagging, stellar ages and the chemo-dynamical evolution of the Galactic disc, Monthly Notices of the Royal Astronomical Society, Volume 438, Issue 4, 11 March 2014, Pages 2753–2764, https://doi.org/10.1093/mnras/stt2320

Chapter 6

Summary and Conclusions

This thesis has presented an original and detailed examination of the empirical grounds for the technique of chemical tagging, which aims to identify long-since dispersed conatal groups of stars via their element abundance signatures. This work is particularly timely due to the impending million star chemical tagging survey, GALAH, and the fact that a quantitative basis for the technique has not previously been established. The first paper presented herein was an abundance analysis of the intermediate age open cluster NGC 3680, providing α and s-process elements to the literature for 11 member stars. The work on this paper led to an enhanced appreciation of abundance analysis and chemical signatures in open clusters, and largely incubated the idea of quantitative chemical tagging, the basis of the other papers in this thesis. We summarise here the main points, related to quantitative chemical tagging, presented in this work.

The goal of quantitative chemical tagging is to understand how well we can identify conatal sub-structure in the real Galaxy at our current measurement capability. To this end, a pairwise difference metric, the $\delta_{\rm C}$ metric, was defined which operates on any number of similarly measured element abundances in two stars, returning the mean absolute deviation of abundances. The metric is resistant to missing measurements, retaining the same scale regardless of input dimensionality. Using a sample of stars compiled from the literature containing some $\sim$ 300 stars with up to 12 chemical species measured over 20 Galactic open clusters, we defined two distinct populations of chemical differences. An appropriate ratio of the chemical difference values in the two populations, the inter-cluster and intra-cluster populations, was shown to give a probability that two stars with a given $\delta_{\rm C}$ value are conatal. The result of this analysis is the empirical chemical tagging probability function, $\rm P_{\delta C}$.

While an empirical function is useful when there are many theoretical unknowns, it is subject

to measurement uncertainties in both the definition of the function itself, as well as the measurements that it applies to. The uncertainties are magnified in the case of $P_{\delta C}$ given the systematic uncertainties associated with abundance measurements from different literature analyses. To understand the magnitude of these effects, we performed a simulation re-evaluating the inter-cluster δ_C distribution in light of systematic uncertainties of a reasonable order, and computed a new probability function. The adjusted probability function shows a shift of 0.02 dex for the 68% probability level, meaning that an increase in precision of 0.02 dex is required to sort stars to the same level. Another way to quantify the difference is that a pair with 68% probability using the empirical function would have roughly a 40% probability with the adjusted function. For several reasons we believe this to be a conservative estimate of the systematic effects, however it elucidates an important point made several times in this thesis: the chemical tagging probability function should be derived from a homogeneous sample of stellar spectral abundance analyses made from the same instrument configuration as the chemical tagging survey. When an open cluster sample is not part of the survey program, a sample from a similar survey may be used. For example, the Gaia-ESO survey will target open cluster stars as a part of its main program, and the UVES high-resolution component could probably be used as a $P_{\delta C}$ calibration for GALAH as well as Gaia-ESO itself.

A practical approach to vetting groups of stars, e.g., those linked with the density based hierarchical group finding code EnLink (Sharma & Johnston 2009), based on their conatal pair probabilities was presented. Grouping chemical sub-structure is not the only thing that can be done with quantitative chemical tagging. We have also shown how the shape of the probability function is affected by removal of particular elements or element groups from the analysis. Not only can we probe the chemical tagging power of individual elements – for example Ba, as previously suspected, has significant power as a chemical tagging dimension – this type of analysis can additionally shed light on early nucleosynthetic processes.

At the end of Chapter 4, an estimation of the efficiency of tagging was made based on a mock experiment using the literature abundance sample. The study finishes on a relatively positive note, even at an efficiency of $\sim 2\%$ (of detecting true conatal pairs), it implies an estimated 4300 clusters might be recovered in the GALAH million star survey.

To perform a real world test of the predictions and procedures using quantitative chemical tagging, we conducted what is likely the first ever *blind* chemical tagging experiment on Galactic field stars. We obtained a sample of homogeneously analysed high-resolution abundances of Hipparcos stars, allowing 3D space motion analysis in addition to abundances with internal errors on the order of 0.05 dex. The sample includes $\sim$ 700 stars, small compared to the upcoming

surveys but sufficient in size to make some predictions about what those surveys may be able to uncover.

Groups were identified in this sample using a $\delta_{\rm C}$ threshold-based approach, where pairs of stars with a conatal pair probability greater than a chosen threshold X were linked successively as described in Appendix C. We chose to analyse two thresholds for the sake of comparison, the 68% threshold being approximately the most sensitive comparison that can be made in light of uncertainties, and the 90% threshold, whose $\delta_{\rm C}$ limit is below the mean internal error of the sample. The first interesting, and surprising, result from group linking was the large percentage of stars tagged to groups in a sample comprising a spherical volume with a radius of just 150 pc around the Sun. The 84 and 47% of stars tagged at the 68 and 90% probability levels, respectively, in groups with more than 2 members, is vastly larger than predictions from the previous paper, even including potential contamination as computed therein.

We explored several possible explanations for this presumed anomaly, among them that the contamination level is simply much higher than predicted in Mitschang et al. (2013). In the same vein, it is possible that the prior, as discussed in 4.1.2, could be underestimated by a large factor, resulting in many pairs linked in simply meaningless associations. A third option is that Galactic mixing is weak, or that mixing occurs on scales larger than the sample volume, in which case the efficiency is not overly large and the groups do represent conatal stars. Lines of evidence, particularly from Galactic dynamical evolution models, argue against such an option, but, indeed, this result could represent observational evidence *against* strong Galactic mixing. These three options cannot be discounted and certainly warrant further investigation; however, there were several lines of evidence that led to the preference of the following option: that instead of chemically tagged groups being made up of stars from a conatal origin, as has been generally accepted, that they are instead only coeval, i.e., born at approximately the same time but not necessarily the same spatial location. Evidence in favour of this explanation includes, for one, that the CMD plots in $T_{\rm eff}$ and log g do not in general exhibit arrangements incompatible with mono-age simple stellar populations. Age-metallicity and -velocity dispersion relations, utilising ages computed via isochrone fitting to chemically tagged groups, further paint a picture that aligns with prevailing theory of Galactic evolution, bolstering the idea that these groups indeed have a physical interpretation.

Assuming that the groups do indeed represent coeval groups of stars, then we are brought to another important implication from this experiment. We have shown that the ages computed from single stars are not compatible with those from the chemically tagged groups for the same stars. The problems with computing an age via isochrone fitting to a single point are obvious, yet

this is still the prevailing way ages are estimated for field stars. To have a method to circumvent that issue would be a powerful astrophysical tool. Even if chemical tagging of field stars cannot deliver on the promise to seek out conatal stellar structure in the Galaxy, if it can be used to deliver more accurate and precise ages for field stars it will be a resounding success.

Though this thesis ends here, the saga of chemical tagging is only just beginning. What does the future hold? First and foremost, the empirical chemical tagging probability function should be evaluated on a high quality homogeneous open cluster abundance dataset. The UVES open cluster survey component of Gaia-ESO clearly shows the most promise in this respect, and will likely be the first of its kind to appear. The same dataset would be well-suited to investigating the $\delta_{\rm C}$ weighting parameter ω as described in Section 4.1.1.

A more concerted effort at modeling the prior on the intra- and inter-cluster distributions that go into the chemical tagging probability function would be useful. A clearly developed theoretical framework that tracks individual stars from their birth over a cosmic evolutionary scale would be most appropriate. Comprehensive models of this type do not seem to exist at present, and the disputes between those theorists who work on such problems as stellar radial migration points to the need for caution in the interpretation of any results from the models that do exist. Once survey data from GALAH and Gaia-ESO become available, combined with the precise kinematic and distance information from Gaia, chemo-dynamical models will have powerful constraints to test against, particularly in conjunction with group identifications from chemical tagging, which may iteratively lead to a better understanding of the Galactic churning processes.

Eventually, the survey data themselves will be tagged using one or many different methods. Ideally, the updated tools discussed above will provide for high confidence in reconstructing coeval groups of stars, regardless of the methods used to link stars together. We can only hope that the results from this work, particularly those discussed in Chapter 5, are carefully considered in the interpretation of the tagged groups. Until proper motion data from Gaia are made available, the detailed kinematic properties of groups will quite likely not be known, making testing an experiment like performed here impossible. Without those added constraints the interpretation of chemically tagged groups is even more fragile.

Notwithstanding the challenges facing chemical tagging, the coming years will be an exciting time for stellar studies of the Galaxy. The author is looking forward eagerly to the many advancements that will surely arise from the coming era of stellar spectroscopic surveys and, in particular, chemical tagging.

Appendix A

Metric Computation and Considerations

Evaluating δ_{C} for a sample of stars in order to link groups requires computing the value for every pair in the sample, $\mathrm{N_{pair}}$, which can be expressed as:

$$N_{pair} = \frac{N_\star \times (N_\star - 1)}{2}$$

The computational procedure for evaluating δ_{C} for a sample of stars is outlined in pseudo code below. For large sample sizes this can be trivially parallelised by distributing the outer loop over multiple CPU cores.

```
For every star i in sample
Do
  For every star j from i+1 in sample to the end
  Do
    For element in elements
    Do
      If star i has element and star j has element
      Do
        delta_C = delta_C + abs(element_i - element_j)
      End
    End

    delta_C = delta_C / (number of elements in common)
```

```
    Append this delta_C to list
  End
End
```

The storage cost, at the very least, is $N_{pair} \times B_{float}$, where B_{float} is the size in bytes of a single precision floating point number, typically 4. In this case, indices of stars, i.e., which two stars comprise a particular δ_{C} value, can be calculated based on the iterating procedure used. Otherwise, space must be allocated for these as well.

For a sample of 1×10^6 stars, the computational costs become non-trivial. The number of pairs is close to 5×10^{11}, which at the simplest storage arrangement mentioned above is almost 20TB. Arguably, the δ_{C} may be calculated as data come in, meaning CPU time is of no consequence, but in the case of reprocessing this cannot be done, and storage is more particularly necessary because an experiment will presumably not be done immediately. Storage needs can be alleviated by saving only those pair probabilities which are greater than some threshold, but in this case it is strictly necessary to store also some index relating the entry to the two stars from which it was computed.

Appendix B

Open Cluster Literature Abundance Database

The literature abundance table used in chapter 4 is included below. The column SID is a unique identifier for a particular star, CID uniquely identifies the cluster it belongs to and Ref is a single alpha-numeric letter code for the article from which the abundance values were compiled, see table B.1 for the codes. The remaining columns are abundance values in the form [X/Fe] (i.e. relative to Solar Fe abundance values). Where uncertainties were given in the literature these appear in parentheses after the abundance value.

SID	CID	Ref	Na	Mg	Al	Si	Ca	Sc	Ti	V	Cr	Mn	Fe	Co	Ni	Cu	Zn	Sr	Y	Zr	Ba	La	Ce	Nd	Sm	Eu
700	14	N	−0.08	−0.12		0.04	0.05		−0.01				0.16				−0.13			−0.1	0.39		0.13	−0.14		
701	14	N	−0.03	−0.04		0.07	0.06		0.07				0.1				−0.01			0.03	0.38	1.09	0.25	−0.15		
702	14	N	−0.09	−0.01		0.02	0.14		0.1				−0.12				−0.05			0.0	0.74		0.15	−0.02		
703	14	N	−0.1	−0.1		0.06	0.02		0.03				0.18				−0.15			−0.05	0.43		0.13	−0.15		
704	14	N	0.0	−0.06		0.07	0.05		0.03				0.09				−0.08			0.01	0.34		0.09	−0.04		
705	14	N	0.02	−0.05		0.0	0.16		0.07				0.3				−0.11			0.11	0.48		0.0	−0.22		
706	14	N	0.01	−0.06		−0.02	0.13		0.04				0.3				−0.03			−0.03	0.45		−0.01	−0.21		
707	14	N	0.02	−0.07		−0.04	0.12		−0.03				0.15				−0.01			0.05	0.46		0.06	−0.22		
708	14	N	−0.04	−0.07		0.0	−0.01		−0.01				0.17				−0.09			−0.19	0.33		0.1	−0.26		
709	14	N	0.0	−0.11		0.09	0.12		0.03				0.11				−0.03			−0.09	0.41		−0.07	−0.18		
710	14	N	0.05	0.01		0.06	0.14		0.0				0.09				0.08			−0.04	0.48		0.1	−0.15		
711	14	N	0.01	−0.03		0.08	0.08		0.02				0.06				−0.08			0.05	0.4		0.13	−0.13		
712	14	N	−0.01	−0.01		0.04	0.13		0.05				0.12				0.0			0.02	0.38	1.05	0.04	−0.18		
713	14	N	−0.02	0.0		0.09	0.04		0.06				0.09				−0.09			−0.04	0.36		0.11	−0.13		
714	14	N	0.01	−0.01		0.03	0.08		0.05				0.15				−0.03			−0.05	0.33		0.08	−0.23		
715	14	N	−0.05	−0.04		0.06	0.08		−0.04				0.1				−0.06			−0.07	0.37	1.06	0.11	−0.16		
716	14	N	0.0	−0.07		0.04	0.0		0.05				0.08				−0.01			−0.08	0.34		0.18	−0.11		
717	14	N	0.0	−0.06		0.05	0.1		0.03				0.09				−0.08			−0.03	0.44	1.1	0.05	−0.16		
718	14	N	0.01	−0.05		0.0	0.13		0.03				0.14				0.02			0.04	0.4	0.98	0.0	−0.22		
719	14	N	0.02	−0.04		0.05	0.11		0.04				0.1				−0.04			−0.06	0.38	1.06	0.09	−0.14		
720	14	N	−0.03	−0.06		0.02	0.05		−0.02				0.15				−0.09			−0.14	0.37	1.04	0.1	−0.18		
721	14	N	−0.02	−0.02		0.09	0.01		0.03				0.08				−0.08			−0.04	0.35		0.12	−0.12		
722	14	N	0.02	−0.07		0.06	0.03		0.02				0.11				−0.08			−0.09	0.33	1.05	0.09	−0.18		
723	14	N	0.05	−0.05		0.05	0.11		0.01				0.09				−0.09			−0.01	0.45	1.06	0.0	−0.18		
724	14	N	−0.04	−0.05		0.06	0.06		−0.04				0.08				−0.02			−0.09	0.38		0.1	−0.14		
725	14	N	−0.05	−0.09		0.06	0.01		0.01				0.13				−0.05			−0.08	0.39	1.06	0.15	−0.17		
726	14	N	−0.01	−0.09		0.03	0.03		0.07				0.13				−0.14			−0.07	0.32	1.09	0.12	−0.12		
727	14	N	−0.01	−0.11		0.02	0.09		0.03				0.12				−0.05			0.01	0.36		0.0	−0.19		
728	14	N	0.04	−0.13		0.07	0.05		0.05				0.09				0.03			−0.04	0.45		0.23	−0.1		
729	14	N	−0.06	−0.05		0.01	0.11		−0.04				0.13				−0.07			−0.08	0.44	1.03	−0.01	−0.2		
730	14	N	−0.05	−0.09		0.05	0.02		0.03				0.13				−0.07			−0.07	0.34		0.1	−0.19		
731	14	N	0.0	−0.08		0.02	0.09		0.0				0.15				−0.12			−0.04	0.4		−0.02	−0.23		
732	14	N	0.01	−0.08		0.0	0.02		−0.01				0.15				−0.1			−0.01	0.35	1.04	0.08	−0.2		
733	14	N	−0.05	−0.02		0.06	0.09		0.03				0.11				−0.05			−0.08	0.37	1.08	0.11	−0.19		
734	14	N	0.08	−0.02		0.05	0.12		0.12				0.08				−0.1			0.01	0.47		0.02	−0.13		
735	14	N	−0.01	−0.05		0.02	0.09		0.03				0.15				−0.02			−0.1	0.31		0.06	−0.22		
736	14	N	0.02	−0.05		0.07	0.09		0.07				0.12				−0.04			−0.1	0.35		0.09	−0.19		
737	14	N	0.01	−0.04		0.07	0.06		0.03				0.09				−0.07			−0.08	0.37		0.14	−0.1		
738	14	N	0.02	−0.06		0.0	0.06		0.02				0.14				−0.05			−0.04	0.36		0.12	−0.17		
739	14	N	0.01	−0.04		0.08	0.08		0.05				0.13				0.0			−0.1	0.33	1.04	0.06	−0.21		
740	14	N	−0.03	−0.11		0.1	0.08		−0.06				0.15				−0.07			−0.04	0.38		0.15	−0.14		
741	14	N	−0.05	−0.08		0.05	0.03		0.02				0.11				−0.1			−0.13	0.35		0.16	−0.1		
742	14	N	−0.08	−0.06		0.05	0.03		0.02				0.08				−0.09			−0.11	0.35	1.07	0.14	−0.1		
743	14	N	0.01	−0.09		0.02	0.02		0.0				0.14				−0.06			−0.05	0.3	1.06	0.07	−0.12		
744	14	N	−0.08	−0.15		0.03	0.03		0.03				0.22				−0.12			−0.06	0.32	1.04	0.17	−0.19		
745	14	N	−0.02	−0.09		0.02	0.02		0.03				0.15				−0.07			−0.04	0.41		0.16	−0.14		
746	32	J	0.0	−0.01	−0.01	−0.01	0.09		0.0		0.0		0.01		−0.04											
747	32	J	0.12	0.03	−0.04	0.1	0.12		0.0		0.09		0.03		0.03											
748	32	J	0.12	0.02	−0.04	0.02	0.07		0.04		0.03		0.0		0.04											
749	32	J	0.04	0.0	−0.06	0.03	0.05		−0.06		−0.04		0.05		−0.07											
750	32	J	0.08	0.0	−0.08	−0.02	0.01		0.0		−0.05		0.07		−0.03											
751	32	J	0.07	−0.02	−0.08	0.03	0.03		0.0		0.0		0.01		−0.03											
752	32	J	0.03	−0.01	0.02	0.05	0.0		−0.05		−0.01		0.02		−0.03											
753	32	J	−0.04	−0.04	−0.09	0.0	0.02		−0.08		−0.04		0.05		−0.05											
754	32	J	−0.06	−0.04	−0.11	−0.03	0.04		−0.04		−0.02		0.06		−0.04											
755	32	J	0.13	0.03	−0.06	0.04	0.03		−0.06		−0.01		0.0		0.03											
756	40	A	−0.1			−0.12			−0.07				0.07		−0.27											
757	40	A	−0.09			−0.06			−0.13				0.02		−0.05											
758	40	A	−0.22			−0.11			−0.02				0.01		−0.17											
759	40	A	−0.15			0.01			−0.14				0.05		−0.13											
760	40	A	0.13			−0.12			−0.05				0.06		−0.19											
761	40	A	−0.38			−0.2			−0.05				0.19		−0.3											
762	40	A	−0.17			−0.12			−0.09				0.08		−0.22											
763	40	A	−0.11			−0.09			−0.16				0.04		−0.17											
764	40	A	−0.15			−0.13			−0.01				0.1		−0.16											
765	40	A	0.17			−0.04			−0.15				0.04		−0.03											
766	40	A	−0.24			−0.06			−0.08				0.08		−0.18											
767	40	A	−0.17			−0.09			−0.14				0.06		−0.17											
768	40	A	−0.16			−0.1			0.06				0.18		−0.27											

SID	CID	Ref	Na	Mg	Al	Si	Ca	Sc	Ti	V	Cr	Mn	Fe	Co	Ni	Cu	Zn	Sr	Y	Zr	Ba	La	Ce	Nd	Sm	Eu
769	40	A	−0.21			−0.05			−0.03				0.09		−0.11											
770	40	A	−0.24			0.0			0.0				0.0		−0.15											
771	40	A	−0.02			−0.05			−0.02				0.13		−0.11											
772	40	A	−0.24			−0.07			−0.11				0.03		−0.17											
773	40	A	−0.22			−0.07			−0.03				0.05		−0.15											
774	40	A	−0.14			−0.06			0.06				0.13		−0.2											
775	40	A	−0.04			−0.06			−0.16				0.08		−0.07											
776	7	F	0.15			−0.05	−0.01		0.05		0.02		0.08		−0.02						0.61					
777	7	F	0.1			0.02	0.06		−0.04		−0.02		0.0		−0.03						0.64					
778	7	F	0.15			0.0	0.13		0.01		0.01		0.03		−0.02						0.58					
779	7	F	0.08			−0.01	0.03		0.01		0.0		0.05		−0.02						0.66					
780	7	F	0.19			0.03	0.01		−0.02		0.01		0.02		−0.06						0.58					
781	8	F	0.14			0.08	0.01		−0.03		0.05		0.0		0.01						0.53					
782	8	F	0.14			−0.01	0.02		0.0		0.06		0.07		−0.04						0.55					
783	8	F	0.18			0.04	0.04		−0.03		0.06		0.0		0.02						0.48					
784	8	F	0.16			0.03	0.0		−0.04		0.03		0.02		−0.03						0.61					
785	8	F	0.2			0.01	−0.01		−0.07		0.0		0.0		0.04						0.52					
786	8	F	0.15			0.11	0.07		−0.04		0.07		0.02		−0.04						0.55					
787	4	F	0.13			0.14	0.1		0.01		−0.04		−0.31		−0.01						0.34					
788	4	F	0.08			0.13	0.14		0.02		−0.02		−0.27		0.02						0.34					
789	4	F	0.19			0.11	0.07		−0.04		−0.08		−0.35		−0.03						0.25					
790	4	F	0.08			0.13	0.01		0.08		−0.09		−0.2		0.0						0.21					
791	4	F	0.1			0.04	0.08		0.11		−0.01		−0.24		−0.04						0.17					
792	4	F	0.09			0.12	0.05		0.06		−0.1		−0.35		0.07						0.21					
793	4	F	0.19			0.17	0.07		−0.03		−0.05		−0.3		0.0						0.3					
794	4	F	0.29			0.09	0.1		−0.02		0.0		−0.33		−0.02						0.27					
795	4	F	0.07			0.19	0.01		−0.04		−0.09		−0.29		0.04						0.52					
796	5	F	0.31			0.05	0.2		−0.07		−0.02		−0.17		−0.08						0.66					
797	5	F	0.43			0.3	0.06		−0.06		−0.05		−0.14		−0.06						0.46					
798	5	F	0.32			−0.05	0.18		−0.1		−0.05		−0.17		−0.11						0.67					
799	5	F	0.31			0.02	0.14		−0.14		−0.05		−0.17		−0.09						0.67					
800	5	F	0.33			0.06	0.12		−0.03		0.01		−0.1		−0.08						0.67					
801	5	F	0.4			0.04	0.21		−0.09		−0.01		−0.27		−0.1						0.61					
802	5	F	0.44			0.02	0.17		−0.09		−0.02		−0.17		−0.1						0.63					
803	6	F	0.16			0.07	−0.03		−0.06		−0.03		0.05		−0.01						0.44					
804	6	F	0.16			0.06	0.0		0.01		0.03		0.05		−0.01						0.45					
805	6	F	0.19			0.08	0.01		0.02		0.01		0.1		0.06						0.55					
806	6	F	0.16			0.07	−0.01		0.0		0.06		0.05		0.02						0.45					
807	6	F	0.2			−0.01	−0.02		−0.01		0.04		0.07		−0.05						0.39					
808	6	F	0.14			0.05	−0.01		0.12		0.03		0.12		−0.02						0.48					
820	13	C		−0.13(0.04)		−0.1(0.02)	−0.13(0.02)		−0.12(0.03)				−0.04(0.02)		−0.16(0.03)											
821	13	C		−0.02(0.08)		−0.11(0.04)	0.0(0.04)		0.08(0.03)				−0.05(0.02)		−0.21(0.01)											
822	13	C		−0.08(0.05)		−0.15(0.02)	−0.14(0.04)		−0.09(0.05)				0.09(0.02)		−0.19(0.02)											
823	13	C		−0.16(0.02)		−0.13(0.02)	−0.05(0.04)		−0.13(0.05)				0.09(0.02)		−0.12(0.01)											
824	13	C		−0.21(0.05)		−0.06(0.05)	−0.26(0.05)		−0.29(0.12)				0.11(0.03)		−0.26(0.05)											
825	13	C		−0.19(0.02)		−0.1(0.04)	−0.07(0.03)		−0.17(0.03)				0.05(0.02)		−0.22(0.03)											
826	13	C		−0.15(0.05)		−0.06(0.04)	−0.07(0.03)		−0.02(0.06)				0.09(0.02)		−0.12(0.03)											
827	13	C		−0.11(0.02)		−0.04(0.04)	−0.08(0.03)		0.02(0.1)				−0.03(0.02)		−0.14(0.04)											
828	9	O	0.87(0.17)	0.31(0.15)	0.37(0.13)	0.13(0.11)	0.29(0.1)	−0.19(0.17)	0.28(0.23)		−0.02(0.19)	0.14(0.07)	−0.32(0.14)	−0.1(0.22)	0.16(0.18)						0.35(0.06)					
829	9	O	0.36(0.08)	0.09(0.17)	0.18(0.19)	0.22(0.21)	0.08(0.13)	0.16(0.14)	−0.06(0.22)		0.07(0.17)	−0.02(0.16)	−0.06(0.13)	−0.12(0.07)	−0.03(0.19)						0.35(0.04)					
830	9	O	0.22(0.03)	0.19(0.23)	0.1(0.14)	0.16(0.12)	−0.01(0.09)	0.06(0.13)	−0.21(0.2)		−0.06(0.19)	0.04(0.16)	−0.02(0.11)	0.11(0.21)	0.02(0.16)						0.15(0.09)					
831	9	O	0.37(0.07)	0.3(0.19)	0.22(0.14)	0.31(0.18)	−0.04(0.08)	0.15(0.14)	−0.15(0.23)		−0.02(0.19)	−0.07(0.1)	−0.08(0.15)	0.0(0.17)	0.12(0.19)						0.34(0.02)					
832	9	O	0.38(0.08)	0.13(0.16)	−0.02(0.18)	0.26(0.19)	−0.04(0.16)	0.15(0.16)	−0.19(0.21)		−0.1(0.15)	−0.06(0.17)	0.01(0.16)	0.13(0.05)	0.0(0.17)						0.38(0.01)					
833	9	O	0.33(0.09)	0.15(0.16)	0.14(0.11)	0.23(0.17)	0.04(0.13)	0.1(0.09)	0.03(0.23)		0.05(0.21)	−0.05(0.14)	0.0(0.15)	−0.06(0.19)	0.19(0.1)						0.3(0.01)					
834	12	B	−0.14(0.07)			0.02(0.1)	−0.02(0.09)		−0.06(0.08)				−0.01(0.06)		−0.01(0.1)											
835	12	B	−0.07(0.08)			0.05(0.11)	0.01(0.08)		−0.02(0.09)				0.0(0.07)		−0.01(0.1)											
836	12	B	−0.35(0.11)			0.03(0.11)	−0.2(0.09)		−0.4(0.08)				0.0(0.08)		0.02(0.09)											
837	12	B	−0.03(0.06)			0.02(0.07)	0.0(0.05)		−0.03(0.06)				−0.01(0.07)		−0.03(0.06)											
838	12	B	0.0(0.08)			−0.04(0.09)	0.03(0.11)		0.0(0.06)				0.0(0.08)		−0.04(0.09)											
839	12	B	0.02(0.06)			−0.02(0.08)	0.02(0.06)		0.01(0.07)				−0.02(0.07)		−0.02(0.07)											
840	12	B	−0.13(0.08)			−0.02(0.09)	0.04(0.09)		−0.07(0.11)				0.02(0.06)		−0.05(0.11)											
841	12	B	−0.12(0.11)			0.01(0.11)	0.0(0.11)		0.02(0.09)				−0.02(0.1)		−0.03(0.13)											
842	11	B	−0.02(0.07)			0.02(0.08)	0.01(0.05)		0.0(0.07)				0.0(0.08)		−0.02(0.07)											
843	11	B	0.02(0.07)			0.02(0.07)	0.01(0.04)		0.03(0.08)				−0.02(0.08)		0.02(0.06)											
844	11	B	−0.31(0.11)			0.0(0.13)	−0.21(0.14)		−0.38(0.07)				0.01(0.08)		−0.02(0.08)											
845	11	B	−0.06(0.09)			0.04(0.09)	0.03(0.07)		−0.03(0.08)				−0.03(0.09)		0.02(0.07)											
846	11	B	−0.12(0.08)			0.01(0.09)	0.03(0.09)		0.02(0.07)				−0.02(0.07)		0.01(0.06)											
847	11	B	−0.34(0.11)			0.06(0.12)	−0.38(0.14)		−0.35(0.17)				0.0(0.09)		0.02(0.12)											
848	11	B	−0.03(0.06)			−0.01(0.08)	0.02(0.06)		0.01(0.04)				0.0(0.06)		−0.03(0.05)											

SID	CID	Ref	Na	Mg	Al	Si	Ca	Sc	Ti	V	Cr	Mn	Fe	Co	Ni	Cu	Zn	Sr	Y	Zr	Ba	La	Ce	Nd	Sm	Eu
849	41	T	0.19	0.08	0.1(0.01)	0.15(0.08)	0.06(0.16)	0.12(0.2)	0.04(0.17)	0.14(0.14)	0.1(0.11)	−0.08(0.12)	−0.02(0.11)	0.05(0.14)	0.07(0.15)	0.15(0.06)			0.02(0.22)	−0.16(0.11)	0.08	0.14(0.04)	0.11(0.02)			0.12
850	41	T	0.05	0.07	0.04(0.07)	0.14(0.08)	−0.03(0.19)	0.15(0.21)	−0.02(0.19)	0.15(0.18)	0.12(0.22)	0.07(0.24)	−0.05(0.12)	0.16(0.17)	0.1(0.15)	0.17(0.03)			0.12(0.25)	−0.3(0.09)	−0.04	0.25(0.01)	0.11(0.16)			0.25
851	41	T	0.17	0.05	0.18(0.05)	0.05(0.1)	0.11(0.18)	0.07(0.2)	0.22(0.22)	0.42(0.14)	0.24(0.17)	−0.04(0.02)	−0.02(0.12)	0.17(0.16)	0.04(0.17)	0.2(0.05)			0.13(0.18)	−0.11(0.11)	0.2	0.19	0.06(0.15)			0.02
852	41	T	0.25	0.11	0.08(0.01)	0.11(0.1)	0.09(0.12)	0.09(0.15)	−0.03(0.17)	0.09(0.12)	0.12(0.17)	0.08(0.24)	−0.01(0.11)	0.05(0.19)	0.05(0.15)	0.08(0.15)			−0.12(0.15)	−0.18(0.19)	0.07	−0.06	0.11(0.09)			0.11
853	41	T	0.21	−0.01	0.14(0.06)	0.05(0.06)	0.06(0.17)	0.1(0.17)	0.02(0.2)	0.06(0.18)	0.03(0.2)	0.04(0.23)	0.01(0.12)	0.08(0.15)	0.04(0.14)	0.11(0.12)			−0.12(0.08)	−0.19(0.21)	0.13	0.05(0.13)	0.09(0.12)			0.09
854	41	T	0.2	0.1	0.16(0.02)	0.07(0.05)	0.07(0.18)	0.09(0.17)	0.03(0.17)	0.13(0.13)	0.07(0.14)	0.11(0.17)	0.0(0.07)	0.04(0.16)	0.06(0.18)	0.17(0.07)			0.02(0.23)	−0.2(0.15)	0.02	0.17(0.02)	0.03(0.21)			0.0
855	41	T	0.18	0.07	0.15(0.01)	0.04(0.07)	0.06(0.2)	0.06(0.22)	0.19(0.21)	0.29(0.17)	0.13(0.2)	0.07(0.28)	−0.02(0.14)	0.1(0.23)	0.0(0.19)	0.21(0.1)			0.16(0.14)	−0.16(0.15)	0.15	0.2(0.01)	0.06(0.12)			−0.03
856	41	T	0.21	0.18	0.18(0.03)	0.18(0.05)	−0.03(0.25)	0.11(0.19)	−0.05(0.2)	0.05(0.14)	0.04(0.22)	−0.15(0.11)	−0.11(0.12)	0.07(0.17)	−0.05(0.18)	0.01(0.19)			−0.14(0.1)	0.0(0.23)	−0.07	0.1(0.01)	0.13(0.1)			−0.04
857	41	T	0.22	0.15	0.21(0.07)	0.09(0.08)	−0.01(0.19)	0.08(0.15)	−0.05(0.18)	−0.04(0.12)	0.03(0.22)	0.01(0.23)	−0.02(0.1)	0.03(0.16)	0.03(0.13)	0.06(0.07)			−0.02(0.11)	−0.27(0.2)	0.05	0.1(0.01)	0.08(0.1)			0.12
858	16	S	−0.26(0.22)	0.08(0.39)		−0.01(0.18)	−0.06(0.18)	−0.07(0.27)	0.01(0.26)	0.24(0.2)	−0.03(0.2)	−0.04(0.2)	0.06(0.15)	−0.27(0.27)	−0.07(0.28)			−0.03(0.15)	0.05(0.17)	0.13(0.25)	0.77(0.27)				
859	16	S	0.14(0.19)	0.0(0.4)		0.15(0.18)	0.28(0.26)	0.06(0.2)	−0.02(0.22)	0.56(0.31)	0.07(0.19)	0.23(0.27)	0.08(0.17)	0.25(0.23)	0.19(0.21)			−0.02(0.18)	0.06(0.19)	0.14(0.21)	0.66(0.28)				
860	16	S	−0.2(0.23)	0.37(0.39)		0.29(0.17)	−0.06(0.16)	−0.11(0.27)	0.06(0.3)	0.51(0.31)	−0.02(0.2)	−0.18(0.21)	0.06(0.16)	−0.07(0.59)	−0.1(0.24)			0.03(0.17)	−0.08(0.19)	0.31(0.26)	0.6(0.26)				
861	16	S	−0.17(0.17)	0.19(0.37)		0.14(0.15)	0.29(0.16)	−0.07(0.23)	0.04(0.23)	0.42(0.4)	0.0(0.17)	0.11(0.18)	0.02(0.09)	0.15(0.17)	0.01(0.22)			0.04(0.09)	0.04(0.15)	0.29(0.16)	0.74(0.25)				
862	16	S	−0.11(0.32)	0.25(0.38)		0.26(0.14)	0.25(0.2)	−0.02(0.29)	0.06(0.25)	0.27(0.34)	0.0(0.18)	0.15(0.23)	0.08(0.11)	−0.38(0.26)	0.12(0.25)			0.04(0.12)	0.03(0.19)	0.57(0.36)	0.72(0.27)				
863	29	G	−0.02(0.11)		−0.06(0.1)	0.0(0.09)	0.03(0.12)		0.02(0.14)		0.04(0.14)		0.11(0.09)		0.0(0.11)											
864	29	G	−0.07(0.11)		−0.09(0.1)	−0.02(0.09)	0.04(0.12)		−0.08(0.13)		0.01(0.14)		0.13(0.09)		−0.03(0.11)											
865	29	G	−0.07(0.11)		−0.18(0.1)	−0.08(0.09)	0.0(0.12)		−0.02(0.14)		0.02(0.15)		0.19(0.09)		−0.02(0.11)											
866	29	G	0.0(0.11)		−0.07(0.1)	−0.05(0.09)	0.06(0.12)		−0.03(0.14)		−0.07(0.14)		0.13(0.09)		−0.03(0.11)											
867	29	G	−0.03(0.11)		−0.1(0.1)	0.04(0.09)	0.03(0.12)		−0.01(0.13)		−0.03(0.13)		0.05(0.09)		−0.04(0.11)											
868	31	G	−0.05(0.12)			−0.01(0.1)	−0.03(0.13)		−0.03(0.15)		−0.03(0.16)		0.22(0.1)		0.0(0.12)											
869	31	G	0.0(0.12)			0.11(0.11)	0.02(0.14)		−0.09(0.15)		−0.06(0.16)		0.27(0.1)		−0.02(0.12)											
870	31	G	0.03(0.12)		0.02(0.11)	−0.02(0.1)	0.03(0.13)		0.0(0.15)		0.07(0.16)		0.28(0.1)		−0.02(0.12)											
871	31	G	−0.06(0.12)		−0.03(0.11)	0.0(0.1)	−0.03(0.14)		−0.01(0.16)		−0.01(0.17)		0.29(0.1)		−0.03(0.12)											
872	31	G	−0.07(0.13)		−0.09(0.12)	−0.03(0.11)	0.0(0.15)		−0.05(0.18)		0.05(0.18)		0.26(0.11)		−0.01(0.13)											
873	31	G	−0.08(0.13)		−0.09(0.12)	−0.06(0.12)	0.0(0.14)		−0.01(0.16)		0.03(0.17)		0.35(0.11)		−0.02(0.14)											
874	31	G	−0.09(0.12)		−0.13(0.11)	−0.04(0.11)	0.01(0.13)		−0.11(0.15)		0.02(0.16)		0.24(0.1)		−0.04(0.13)											
875	30	G	−0.03(0.11)		0.06(0.1)	−0.12(0.09)	0.05(0.12)		−0.01(0.15)		0.08(0.15)		0.07(0.09)		−0.07(0.1)											
876	30	G	−0.03(0.12)		−0.07(0.11)	−0.04(0.1)	0.06(0.13)		0.01(0.15)		0.08(0.16)		0.03(0.1)		0.02(0.12)											
877	30	G	0.02(0.11)		−0.05(0.1)	0.01(0.09)	0.04(0.12)		0.06(0.13)		0.01(0.14)		0.07(0.09)		0.0(0.11)											
878	30	G	−0.01(0.12)			0.01(0.1)	0.02(0.13)		−0.02(0.15)		0.03(0.16)		0.01(0.1)		0.03(0.12)											
879	30	G	0.01(0.11)		−0.15(0.1)	0.0(0.09)	0.03(0.12)		−0.03(0.13)		−0.01(0.14)		0.03(0.09)		−0.01(0.11)											
880	30	G	−0.04(0.11)			−0.01(0.09)	−0.01(0.12)		−0.12(0.13)		−0.03(0.14)		−0.04(0.09)		−0.06(0.11)											
881	15	R	−0.13(0.06)	0.21(0.22)		0.01(0.11)		−0.09(0.09)	−0.09(0.11)	0.35(0.16)	−0.04(0.11)	−0.15(0.09)	0.09(0.05)	−0.1(0.26)	0.04(0.09)			0.11(0.16)	−0.09(0.09)	−0.05(0.12)	0.77(0.11)				
882	15	R	−0.18(0.25)	0.26(0.25)		0.07(0.2)		−0.26(0.23)	−0.18(0.23)	0.43(0.25)	−0.08(0.19)	−0.15(0.19)	0.19(0.17)	0.25(0.31)	0.02(0.28)			−0.2(0.17)	−0.18(0.18)	−0.23(0.19)	0.45(0.29)				
883	15	R	0.02(0.26)	0.38(0.24)		0.2(0.18)		0.07(0.23)	0.08(0.22)	0.5(0.37)	0.12(0.2)	0.16(0.19)	−0.08(0.16)	0.72(0.21)	0.04(0.18)			0.23(0.16)	0.12(0.18)	0.58(0.22)	0.73(0.26)				
884	15	R	−0.09(0.16)	0.27(0.2)		0.08(0.11)		−0.22(0.19)	0.03(0.19)	0.42(0.45)	−0.07(0.2)	−0.1(0.11)	0.18(0.08)	0.11(0.26)	−0.2(0.2)			−0.06(0.13)	0.06(0.21)	0.2(0.12)	0.41(0.18)				
885	15	R	−0.19(0.06)	0.14(0.19)		0.13(0.13)		−0.14(0.09)	0.05(0.08)	0.59(0.11)	0.01(0.09)	−0.08(0.08)	0.09(0.05)	−0.19(0.33)	−0.15(0.07)			0.05(0.18)	0.01(0.13)	0.04(0.18)	0.75(0.11)				
886	15	R	0.01(0.15)	0.24(0.14)		−0.02(0.29)		−0.09(0.17)	0.1(0.13)	0.3(0.34)	−0.13(0.12)	−0.35(0.32)	0.15(0.09)	−0.17(0.26)	0.06(0.14)			0.12(0.22)	−0.09(0.22)	−0.28(0.17)	0.28(0.17)				
887	15	R	−0.28(0.13)	0.25(0.22)					0.03(0.26)	0.49(0.29)	0.18(0.15)	0.0(0.18)	0.15(0.13)	−0.45(0.31)	−0.03(0.15)					−0.01(0.21)	0.41(0.16)				
888	15	R	−0.14(0.24)	0.14(0.21)					0.17(0.17)	0.11(0.38)	0.37(0.14)	0.12(0.17)	0.01(0.11)	−0.36(0.32)	0.08(0.14)					0.02(0.2)	0.53(0.15)				
889	15	R	−0.01(0.25)	0.17(0.21)					0.19(0.18)	0.52(0.27)	0.33(0.14)	0.06(0.13)	0.05(0.11)	−0.35(0.36)	0.03(0.14)					−0.11(0.2)	0.54(0.15)				
890	15	R	0.03(0.24)	0.14(0.23)					0.1(0.21)	0.57(0.18)	0.23(0.16)	−0.45(0.18)	−0.01(0.14)	−0.28(0.21)	0.04(0.19)					−0.49(0.22)	0.3(0.17)				
891	15	R		0.44(0.25)					0.02(0.27)	0.43(0.17)			−0.03(0.17)	0.48(0.41)	0.32(0.22)					−0.01(0.24)	0.4(0.2)				
893	36	E		0.0		−0.01	−0.13		−0.19		0.14				0.04											
894	36	E		0.0		0.0	−0.02		−0.02		0.0				−0.02											
895	36	E		−0.04		0.0	0.04		0.09		−0.06				−0.08											
896	36	E		−0.05		−0.14	−0.01		−0.1		−0.09				−0.1											
897	36	E		0.37		−0.19	0.22		0.25		0.01				−0.08											
898	36	E		0.23		0.02	0.13		0.09		−0.09				−0.09											
899	36	E		−0.03		0.08	0.06		0.11		0.02				−0.06											
900	36	E		0.06		0.01	−0.11		0.61		−0.01				0.21											
901	36	E		−0.05		0.28	0.14		0.07		−0.18				−0.13											
902	36	E		−0.13		−0.13	0.19		0.28		0.08				−0.03											
903	36	E		0.07		0.14	0.04		0.44		0.17				0.19											
904	36	E		−0.02		−0.04	−0.09		0.48		0.25				0.22											
905	36	E		0.08		0.25	0.15		0.24		−0.2				−0.09											
906	36	E		0.01		−0.03	0.17		0.19		−0.04				−0.04											
907	36	E		−0.15		0.4	0.14		0.25		−0.11				0.04											
908	36	E		0.15		0.3	−0.23		0.31		−0.12				0.33											
909	36	E		−0.05		0.48	−0.1		0.3		−0.01				0.34											
910	36	E		0.17		0.27	−0.06		0.38		−0.12				0.3											
911	38	M		−0.02		0.04(0.09)	0.07(0.1)	0.01	−0.04(0.11)	0.03(0.14)	0.03(0.08)			0.05(0.11)	−0.02(0.05)											
912	38	M		−0.05		0.1(0.07)	0.03(0.05)	0.19	−0.03(0.16)	0.09(0.12)	0.11(0.1)			0.12(0.15)	0.03(0.09)											
913	38	M		−0.06		0.1(0.09)	−0.05(0.04)	0.02	−0.06(0.05)	0.01(0.15)	−0.04(0.18)			0.05(0.19)	−0.01(0.05)											
914	38	M		−0.05		0.01(0.06)	0.04(0.09)	0.03	−0.04(0.1)	−0.06(0.08)	0.05(0.08)			0.02(0.14)	−0.02(0.05)											
915	38	M		−0.07		0.02(0.04)	0.04(0.09)	0.07	−0.06(0.04)	−0.05(0.07)	0.03(0.09)			0.06(0.14)	−0.01(0.05)											
916	37	M		−0.07		0.06(0.06)	0.1(0.12)	−0.04	−0.01(0.08)	−0.01(0.09)	0.0(0.1)			0.03(0.13)	−0.01(0.07)											
917	37	M		−0.03		0.14(0.09)	0.02(0.06)	−0.07	−0.04(0.08)	−0.04(0.13)	−0.04(0.11)			0.01(0.14)	0.0(0.07)											
918	37	M		−0.03		0.08(0.16)	0.15(0.12)	−0.08	−0.03(0.13)	0.05(0.1)	0.06(0.17)			0.12(0.14)	−0.01(0.08)											

SID	CID	Ref	Na	Mg	Al	Si	Ca	Sc	Ti	V	Cr	Mn	Fe	Co	Ni	Cu	Zn	Sr	Y	Zr	Ba	La	Ce	Nd	Sm	Eu
919	37	M		0.0		0.09(0.11)	0.13(0.11)	0.04	−0.02(0.1)	0.02(0.14)	0.03(0.06)			0.1(0.18)	−0.01(0.09)											
920	37	M		−0.23		0.14(0.11)	0.04(0.04)	0.12	0.01(0.09)	0.16(0.16)	−0.01(0.13)			0.13(0.25)	0.16(0.15)											
921	39	M		−0.01		0.06(0.07)	0.03(0.15)	0.0	0.04(0.04)	0.05(0.14)	0.06(0.1)			0.1(0.15)	0.01(0.06)											
922	39	M		−0.02		−0.04(0.04)	0.0(0.06)	−0.17	−0.02(0.1)	0.0(0.08)	0.03(0.1)			0.03(0.15)	−0.03(0.05)											
923	39	M		0.03		0.17(0.08)	0.06(0.14)	0.06	−0.04(0.06)	0.02(0.13)	0.04(0.1)			0.08(0.15)	0.05(0.05)											
924	39	M				0.13(0.12)	−0.02(0.06)	0.03	−0.02(0.08)	0.11(0.16)	−0.03(0.17)			0.06(0.2)	0.05(0.09)											
925	39	M				0.11(0.09)	0.0(0.08)	0.03	−0.01(0.08)	0.12(0.15)	0.02(0.07)			0.12(0.2)	0.08(0.13)											
926	17	L	0.23(0.14)		0.12(0.1)	0.05(0.1)	0.0(0.08)	0.0(0.07)	0.06(0.15)						0.0(0.1)						0.18(0.12)				0.0(0.15)
927	17	L	0.24(0.12)		0.22(0.1)	0.25(0.1)	0.0(0.09)	0.0(0.06)	0.01(0.12)					0.0(0.15)	0.0(0.1)						0.03(0.12)				0.0(0.15)
928	17	L	0.03(0.13)		0.22(0.1)	0.27(0.1)	0.0(0.07)	0.08(0.07)	0.08(0.15)					0.0(0.15)	0.0(0.1)						0.27(0.12)				0.0(0.15)
929	17	L	0.32(0.14)		0.22(0.1)	0.35(0.1)	0.0(0.07)	0.0(0.07)	0.01(0.12)					0.0(0.15)	0.0(0.1)						0.18(0.12)				0.0(0.15)
930	33	D				−0.01(0.22)	0.09(0.18)		−0.01(0.2)		−0.1(0.18)				−0.1(0.17)						0.4(0.25)				
931	33	D				0.13(0.28)	0.12(0.2)		0.02(0.2)		−0.06(0.2)				0.01(0.18)						0.46(0.37)				
932	33	D				−0.01(0.16)	0.14(0.18)		0.07(0.19)		−0.1(0.2)				−0.03(0.2)						0.46(0.4)				
933	33	D				0.05(0.12)	0.04(0.16)		0.06(0.15)		−0.13(0.16)				−0.08(0.13)						0.37(0.17)				
934	33	D				−0.05(0.16)	0.08(0.19)		−0.03(0.19)		−0.11(0.18)				−0.04(0.2)						0.37(0.2)				
935	33	D				0.05(0.14)	0.12(0.15)		0.42(0.22)		0.03(0.29)				0.08(0.21)						0.53(0.12)				
936	35	D				0.13(0.09)	0.15(0.18)		−0.02(0.14)		−0.01(0.15)				−0.02(0.11)						0.32(0.13)				
937	35	D				0.14(0.1)	0.09(0.15)		−0.02(0.14)		0.02(0.15)				−0.01(0.14)						0.3(0.1)				
938	35	D				0.1(0.1)	0.1(0.17)		0.01(0.13)		−0.06(0.11)				−0.05(0.12)						0.29(0.1)				
939	35	D				0.14(0.11)	0.07(0.14)		−0.05(0.12)		−0.05(0.14)				−0.02(0.11)						0.47(0.09)				
940	35	D				0.1(0.1)	0.06(0.13)		0.08(0.11)		−0.02(0.13)				0.0(0.09)						0.26(0.1)				
941	35	D				0.16(0.11)	0.08(0.14)		0.01(0.11)		0.03(0.15)				0.03(0.11)						0.36(0.1)				
942	34	D				0.17(0.22)	0.03(0.2)		0.24(0.2)		0.08(0.21)				0.08(0.18)						0.3(0.11)				
943	34	D				0.03(0.16)	−0.04(0.2)		−0.03(0.17)		−0.05(0.18)				0.0(0.16)						0.26(0.13)				
944	34	D				0.14(0.19)	−0.12(0.14)		0.06(0.15)		−0.04(0.17)				0.11(0.16)						0.29(0.12)				
945	34	D				0.03(0.25)	−0.03(0.15)		0.22(0.19)		0.04(0.19)				0.1(0.17)						0.23(0.1)				
946	34	D				0.07(0.15)	−0.03(0.16)		0.07(0.14)		0.1(0.18)				0.06(0.14)						0.31(0.09)				
947	34	D				0.09(0.12)	−0.03(0.15)		0.14(0.16)		0.07(0.18)				0.04(0.17)						0.25(0.09)				
948	34	D				0.09(0.18)	−0.07(0.16)		−0.01(0.15)		0.0(0.19)				0.11(0.17)						0.31(0.11)				
1004	10	I	0.28(0.08)	0.07(0.06)		0.24(0.05)	0.08(0.06)					0.01(0.04)	0.0(0.03)		−0.08(0.05)					0.03(0.13)	0.02(0.08)					
1005	10	I	0.16(0.08)	0.2(0.06)		0.23(0.05)	−0.08(0.06)					0.0(0.04)	−0.01(0.03)		−0.1(0.05)					0.06(0.13)	0.04(0.08)					
1006	10	I	0.11(0.08)	0.13(0.06)		0.13(0.05)	−0.02(0.06)					−0.07(0.04)	0.0(0.03)		−0.01(0.05)					0.06(0.13)	0.01(0.08)					
1007	10	I	0.03(0.08)	0.22(0.06)		0.13(0.05)	0.03(0.06)					−0.04(0.04)	−0.03(0.03)		0.01(0.05)					−0.19(0.13)	0.0(0.08)					
1008	10	I	0.09(0.08)	0.11(0.06)		0.21(0.05)	0.01(0.06)					0.0(0.04)	−0.02(0.03)		0.02(0.05)					−0.03(0.13)	0.04(0.08)					
1009	10	I	0.12(0.08)	0.09(0.06)		0.11(0.05)	−0.07(0.06)					0.0(0.04)	−0.01(0.03)		−0.06(0.05)					0.1(0.13)	0.0(0.08)					
1010	10	I	−0.01(0.08)	0.13(0.06)		0.2(0.05)	0.01(0.06)					−0.05(0.04)	0.02(0.03)		−0.09(0.05)					−0.15(0.13)	0.01(0.08)					
1011	10	I	0.15(0.08)	0.17(0.06)		0.25(0.05)	0.02(0.06)					−0.1(0.04)	−0.01(0.03)		−0.03(0.05)					−0.29(0.13)	0.02(0.08)					
1012	10	I	0.32(0.08)	0.31(0.06)		0.3(0.05)	0.25(0.06)					0.05(0.04)	0.04(0.03)		0.08(0.05)					0.13(0.13)	0.24(0.08)					
1013	10	I	0.13(0.08)	0.17(0.06)		0.23(0.05)	0.07(0.06)					−0.05(0.04)	0.01(0.03)		−0.04(0.05)					0.04(0.13)	0.0(0.08)					
1014	10	I	0.11(0.08)	0.11(0.06)		0.15(0.05)	−0.03(0.06)					−0.04(0.04)	−0.03(0.03)		−0.07(0.05)					−0.06(0.13)	0.01(0.08)					
1015	10	I	0.11(0.08)	0.03(0.06)		0.11(0.05)	−0.04(0.06)					−0.04(0.04)	−0.01(0.03)		−0.1(0.05)					−0.03(0.13)	0.02(0.08)					
1016	44	P		0.18()	−0.03(0.19)	0.03(0.22)	0.04(0.18)	0.05(0.19)	−0.08(0.2)		−0.2()				0.03(0.28)				0.04(0.26)	0.09(0.17)		0.29(0.22)	0.02(0.26)	0.22(0.28)		
1017	44	P		0.17()	−0.04(0.2)	−0.08(0.19)	−0.09(0.17)	−0.1(0.2)	−0.1(0.07)		0.06()				0.01(0.19)					−0.21(0.28)		−0.17(0.17)				
1018	44	P		0.6()	0.17(0.16)	0.36(0.17)	0.13(0.12)	−0.01(0.15)	−0.15(0.13)		0.18(0.13)				−0.1(0.2)				0.02(0.14)			0.02(0.22)	0.13(0.27)	0.26(0.24)		
1019	44	P		0.17()	−0.16(0.18)	0.0(0.21)	0.0(0.21)	0.0(0.25)	−0.27(0.19)		−0.05()				−0.07(0.22)				−0.02(0.31)	−0.16(0.18)		0.26(0.23)	0.17(0.26)	0.34()		
1020	44	P		0.2(0.17)	0.07(0.17)	0.07(0.18)	−0.1(0.15)	−0.15(0.12)	0.05(0.19)		−0.13()				−0.13(0.17)				−0.04(0.08)	0.2(0.09)		0.25(0.19)	0.17(0.19)	0.26(0.14)		
1021	44	P			0.16(0.32)	0.31(0.21)	0.1(0.25)	0.1(0.23)	−0.13()		−0.11()				−0.08(0.22)				−0.04(0.25)	−0.06(0.2)		0.25(0.23)	0.23(0.26)	0.18(0.2)		
1022	44	P				0.16(0.21)	−0.11()	0.2(0.23)	−0.22()		−0.2()				−0.15(0.24)					−0.06(0.08)		0.29()	0.12()	0.31(0.17)		
1023	46	H		0.1(0.1)	0.05(0.2)	0.23(0.15)	−0.24(0.15)		0.08(0.13)		0.2(0.14)		0.05(0.09)		−0.05(0.13)											
1024	46	H		−0.04(0.16)	−0.03(0.14)	−0.07(0.14)	−0.18(0.13)		−0.15(0.14)		−0.02(0.16)		0.07(0.09)		0.13(0.13)											
1025	46	H		−0.05(0.16)	0.15(0.14)	0.14(0.12)	−0.26(0.12)		−0.07(0.12)		−0.02(0.11)		0.2(0.09)		0.17(0.13)											
1026	46	H		0.0(0.11)	−0.05(0.08)	0.08(0.14)	−0.13(0.13)		0.12(0.12)		−0.04(0.14)		0.11(0.1)		0.0(0.15)											
1027	45	H		−0.16(0.16)	−0.08(0.14)	0.14(0.14)	−0.08(0.13)		−0.09(0.14)		−0.09(0.14)		0.19(0.07)		0.02(0.13)											
1028	45	H		−0.01(0.16)	0.14(0.14)	0.0(0.12)	0.02(0.12)		0.03(0.12)		0.04(0.11)		0.08(0.08)		−0.11(0.13)											
1029	45	H		−0.07(0.11)	0.03(0.2)	0.0(0.15)	−0.04(0.15)		−0.02(0.13)		−0.03(0.14)		0.13(0.1)		−0.05(0.13)											
1030	45	H		−0.04(0.11)	0.03(0.08)	0.05(0.14)	−0.09(0.13)		−0.04(0.12)		0.01(0.11)		0.07(0.08)		−0.05(0.15)											
1031	47	K	0.21(0.04)	0.0(0.04)	−0.12(0.01)	0.01(0.19)	0.0(0.1)	−0.06()				0.03(0.1)			−0.05(0.27)						0.13(0.14)					0.03()
1032	47	K	0.23(0.07)	0.02(0.09)	−0.19(0.07)	0.07(0.21)	−0.06(0.1)	−0.06()				0.1(0.09)			−0.05(0.27)						0.18(0.21)					0.03()
1033	47	K	0.18	0.05(0.04)	−0.09(0.01)	0.14(0.2)	−0.16(0.13)	−0.06()				0.07(0.08)			−0.05(0.27)						0.13(0.14)					0.03()
1034	47	K	0.23(0.07)	−0.03(0.01)	0.1(0.01)	0.14(0.13)	0.13(0.15)	−0.05(0.1)				−0.05(0.14)			−0.05(0.02)						0.2(0.16)					0.03()
1035	48	K		0.24(0.09)	−0.24(0.01)	−0.06(0.17)	−0.16(0.08)	−0.23(0.14)	0.01()			0.13(0.16)			0.0(0.23)						0.43(0.1)					
1036	48	K		0.24(0.14)	−0.17(0.01)	0.12(0.17)	−0.06()	−0.08(0.13)	−0.04()			0.1(0.22)			−0.03(0.33)						0.31(0.03)					
1037	48	K		0.18(0.23)	−0.32(0.01)	−0.11(0.1)	−0.26()	−0.1(0.09)	0.16()			0.1(0.1)			−0.15(0.13)						0.21(0.2)					
1038	48	K		0.14(0.15)	−0.12(0.01)	0.02(0.11)	−0.13(0.19)	−0.1(0.01)	0.01()			−0.03(0.03)			−0.08(0.33)						0.15(0.18)					
1039	49	U	0.13(0.05)	−0.01(0.07)	0.19(0.04)	0.12(0.05)	0.01(0.07)	0.07(0.04)	−0.03(0.06)	0.11(0.06)	−0.02(0.05)	−0.11()	−0.04(0.05)	−0.03(0.05)	0.01(0.03)	−0.03()	−0.09		0.03(0.01)	0.06(0.01)	0.14()	0.15(0.06)	0.13()	0.07(0.09)	0.08()	0.1()
1040	49	U	0.1(0.03)	0.02(0.05)	0.11(0.03)	0.03(0.05)	0.03(0.05)	0.06(0.1)	−0.14(0.04)	−0.05(0.07)	−0.07(0.04)	−0.18()	−0.02(0.06)	−0.08(0.05)	−0.04(0.06)	−0.12()			−0.01(0.04)	−0.05(0.01)	0.12()	0.07(0.08)	0.08()	0.02(0.04)		0.0()
1041	49	U	0.14(0.02)	−0.06(0.05)	0.14(0.04)	0.11(0.07)	0.06(0.05)	0.12(0.03)	−0.02(0.06)	0.05(0.04)	−0.04(0.07)	−0.12()	−0.05(0.05)	0.0(0.08)	−0.01(0.05)	−0.15()	−0.07		0.06(0.02)	0.16(0.02)	0.16()	0.14(0.06)	0.14()	0.06(0.03)	0.07()	0.09()
1042	49	U	0.13(0.07)	−0.01(0.04)	0.17(0.02)	0.18(0.06)	0.01(0.06)	0.03(0.05)	−0.08(0.06)	0.03(0.05)	0.0(0.06)	−0.1()	−0.04(0.05)	0.04(0.06)	0.0(0.05)	−0.13()	−0.14		0.03(0.03)	0.06(0.01)	0.11()	0.16(0.06)	0.16()	0.1(0.04)	0.11()	0.08()

SID	CID	Ref	Na	Mg	Al	Si	Ca	Sc	Ti	V	Cr	Mn	Fe	Co	Ni	Cu	Zn	Sr	Y	Zr	Ba	La	Ce	Nd	Sm	Eu
1043	50	U	0.14(0.07)	−0.06(0.01)	0.18(0.06)	0.14(0.06)	0.03(0.05)	0.19(0.01)	0.04(0.04)	0.23(0.05)	0.0(0.05)	−0.14()	−0.07(0.07)	0.17(0.07)	−0.02(0.06)	−0.2()			0.14(0.03)	0.13(0.02)	0.06()		0.18()		0.13()	
1044	50	U	0.23(0.06)	0.13(0.07)	0.0(0.01)	0.18(0.06)	0.14(0.06)	0.14(0.06)	0.02(0.07)	0.04(0.06)	0.02(0.06)	−0.18()	−0.13(0.05)	0.0(0.07)	0.01(0.04)	−0.16()	0.05		0.08(0.05)	0.16(0.01)	0.13()	0.17(0.1)	0.19()			
1045	50	U	0.21(0.05)	0.13(0.08)	0.19(0.05)	0.14(0.05)	0.16(0.04)	0.05(0.06)	0.01(0.05)	0.06(0.05)	0.02(0.03)	−0.2()	−0.05(0.06)	0.05(0.06)	0.02(0.06)	−0.23()			−0.04(0.06)	0.1(0.06)	0.11()	0.17(0.09)			0.12()	
1046	50	U	0.24(0.04)	0.1(0.04)	−0.01(0.05)	0.16(0.06)	0.13(0.06)	−0.1(0.06)	−0.18(0.07)	−0.01(0.07)	0.02(0.05)		−0.06(0.07)	0.03(0.09)	0.04(0.08)	−0.13()	0.03		0.07(0.06)	−0.06(0.06)		0.08(0.09)			0.13()	
1217	28	Q	0.05(0.11)	−0.05(0.07)	−0.06(0.07)	0.04(0.08)	−0.15(0.09)		0.18(0.06)		0.01(0.07)		0.04(0.08)		−0.07(0.08)		−0.34(0.06)		0.25(0.1)		0.16(0.07)	0.36(0.06)		0.56(0.08)		
1219	28	Q	0.13(0.11)	0.0(0.07)	0.12(0.07)	0.07(0.08)	−0.09(0.09)		0.22(0.06)		0.09(0.07)		−0.01(0.08)		0.01(0.08)		−0.38(0.06)		0.23(0.1)		0.16(0.07)	0.31(0.06)		0.56(0.08)		
1226	28	Q	0.22(0.11)	−0.14(0.07)	0.08(0.07)	0.1(0.08)	−0.09(0.09)		0.24(0.06)		0.04(0.07)		0.06(0.08)		−0.05(0.08)		−0.31(0.06)		0.1(0.1)		0.18(0.07)	0.24(0.06)		0.44(0.08)		
1232	28	Q	0.12(0.11)	−0.01(0.07)	0.16(0.07)	0.01(0.08)	−0.03(0.09)		0.29(0.06)		0.11(0.07)		0.09(0.08)		−0.03(0.08)		−0.43(0.06)		0.13(0.1)		0.12(0.07)	0.29(0.06)		0.51(0.08)		
1233	28	Q	0.16(0.11)	−0.01(0.07)	0.1(0.07)	−0.02(0.08)	−0.11(0.09)		0.21(0.06)		0.1(0.07)		0.04(0.08)		−0.1(0.08)		−0.5(0.06)		0.09(0.1)		0.06(0.07)	0.26(0.06)		0.56(0.08)		
1240	28	Q	0.04(0.11)	−0.15(0.07)	0.02(0.07)	−0.03(0.08)	−0.09(0.09)		0.07(0.06)		0.07(0.07)		−0.11(0.08)		−0.04(0.08)		−0.48(0.06)		0.19(0.1)		0.21(0.07)			0.21(0.08)		
1247	28	Q	0.11(0.11)	−0.01(0.07)	0.18(0.07)	0.03(0.08)	−0.06(0.09)		0.25(0.06)		0.12(0.07)		0.03(0.08)		0.0(0.08)		−0.42(0.06)		0.11(0.1)		0.13(0.07)	0.27(0.06)		0.55(0.08)		
1250	28	Q	0.18(0.11)	0.05(0.07)	0.27(0.07)	0.15(0.08)	−0.03(0.09)		0.21(0.06)		0.14(0.07)		−0.13(0.08)		−0.03(0.08)		−0.49(0.06)		0.24(0.1)		0.03(0.07)	0.43(0.06)		1.09(0.08)		
1230	28	Q	−0.16(0.12)	−0.16(0.05)		0.0(0.08)	−0.05(0.06)		0.15(0.07)		0.04(0.17)		−0.07(0.07)		−0.03(0.07)		−0.29(0.03)		0.11(0.04)							
1241	28	Q	−0.06(0.12)	−0.11(0.05)		0.01(0.08)	−0.04(0.06)		0.07(0.07)		−0.07(0.17)		−0.15(0.07)		−0.1(0.07)		−0.23(0.03)		0.12(0.04)							
1211	28	Q	−0.15(0.12)	−0.11(0.05)		0.01(0.08)	−0.01(0.06)		0.11(0.07)		−0.16(0.17)		−0.17(0.07)		−0.09(0.07)		−0.16(0.03)		0.11(0.04)							

TABLE B.1: Sources and designations used in the literature abundance database

Source reference	Label
Soderblom et al. (2009)	A
D'Orazi & Randich (2009)	B
Ford et al. (2005)	C
Sestito et al. (2008b)	D
Shen et al. (2005)	E
Bragaglia et al. (2008b)	F
Pace et al. (2008a)	G
Magrini et al. (2010)	H
De Silva et al. (2007a)	I
Randich et al. (2006)	J
Carretta et al. (2007)	K
Gonzalez & Wallerstein (2000b)	L
De Silva et al. (2006), Paulson et al. (2003)	N
Carretta et al. (2005)	O
Pereira & Quireza (2010)	P
Mitschang et al. (2012)	Q
Gebran et al. (2008)	R
Gebran & Monier (2008)	S
Tautvaišiene et al. (2000b)	T
Reddy et al. (2012)	U

Appendix C

Procedure for Group Finding

Herein is described, in greater detail, the group finding procedure used in Mitschang et al. (2014) to identify coeval associations of stars. The procedure is physically, as opposed to statistically, motivated, meaning that each star can only be associated with a single group. The preferred association for a single star with multiple possible associations is that which has the highest conatal pair probability to a star already associated with that group.

The following steps are carried out. In this description, a vector is represented with angle brackets, e.g. vector X is denoted as $\langle X \rangle$. Square brackets denote a vector element, indexing from 0, e.g. $X[0]$ would be the first element of X.

1.) $\delta_{\rm C}$ values are calculated for all pairs of stars in the sample, collated as $\langle D \rangle$, where each element of $\langle D \rangle$ is a $\delta_{\rm C}$ value associated with a single pair of stars.

2.) $\langle D \rangle$ is sorted so that $D[0] = min(\langle D \rangle)$

3.) All $\delta_{\rm C}$ in $\langle D \rangle$ whose value is greater than $\delta_{\rm C}(P_{\rm lim})$ are removed, creating $\langle D_p \rangle$

4.) Set index i to 0

5.) let A be one star associated with the $\delta_{\rm C}$ pair at $D_p[i]$, and B be the other star associated with that same pair.

6.) If neither A nor B are already members of some group, a new group G is established with A and B.

7.) If A(or B) is a member of some group G and if all pairings of B(or A) with members of G exist within $\langle D_p \rangle$, then B(or A) becomes a member of G.

8.) Set index $i = i + 1$

9.) Goto step 5

Below is the complete table of HIP number to group number (Table 2 of Chapter 5) for the 68% probability threshold chemical tagging of the Bensby et al. (2014) sample.

HIP	GID	HIP	GID	HIP	GID	HIP	GID	HIP	GID	HIP	GID
80	6	17147	8	44896	14	73650	3	92864	1	109110	15
305	13	17378	39	44915	1	74033	8	92880	21	109144	19
407	1	17970	41	45283	28	74067	8	92973	44	109207	24
699	18	17987	4	45514	2	74079	47	93185	22	109214	21
768	19	18331	60	45733	48	74389	1	93377	7	109378	30
910	25	18612	3	46685	17	74500	5	93889	5	109381	13
950	15	18802	47	46888	18	74537	12	93966	39	109450	7
1128	28	19233	3	47048	52	74831	48	94645	49	109650	22
1349	9	19773	9	47588	2	75181	2	94678	12	109795	18
1599	18	20199	20	48468	27	75487	33	95106	16	109821	3
1746	4	20242	26	49285	12	76226	34	95262	4	110028	1
1877	26	20489	5	49793	6	76394	19	95447	65	110035	38
1931	11	20638	4	49942	2	76899	20	96124	2	110084	2
1976	13	21079	15	50274	53	76984	13	96160	16	110102	26
2021	19	21731	30	50316	1	77358	1	96258	31	110109	14
2057	21	21832	35	50671	25	77439	6	96425	29	110341	31
2194	64	21839	20	50907	65	77536	27	96536	42	110454	23
2319	34	22162	42	50941	8	77637	8	96854	24	110468	62
2711	61	22263	15	51028	33	77641	24	96881	29	110512	2
2909	12	22278	1	51078	5	78330	4	97024	2	110712	32
3026	58	22325	49	51579	5	78425	21	97213	5	110843	5
3086	20	22336	5	51614	27	78551	7	97358	15	111274	12
3142	25	22349	2	51933	18	78556	2	97676	1	111312	26
3170	26	22395	32	51938	4	78955	11	97779	16	111517	2
3182	2	22824	21	52325	7	79073	60	98355	9	111565	4
3391	63	23383	12	52990	32	79137	30	98416	19	111648	40
3479	21	23555	56	53122	50	79138	10	98565	52	111746	10
3497	2	24037	4	53719	29	79576	8	98767	30	112151	43
3704	14	24682	10	53765	23	79715	1	98785	61	112201	1
3734	31	24722	2	53982	27	79792	1	98964	17	112243	55
3909	16	24819	57	54043	28	80013	12	99100	17	113044	5
4830	1	24829	42	54469	48	80221	35	99139	4	113113	3
4892	14	25209	61	54779	4	80337	15	99174	56	113137	30
5264	13	25905	14	54924	8	80423	6	99224	17	113357	5
5301	38	26273	41	55210	53	80587	45	99240	11	113386	7
5315	40	27072	67	55278	5	80686	15	99551	12	113421	11
5700	3	27080	35	55805	66	80700	7	99799	10	113454	22
5862	36	27128	8	56004	13	80722	37	100405	41	113543	26
6177	51	27910	29	56336	9	81041	44	100412	14	113677	21
6607	4	28044	20	56389	3	81269	39	100568	58	113688	3
6653	1	28066	12	56557	7	81300	46	100792	58	113777	2
6949	4	28159	4	56664	33	81461	6	100942	1	114040	17
7080	11	28267	17	56845	2	81520	54	100970	3	114333	1
7091	7	28403	10	56868	4	81580	34	101346	9	114450	3
7276	11	29271	29	57017	23	81603	7	101399	30	114460	7
7961	28	29716	31	57216	10	81749	4	101857	3	114576	7
7978	15	30158	7	58145	66	82062	9	102018	36	114584	22
8398	5	30439	6	58153	6	82265	13	102046	66	114590	5
8498	1	30476	55	58401	62	82588	16	102200	54	114615	16
8758	1	30480	11	58517	1	82621	32	102264	22	114709	23
8798	2	30503	1	58576	11	83204	37	102548	22	114743	12
8859	23	30545	19	58843	8	83229	4	102580	32	115286	20
9085	22	31030	9	58950	14	83241	3	102610	37	115411	41
9137	23	32649	2	59021	19	83276	3	102762	1	115577	17
9316	63	33094	17	59380	9	83489	2	102793	44	115662	1
9381	2	33324	6	59639	51	83562	2	102838	2	115792	31
9471	17	33582	44	59699	6	83601	49	103458	45	115803	16
9629	53	33642	12	60019	22	83867	22	103498	59	115917	9
9818	12	34065	10	60288	13	84255	9	103572	6	116033	3
9911	13	34069	53	60462	41	84551	42	103609	40	116410	10
10116	1	34212	19	60574	50	84636	11	103654	1	116421	43
10483	3	34254	19	60729	36	84781	2	103682	11	116478	7
10492	11	34410	37	60825	33	84905	43	103692	63	116906	1
10694	7	34511	16	60956	35	84907	38	103735	26	117320	36
10798	54	34739	2	61619	67	84988	6	103773	18	117364	3
10977	46	34961	4	61971	34	85007	23	103881	52	117526	56
11072	19	35139	9	62534	4	85042	7	103896	18	117627	10
11205	7	35148	20	62607	64	85320	21	103990	27	117880	39
11309	25	35318	9	62857	1	85757	6	104045	1	117902	24
11586	52	35718	17	63918	6	85963	33	104075	15	117961	13
12048	36	35750	46	64345	6	85969	1	104152	1	118010	3
12186	39	36210	1	64408	5	86013	8	104294	10	118115	3
12306	45	36491	59	64426	45	86193	13	104560	9	118141	23
12381	18	36515	15	64444	48	86516	18	104659	59	118143	32
12411	21	36795	31	64459	10	86731	5	104672	3		
12444	15	36849	47	64673	1	86796	5	104766	18		
12483	6	36855	24	64698	20	87154	27	104922	1		
12611	65	36874	46	64706	51	87443	1	105083	37		
12653	49	36993	56	64747	14	87523	25	105214	13		
12889	21	37233	43	64792	60	87533	3	105521	5		
13315	37	37419	10	64924	7	87539	8	105541	21		
13341	1	37520	11	66238	20	87679	24	105606	11		
13350	14	37853	8	66814	35	87769	1	105790	2		
13366	6	38134	8	67371	5	87841	1	105858	34		
13848	24	38750	50	67534	11	88622	4	106006	5		
13902	14	38782	7	67784	16	88631	30	106560	6		
13938	27	38862	20	67863	8	88945	15	106678	17		
14016	12	38926	25	68273	4	89036	3	106701	16		
14023	29	39911	47	68468	1	89076	1	106931	14		
14086	28	40613	28	68796	54	89105	16	106951	20		
14241	40	40761	5	69220	3	89207	16	107607	6		
14339	38	40794	2	69645	32	89583	2	107618	10		
14879	18	41471	1	69780	64	89589	3	107708	25		
14954	11	42356	1	69796	38	89733	6	107857	8		
15131	9	42612	3	70140	6	89952	9	107877	18		
15158	1	42734	43	70182	45	90004	2	108068	4		
15371	14	42889	2	70330	36	90442	4	108095	23		
15381	7	43054	3	70922	8	90485	42	108158	17		
15510	40	43393	35	71019	4	90896	5	108288	10		
15940	4	44075	8	71470	34	91095	12	108468	38		
16169	44	44319	13	71735	10	91438	14	108473	19		
16365	50	44441	31	71844	33	91471	55	108598	62		
16391	55	44713	39	72479	51	91582	29	108736	2		
16492	6	44821	57	72673	9	92270	67	109012	24		
16852	19	44860	28	72688	57	92288	12	109086	1		

References

Abadi, M. G., Navarro, J. F., Steinmetz, M., & Eke, V. R. 2003, ApJ, 597, 21
Adibekyan, V. Z., Delgado Mena, E., Sousa, S. G., et al. 2012, A&A, 547, A36
Anders, E., & Grevesse, N. 1989, Geochim. Cosmochim. Acta, 53, 197
Andrievsky, S. M., Spite, M., Korotin, S. A., et al. 2007, A&A, 464, 1081
Anguiano, B., Freeman, K. C., Steinmetz, M., & Wylie de-Boer, E. in prep.
Anthony-Twarog, B. J., Deliyannis, C. P., Twarog, B. A., Croxall, K. V., & Cummings, J. D. 2009, AJ, 138, 1171
Asplund, M., Grevesse, N., Sauval, A. J., & Scott, P. 2009, ARA&A, 47, 481
Barden, S. C., Jones, D. J., Barnes, S. I., et al. 2010, in Society of Photo-Optical Instrumentation Engineers (SPIE) Conference Series, Vol. 7735, Society of Photo-Optical Instrumentation Engineers (SPIE) Conference Series, 9–19
Batista, S. F. A., & Fernandes, J. 2012, New A, 17, 514
Baumueller, D., Butler, K., & Gehren, T. 1998, A&A, 338, 637
Bekki, K., & Freeman, K. C. 2003, MNRAS, 346, L11
Belokurov, V., Zucker, D. B., Evans, N. W., et al. 2006a, ApJ, 647, L111
—. 2006b, ApJ, 642, L137
Bensby, T., Feltzing, S., & Lundström, I. 2003, A&A, 410, 527
Bensby, T., Feltzing, S., Lundström, I., & Ilyin, I. 2005, A&A, 433, 185
Bensby, T., Feltzing, S., & Oey, M. S. 2014, A&A, 562, A71
Bensby, T., Adén, D., Meléndez, J., et al. 2011, A&A, 533, A134
Bland-Hawthorn, J., & Freeman, K. C. 2004a, PASA, 21, 110
—. 2004b, PASA, 21, 110
Bland-Hawthorn, J., Karlsson, T., Sharma, S., Krumholz, M., & Silk, J. 2010a, ApJ, 721, 582
Bland-Hawthorn, J., Krumholz, M. R., & Freeman, K. 2010b, ApJ, 713, 166
Boeche, C., Siebert, A., Piffl, T., et al. 2013, A&A, 559, A59
Bovy, J., Rix, H.-W., & Hogg, D. W. 2012, ApJ, 751, 131
Bragaglia, A., Sestito, P., Villanova, S., et al. 2008a, A&A, 480, 79
—. 2008b, A&A, 480, 79
Bruntt, H., Frandsen, S., Kjeldsen, H., & Andersen, M. I. 1999, A&AS, 140, 135
Bubar, E. J., & King, J. R. 2010, AJ, 140, 293
Busso, M., Gallino, R., Lambert, D. L., Travaglio, C., & Smith, V. V. 2001, ApJ, 557, 802
Busso, M., Gallino, R., & Wasserburg, G. J. 1999, ARA&A, 37, 239

Carrera, R., & Pancino, E. 2011, A&A, 535, A30
Carretta, E., Bragaglia, A., & Gratton, R. G. 2007, A&A, 473, 129
Carretta, E., Bragaglia, A., Gratton, R. G., Lucatello, S., & D'Orazi, V. 2012, ApJ, 750, L14
Carretta, E., Bragaglia, A., Gratton, R. G., et al. 2010, A&A, 516, A55
Carretta, E., Bragaglia, A., Gratton, R. G., & Tosi, M. 2005, A&A, 441, 131
Casagrande, L., Schönrich, R., Asplund, M., et al. 2011, A&A, 530, A138
Castelli, F., & Kurucz, R. L. 2004, ArXiv Astrophysics e-prints
Conn, A. R., Lewis, G. F., Ibata, R. A., et al. 2013, ApJ, 766, 120
De Silva, G. M., D'Orazi, V., Melo, C., et al. 2013, MNRAS, 431, 1005
De Silva, G. M., Freeman, K. C., Asplund, M., et al. 2007a, AJ, 133, 1161
De Silva, G. M., Freeman, K. C., & Bland-Hawthorn, J. 2009a, PASA, 26, 11
De Silva, G. M., Freeman, K. C., Bland-Hawthorn, J., Asplund, M., & Bessell, M. S. 2007b, AJ, 133, 694
De Silva, G. M., Freeman, K. C., Bland-Hawthorn, J., et al. 2011, MNRAS, 415, 563
De Silva, G. M., Gibson, B. K., Lattanzio, J., & Asplund, M. 2009b, A&A, 500, L25
De Silva, G. M., Sneden, C., Paulson, D. B., et al. 2006, AJ, 131, 455
Demarque, P., Woo, J.-H., Kim, Y.-C., & Yi, S. K. 2004, ApJS, 155, 667
Den Hartog, E. A., Lawler, J. E., Sneden, C., & Cowan, J. J. 2006, ApJS, 167, 292
Derouich, M., Trujillo Bueno, J., & Manso Sainz, R. 2007, A&A, 472, 269
D'Orazi, V., Magrini, L., Randich, S., et al. 2009, ApJ, 693, L31
D'Orazi, V., & Randich, S. 2009, A&A, 501, 553
Edvardsson, B., Andersen, J., Gustafsson, B., et al. 1993, A&A, 275, 101
Eggen, O. J. 1963, AJ, 68, 697
Eggen, O. J. 1994, in Galactic and Solar System Optical Astrometry, ed. L. V. Morrison & G. F. Gilmore, 191
Feltzing, S., Bensby, T., & Lundström, I. 2003, A&A, 397, L1
Feltzing, S., & Holmberg, J. 2000, A&A, 357, 153
Feltzing, S., Holmberg, J., & Hurley, J. R. 2001, A&A, 377, 911
Ford, A., Jeffries, R. D., & Smalley, B. 2005, MNRAS, 364, 272
Freeman, K., & Bland-Hawthorn, J. 2002, ARA&A, 40, 487
Freeman, K. C., Bland-Hawthorn, J., SMG, & GALAH team. 2014, in prep.
Friel, E. D. 1995, ARA&A, 33, 381
Friel, E. D., Jacobson, H. R., Barrett, E., et al. 2003, AJ, 126, 2372
Friel, E. D., Janes, K. A., Tavarez, M., et al. 2002, AJ, 124, 2693

Fuhrmann, K. 1998, A&A, 338, 161
Gebran, M., & Monier, R. 2008, A&A, 483, 567
Gebran, M., Monier, R., & Richard, O. 2008, A&A, 479, 189
Gilmore, G., & Reid, N. 1983, MNRAS, 202, 1025
Gilmore, G., Randich, S., Asplund, M., et al. 2012, The Messenger, 147, 25
Gonzalez, G., & Wallerstein, G. 2000a, PASP, 112, 1081
—. 2000b, PASP, 112, 1081
Gratton, R. G., Bonifacio, P., Bragaglia, A., et al. 2001, A&A, 369, 87
Guedes, J., Callegari, S., Madau, P., & Mayer, L. 2011, ApJ, 742, 76
Haywood, M. 2006, MNRAS, 371, 1760
—. 2008, MNRAS, 388, 1175
Haywood, M., Di Matteo, P., Lehnert, M. D., Katz, D., & Gómez, A. 2013, A&A, 560, A109
Heijmans, J., Asplund, M., Barden, S., et al. 2012, in Society of Photo-Optical Instrumentation Engineers (SPIE) Conference Series, Vol. 8446, Society of Photo-Optical Instrumentation Engineers (SPIE) Conference Series
Høg, E., Fabricius, C., Makarov, V. V., et al. 2000, A&A, 355, L27
Hyde, E. A. 2014, PhD thesis, Macquarie University, Sydney, Australia
Ibata, R. A., Gilmore, G., & Irwin, M. J. 1994, Nature, 370, 194
Iben, J. 1967, ApJ, 147, 624
Irwin, M. J., Davies, J. I., Disney, M. J., & Phillipps, S. 1990, MNRAS, 245, 289
Janes, K. A., & Phelps, R. L. 1994, AJ, 108, 1773
Janes, K. A., Tilley, C., & Lynga, G. 1988, AJ, 95, 771
Kaluzny, J., & Rucinski, S. M. 1995, A&AS, 114, 1
Karakas, A., & Lattanzio, J. C. 2007, PASA, 24, 103
Karlsson, T., Bland-Hawthorn, J., Freeman, K. C., & Silk, J. 2012, ApJ, 759, 111
Kobayashi, C., Umeda, H., Nomoto, K., Tominaga, N., & Ohkubo, T. 2006, ApJ, 653, 1145
Kraft, R. P., Sneden, C., Smith, G. H., et al. 1997, AJ, 113, 279
Kratz, K.-L., Farouqi, K., Pfeiffer, B., et al. 2007, ApJ, 662, 39
Kupka, F., Piskunov, N., Ryabchikova, T. A., Stempels, H. C., & Weiss, W. W. 1999, A&AS, 138, 119
Lada, C. J., & Lada, E. A. 2003, ARA&A, 41, 57
Liu, W. M., & Chaboyer, B. 2000, ApJ, 544, 818
Loebman, S. R., Roškar, R., Debattista, V. P., et al. 2011, ApJ, 737, 8
Luck, R. E., Kovtyukh, V. V., & Andrievsky, S. M. 2006, AJ, 132, 902

Magrini, L., Randich, S., Zoccali, M., et al. 2010, A&A, 523, A11
Martin, N. F., Ibata, R. A., Conn, B. C., et al. 2004, MNRAS, 355, L33
Martin, N. F., McConnachie, A. W., Irwin, M., et al. 2009, ApJ, 705, 758
McGaugh, S. S. 2014, ArXiv e-prints
McKee, C. F., & Tan, J. C. 2002, Nature, 416, 59
McWilliam, A. 1998, AJ, 115, 1640
Mermilliod, J.-C., Andersen, J., Nordstroem, B., & Mayor, M. 1995, A&A, 299, 53
Minchev, I., Chiappini, C., & Martig, M. 2013, A&A, 558, A9
Minchev, I., Famaey, B., Combes, F., et al. 2011, A&A, 527, A147
Minchev, I., Famaey, B., Quillen, A. C., et al. 2012, A&A, 548, A127
Mitschang, A. W., De Silva, G., Sharma, S., & Zucker, D. B. 2013, MNRAS, 428, 2321
Mitschang, A. W., De Silva, G., Zucker, D. B., et al. 2014, MNRAS, 438, 2753
Mitschang, A. W., De Silva, G. M., & Zucker, D. B. 2012, MNRAS, 422, 3527
Montes, D., López-Santiago, J., Gálvez, M. C., et al. 2001, MNRAS, 328, 45
Muench, A., Getman, K., Hillenbrand, L., & Preibisch, T. 2008, Star Formation in the Orion Nebula I: Stellar Content, ed. B. Reipurth, 483
Navarro, J. F., Abadi, M. G., Venn, K. A., Freeman, K. C., & Anguiano, B. 2011, MNRAS, 412, 1203
Ng, Y. K., & Bertelli, G. 1998, A&A, 329, 943
Nordstroem, B., Andersen, J., & Andersen, M. I. 1997, A&A, 322, 460
Nordström, B., Andersen, J., Holmberg, J., et al. 2004, PASA, 21, 129
Pace, G., Pasquini, L., & François, P. 2008a, A&A, 489, 403
Pace, G., Pasquini, L., & François, P. 2008b, A&A, 489, 403
Pancino, E., Carrera, R., Rossetti, E., & Gallart, C. 2010, A&A, 511, A56+
Pasquini, L., Randich, S., & Pallavicini, R. 2001, A&A, 374, 1017
Paulson, D. B., Sneden, C., & Cochran, W. D. 2003, AJ, 125, 3185
Pereira, C. B., & Quireza, C. 2010, in IAU Symposium, Vol. 266, IAU Symposium, ed. R. de Grijs & J. R. D. Lépine, 495–498
Perryman, M. A. C., Lindegren, L., Kovalevsky, J., et al. 1997, A&A, 323, L49
Phelps, R. L., Janes, K. A., & Montgomery, K. A. 1994, AJ, 107, 1079
Pompéia, L., Masseron, T., Famaey, B., et al. 2011, MNRAS, 415, 1138
Quillen, A. C., & Garnett, D. R. 2001, in Astronomical Society of the Pacific Conference Series, Vol. 230, Galaxy Disks and Disk Galaxies, ed. J. G. Funes & E. M. Corsini, 87–88
Quinn, P. J., Hernquist, L., & Fullagar, D. P. 1993, ApJ, 403, 74

Randich, S., Pace, G., Pastori, L., & Bragaglia, A. 2009, A&A, 496, 441
Randich, S., Sestito, P., Primas, F., Pallavicini, R., & Pasquini, L. 2006, A&A, 450, 557
Reddy, A. B. S., Giridhar, S., & Lambert, D. L. 2012, MNRAS, 419, 1350
Reddy, B. E., Lambert, D. L., & Allende Prieto, C. 2006, MNRAS, 367, 1329
Reddy, B. E., Tomkin, J., Lambert, D. L., & Allende Prieto, C. 2003, MNRAS, 340, 304
Richardson, J. C., Irwin, M. J., McConnachie, A. W., et al. 2011, ApJ, 732, 76
Rix, H.-W., & Bovy, J. 2013, A&A Rev., 21, 61
Rocha-Pinto, H. J., Maciel, W. J., Scalo, J., & Flynn, C. 2000, A&A, 358, 850
Roškar, R., Debattista, V. P., & Loebman, S. R. 2013, MNRAS, 433, 976
Roškar, R., Debattista, V. P., Quinn, T. R., Stinson, G. S., & Wadsley, J. 2008a, ApJ, 684, L79
Roškar, R., Debattista, V. P., Stinson, G. S., et al. 2008b, ApJ, 675, L65
Salaris, M., Cassisi, S., & Weiss, A. 2002, PASP, 114, 375
Santos, N. C., Lovis, C., Pace, G., Melendez, J., & Naef, D. 2009, A&A, 493, 309
Schlesinger, K. J., Johnson, J. A., Rockosi, C. M., et al. 2012, ApJ, 761, 160
Schuler, S. C., King, J. R., Fischer, D. A., Soderblom, D. R., & Jones, B. F. 2003, AJ, 125, 2085
Sellwood, J. A., & Binney, J. J. 2002, MNRAS, 336, 785
Sestito, P., Bragaglia, A., Randich, S., et al. 2008a, A&A, 488, 943
—. 2008b, A&A, 488, 943
Sharma, S., & Johnston, K. V. 2009, ApJ, 703, 1061
Shen, Z.-X., Jones, B., Lin, D. N. C., Liu, X.-W., & Li, S.-L. 2005, ApJ, 635, 608
Shu, F. H., Adams, F. C., & Lizano, S. 1987, ARA&A, 25, 23
Skrutskie, M. F., Cutri, R. M., Stiening, R., et al. 2006, AJ, 131, 1163
Sneden, C., & Parthasarathy, M. 1983, ApJ, 267, 757
Sneden, C. A. 1973, PhD thesis, The University of Texas at Austin.
Soderblom, D. R. 2010, ARA&A, 48, 581
Soderblom, D. R., Laskar, T., Valenti, J. A., Stauffer, J. R., & Rebull, L. M. 2009, AJ, 138, 1292
Soubiran, C., Bienaymé, O., Mishenina, T. V., & Kovtyukh, V. V. 2008, A&A, 480, 91
Sousa, S. G., Santos, N. C., Israelian, G., Mayor, M., & Monteiro, M. J. P. F. G. 2007, A&A, 469, 783
Sousa, S. G., Santos, N. C., Mayor, M., et al. 2008, A&A, 487, 373
Springel, V., Wang, J., Vogelsberger, M., et al. 2008, MNRAS, 391, 1685
Steinmetz, M., Zwitter, T., Siebert, A., et al. 2006, AJ, 132, 1645
Tabernero, H. M., Montes, D., & González Hernández, J. I. 2012, A&A, 547, A13
Tautvaišiene, G., Edvardsson, B., Tuominen, I., & Ilyin, I. 2000a, A&A, 360, 499

—. 2000b, A&A, 360, 499
Ting, Y. S., Freeman, K. C., Kobayashi, C., de Silva, G. M., & Bland-Hawthorn, J. 2012, MNRAS, 421, 1231
Torres, C. A. O., Quast, G. R., Melo, C. H. F., & Sterzik, M. F. 2008, Young Nearby Loose Associations, ed. B. Reipurth, 757
Tsikoudi, V. 1980, ApJS, 43, 365
Wallerstein, G., Iben, J., Parker, P., et al. 1997, Reviews of Modern Physics, 69, 995
Willman, B., Dalcanton, J. J., Martinez-Delgado, D., et al. 2005, ApJ, 626, L85
Xin, Y., & Deng, L. 2005, ApJ, 619, 824
Yanny, B., Rockosi, C., Newberg, H. J., et al. 2009, AJ, 137, 4377
Yoachim, P., & Dalcanton, J. J. 2006, AJ, 131, 226
York, D. G., Adelman, J., Anderson, Jr., J. E., et al. 2000, AJ, 120, 1579
Zucker, D. B., Belokurov, V., Evans, N. W., et al. 2006, ApJ, 643, L103
Zuckerman, B., & Song, I. 2004, ARA&A, 42, 685